

DETECTOR DESIGN AND ESTIMATION FOR A DIGITAL COMMUNICATION SYSTEM

by
Nickos Sotirios Kontoyannis

Thesis submitted to the Faculty of the
Virginia Polytechnic Institute and State University
in partial fulfillment of the requirements for the degree of

Master of Science
in
Electrical Engineering

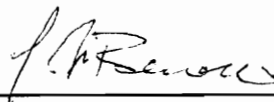


APPROVED:

A. A. (Louis) Beex, Chairman



H. F. VanLandingham



I. M. Besieris

July 1991
Blacksburg, Virginia

c.2

LD

5655

V855

1991

K658

C.2

DETECTOR DESIGN AND ESTIMATION FOR A DIGITAL COMMUNICATION SYSTEM

by

Nickos Sotirios Kontoyannis

Committee Chairman: A. A. (Louis) Beex

Electrical Engineering

(ABSTRACT)

This thesis investigates the behavior of two digital communication systems based on Moving-Average Matched Filters (MAMF). In general, matched filters are instrumental in detecting signals corrupted by noise as they are designed to maximize the probability of detection of the transmitted signals. The MAMF represents a subset of the class of matched filters.

The two communication systems under investigation are the classical MAMF system and one of its modifications, the proposed MAMF system. In the traditional system the N -dimensional signal vector, which encodes the bit to be communicated, remains fixed throughout the whole communication process (transmission and reception). In the proposed system the encoding N -dimensional signal vector is composed of K linearly independent basis vectors spanning a signal vector subspace of dimension $M (= N/K)$. By combining these basis vectors in the receiver, any vector in the signal vector subspace can be formed in order to maximize the Output Signal-to-Noise Ratio (OSNR).

The relative measure of comparison for the two systems is the Signal-to-Noise Ratio Improvement (SNRI). The SNRI is the ratio of the OSNR, which is measured at the output of the receiver, to the Input Signal-to-Noise Ratio (ISNR), which is measured at the input of the receiver. Since the ISNR is fixed for a particular transmitted signal vector and noise characteristics, an attempt is made to maximize the SNRI by maximizing the OSNR.

The OSNR of a MAMF is a function of the signal vector and the

autocorrelation of the noise. The OSNR reaches an absolute maximum when the signal vector is the eigenvector associated with the smallest eigenvalue of the Toeplitz matrix formed from the actual noise autocorrelation. For a practical implementation the noise autocorrelation is estimated from the noise samples obtained from gaps between transmissions; thus producing estimates. Since there is a limit to the number of noise samples taken, the estimated autocorrelation will stochastically deviate from the actual autocorrelation. Therefore the OSNR random variable will approach its optimal value as the estimated autocorrelation approaches the actual autocorrelation but it will not attain that optimal value unless the signal vector is the correct eigenvector. Under these conditions the SNRI varies accordingly and can sometimes become negative on the decibel scale; a situation which is, of course, highly undesirable in communications. This results from bad autocorrelation estimates or poor selection of the signal vectors to be transmitted. The latter can be a result of optimizing the system for one environment while subsequently subjecting it to an entirely different one.

The two systems are compared and their performance evaluated in terms of SNRI, for different signal vectors and over various noise colors. The noise is assumed to be narrowband Gaussian. In addition, the colored noise is assumed to be stationary for a single bit transmission. Initially, the comparison takes place using the actual autocorrelation sequence and is then repeated using the autocorrelation sequence estimates, obtained with the classical biased estimator. The procedure is then repeated for more broadband stationary Gaussian noise.

The SNRI comparisons provide only a relative and not an absolute measure of performance of the two systems. The latter is obtained by measuring Bit Error Rates (BER) as a function of ISNR. For this purpose an optimal detector design is presented in this work. Using the noise corrupted signal vector, the encoding signal vectors, and the noise autocorrelation matrix, the detector can make a decision on which signal vector was most likely transmitted and hence which bit was most likely communicated. The Receiver Operating Characteristic (ROC) is unique for each detector and is presented by plotting the probability of error as a function of OSNR. The ROC represents the theoretical

basis for the BER results. The close correlation existing between the ROC and the BER, as will be shown, enables the prediction of the performance of the detector under various ISNR, noise colors, and choices of encoding signal vectors.

The flexibility that is introduced by the proposed system as a result of linear combining creates the expectation that a more robust system can be developed than the traditional MAMF. In other words, the proposed system will deteriorate to a lesser degree than the traditional system when the detector design is based on autocorrelation estimates. This is indeed established by the SNRI and BER results, for a subset of the possible noise colors. Thus, the need arises for a selector which, for every single bit transmission, will suggest the system (proposed or traditional) to be used for most error-free detection, based on SNRI as well as colored noise center frequency and bandwidth (pole location) parameter estimates. The parameter estimator which will estimate the color of the noise from the noise samples is implemented by the Burg method. It will be shown that the [traditional/proposed] MAMF communication system which incorporates the selector design, outperforms both the proposed and the traditional MAMF communication systems.

Acknowledgements

My gratitude and sincere appreciation are extended to Dr. A. A. Beex for his valuable guidance, continuous encouragement, and patience during the development of this study; Dr. H. F. VanLandingham and Dr. I. M. Besieris who served on my committee; and the Naval Surface Weapons Center (NSWC) in Dahlgren, VA for their financial support of this project.

A special acknowledgement is given to my family. I was able to reach this point, only because of their lifetime efforts, love, and understanding. This work is dedicated to them.

And last but not least, thanks to all my friends and especially Dolly Kylpassis and George Tsoflias for their moral support, valuable suggestions, and extreme tolerance.

TABLE OF CONTENTS

1.0 INTRODUCTION.....	1
2.0 THEORETICAL DEVELOPMENT	11
2.1 NOISE CHARACTERISTICS	12
2.2 TRANSMISSION AND RECEPTION OF SIGNALS	16
2.2.1 Transmission of Signals	16
2.2.2 Linear Combination.....	18
2.2.3 Effects of Linear Combination on the Noise Autocorrelation Matrix.....	20
2.2.4 Methods of Transmission of Signals	21
2.3 AUTOCORRELATION ESTIMATOR.....	26
2.4 MAMF-BASED RECEIVER SYSTEM.....	28
2.4.1 MAMF Characteristics	28
2.4.2 MAMF Theoretical Performance.....	30
2.4.3 MAMF Practical Performance	32
2.4.4 Optimal Detector Design	33
2.4.5 Optimal Detector Performance	41
3.0 SIMULATION	50
3.1 COLORED NOISE GENERATION	51
3.2 SYSTEM DESCRIPTIONS.....	57
3.2.1 Proposed System Description.....	57
3.2.2 Traditional System Description	68
4.0 RESULTS ON MAMF RECEIVER PERFORMANCE.....	75

4.1 GENERAL SNRI COMPARISONS	76
4.1.1 Maximum SNRI curves	76
4.1.2 Optimal Traditional System vs. Proposed System.....	77
4.2 SNRI AND BER RESULTS	87
4.2.1 BER Performance.....	87
4.2.2 Optimal Traditional System vs. Optimal Proposed System.....	89
4.2.3 Optimal Proposed System vs. Traditional System.....	98
 5.0 RECEIVER SELECTOR DESIGN.....	118
5.1 COLORED NOISE CENTER FREQUENCY AND BANDWIDTH ESTIMATOR	119
5.2 DECISION ON MAMF RECEIVER SYSTEM.....	122
5.2.1 Lagrange Interpolation of mean SNRI data.....	122
5.2.2 Estimator / Selector Implementation.....	128
 6.0 SUMMARY AND CONCLUSIONS	140
 APPENDICES	143
 BIBLIOGRAPHY	148
 VITA	151

LIST OF ILLUSTRATIONS

FIGURE 1. A GENERAL DIGITAL COMMUNICATION SYSTEM.....	7
FIGURE 2. TRADITIONAL SYSTEM vs. PROPOSED SYSTEM TRANSMITTERS.....	8
FIGURE 3. TRADITIONAL MAMF COMMUNICATION SYSTEM RECEIVER.....	9
FIGURE 4. PROPOSED MAMF COMMUNICATION SYSTEM RECEIVER.....	10
FIGURE 5A. CONDITIONAL PROBABILITY DENSITY FUNCTIONS ($\sigma_G^2 = 9$).....	48
FIGURE 5B. CONDITIONAL PROBABILITY DENSITY FUNCTIONS ($\sigma_G^2 = 49$).....	49
FIGURE 6. COLORED NOISE AR(2) FILTER CHARACTERISTICS	54
FIGURE 7A. COLORED NOISE AR(2) FILTER MAGNITUDE RESPONSE	55
FIGURE 7B. COLORED NOISE AR(2) FILTER MAGNITUDE RESPONSE	56
FIGURE 8. PROPOSED MAMF COMMUNICATION SYSTEM DETECTOR	66
FIGURE 9. ROC FOR THE PROPOSED SYSTEM AS A FUNCTION OF OSNR	67
FIGURE 10. TRADITIONAL MAMF COMMUNICATION SYSTEM DETECTOR	73
FIGURE 11. ROC FOR THE TRADITIONAL SYSTEM AS A FUNCTION OF OSNR	74
FIGURE 12. MAXIMUM SNRI vs. θ FOR $\rho = 0.95$	80
FIGURE 13. MAXIMUM SNRI vs. θ FOR $\rho = 0.8$	81
FIGURE 14. MAXIMUM SNRI vs. θ FOR $\rho = 0.5$	82
FIGURE 15. SNRI vs. θ FOR $\rho = 0.95$ (OPT. TRAD @ $\theta = 0$ vs. SYMMETRIC PROP)....	83
FIGURE 16. SNRI vs. θ FOR $\rho = 0.95$ (OPT. TRAD @ $\theta = 0$ vs. SKEW-SYMM. PROP) ..	84
FIGURE 17. SNRI vs. θ FOR $\rho = 0.95$ (OPT. TRAD @ $\theta = \frac{\pi}{2}$ vs. SYMMETRIC PROP) ...	85
FIGURE 18. SNRI vs. θ FOR $\rho = 0.95$ (OPT. TRAD @ $\theta = \frac{\pi}{2}$ vs. SKEW-SYMM. PROP) ..	86
FIGURE 19. SNRI vs. θ FOR $\rho = 0.95$ (OPT. TRAD @ $\theta = 0$ vs. OPT. PROP)	92
FIGURE 20. ROC AND BER COMPARISON, TRADITIONAL SYSTEM, ACTUAL AC..	96
FIGURE 21. ROC AND BER COMPARISON, PROPOSED SYSTEM, ACTUAL AC.....	97
FIGURE 22. SNRI vs. θ FOR $\rho = 0.95$ (TRAD & PROP USE OPT. PROP VECTORS)...	101

FIGURE 23. $\hat{\text{SNRI}}$ vs. θ FOR $\rho = 0.95$ (TRAD & PROP USE OPT. PROP VECTORS)...	102
FIGURE 24. SNRI vs. θ FOR $\rho = 0.8$ (TRAD & PROP USE OPT. PROP VECTORS).....	103
FIGURE 25. $\hat{\text{SNRI}}$ vs. θ FOR $\rho = 0.8$ (TRAD & PROP USE OPT. PROP VECTORS).....	104
FIGURE 26. SNRI vs. θ FOR $\rho = 0.5$ (TRAD & PROP USE OPT. PROP VECTORS).....	105
FIGURE 27. $\hat{\text{SNRI}}$ vs. θ FOR $\rho = 0.5$ (TRAD & PROP USE OPT. PROP VECTORS).....	106
FIGURE 28. ROC AND BER COMPARISON, TRADITIONAL SYSTEM, EST. AC	107
FIGURE 29. ROC AND BER COMPARISON, PROPOSED SYSTEM, EST. AC.....	108
FIGURE 30. $\overline{\text{SNRI}}$ vs. $\hat{\rho}$ FOR $\theta = 0$, TRADITIONAL & PROPOSED SYSTEMS.....	125
FIGURE 31. $\overline{\text{SNRI}}$ vs. $\hat{\rho}$ FOR $\theta = \frac{\pi}{2}$, TRADITIONAL & PROPOSED SYSTEMS.....	126
FIGURE 32. $\overline{\text{SNRI}}$ vs. $\hat{\rho}$ FOR $\theta = \pi$, TRADITIONAL & PROPOSED SYSTEMS.....	127

LIST OF TABLES

TABLE 1. BER vs. ISNR ($\theta = 0^\circ$, $\rho = 0.95$, OPT. TRAD @ $\theta = 0$ vs. OPT. PROP)	93
TABLE 2. BER vs. ISNR ($\theta = 105.4^\circ$, $\rho = 0.95$, OPT. TRAD @ $\theta = 0$ vs. OPT. PROP)	94
TABLE 3. BER vs. ISNR ($\theta = 135^\circ$, $\rho = 0.95$, OPT. TRAD @ $\theta = 0$ vs. OPT. PROP)	95
TABLE 4. BER vs. ISNR ($\theta = 0$, $\rho = 0.95$, TRAD & PROP USE OPT. PROP VEC.)	109
TABLE 5. BER vs. ISNR ($\theta = \frac{\pi}{2}$, $\rho = 0.95$, TRAD & PROP USE OPT. PROP VEC.)	110
TABLE 6. BER vs. ISNR ($\theta = \pi$, $\rho = 0.95$, TRAD & PROP USE OPT. PROP VEC.)	111
TABLE 7. BER vs. ISNR ($\theta = 0$, $\rho = 0.8$, TRAD & PROP USE OPT. PROP VEC.)	112
TABLE 8. BER vs. ISNR ($\theta = \frac{\pi}{2}$, $\rho = 0.8$, TRAD & PROP USE OPT. PROP VEC.)	113
TABLE 9. BER vs. ISNR ($\theta = \pi$, $\rho = 0.8$, TRAD & PROP USE OPT. PROP VEC.)	114
TABLE 10. BER vs. ISNR ($\theta = 0$, $\rho = 0.5$, TRAD & PROP USE OPT. PROP VEC.)	115
TABLE 11. BER vs. ISNR ($\theta = \frac{\pi}{2}$, $\rho = 0.5$, TRAD & PROP USE OPT. PROP VEC.)	116
TABLE 12. BER vs. ISNR ($\theta = \pi$, $\rho = 0.5$, TRAD & PROP USE OPT. PROP VEC.)	117
TABLE 13. STATS & BER vs. ISNR ($\theta = 0^\circ$, $\rho = 0.95$, TRAD vs. PROP vs. SELEC)	131
TABLE 14. STATS & BER vs. ISNR ($\theta = 90^\circ$, $\rho = 0.95$, TRAD vs. PROP vs. SELEC)	132
TABLE 15. STATS & BER vs. ISNR ($\theta = 126^\circ$, $\rho = 0.95$, TRAD vs. PROP vs. SELEC)	133
TABLE 16. RECEIVER SYSTEM BER AVERAGES FOR $\rho = 0.95$	137
TABLE 17. RECEIVER SYSTEM \hat{P}_e AVERAGES FOR $\rho = 0.95$	138
TABLE 18. RECEIVER SYSTEM \hat{P}_e AVERAGES $\times 10^{-6}$ FOR $\rho = 0.95$	139

1.0 INTRODUCTION

A *digital communication system* is a system whose transmitter must convey to its receiver a sequence of messages from a finite alphabet of a set dimension L (Figure 1). This is accomplished by sequentially transmitting one of these L different signal vectors, during a specified interval of time. These messages might correspond to a set of numbers, or a digital representation of an analog variable, or even numerical representations of symbols of an alphabet.

The physical medium through which the signal vector must travel between the transmitter and the receiver is the *channel*. A common example of a communication channel is the atmosphere through which electromagnetic radiation travels. Additional examples are media which transmit acoustical waveforms. Water, for instance, is the transmission medium for sonar systems, which analyze high-frequency vibrations generated by, or reflected from, an object. Sonar systems could be used to detect a submarine, or to study an underwater canyon of unknown depth and size. Cables and wires, such as telephone lines, are also channels.

If the channel were noiseless, so that the transmitted signal vector reached the receiver undistorted, then the receiver would have no difficulty to distinguish which message had been transmitted. Obviously, this is hardly a realistic situation. Since the very initial developments of communication systems, the processing of signals corrupted by noise has been a topic of considerable study and importance in that field [4,5,13,16,17,19,20,23].

The distortion in a radio-communication channel is characterized by the type of interference that is placed on the reception of electromagnetic energy

radiated from the transmitter. One form of interference always present is thermal noise in the antenna and the front-end components of the receiver [7,14,15]. Another form of disturbance is electromagnetic radiation at frequencies within the received band, or noise of a specific frequency content which is known as *colored noise*. This work investigates the particular problem of colored noise corrupting the transmitted signal vectors in the channel.

The major purpose of this thesis is to design an optimal detector for a Moving-Average Matched Filter (MAMF) communication system after examining the behavior of the system under ideal and estimated conditions. Since the matched filter is designed to maximize the discrimination and probability of detection of the corrupted signals, it is a key component of the receiver system. The MAMF is a Finite Impulse Response (FIR) digital filter and represents a subset of the class of matched filters. These FIR filters are widely used due to their guarantee of stability, ease of implementation, and efficient design.

Although there are many examples of previous work done on detection in colored noise [4,5,9,18,22], this thesis specifically presents the discrete-time derivation of the detector design as it focuses on two digital communication systems, the traditional MAMF system and one of its modifications, the proposed MAMF system [4]. The general structure of the traditional MAMF communication system is presented in Figures 2 and 3. The system is composed of the transmitter (Figure 2) and the receiver (Figure 3) separated by the transmission medium or the channel. The data to be communicated, \mathbf{d} , is encoded in the transmitter. Each individual bit of data is encoded in a fixed N -dimensional signal vector, \mathbf{s}_j . This vector is then transmitted through the medium where it is subject to additive colored noise \mathbf{w} . The resulting measurement vector \mathbf{r} , next, enters the receiver. The Input Signal-to-Noise Ratio (ISNR) of the vector \mathbf{r} is measured at this point.

In order to design the MAMF, the set of encoding signals $\{\mathbf{s}_0, \mathbf{s}_1, \dots, \mathbf{s}_{L-1}\}$ as well as the colored noise autocorrelation sequence \mathbf{r}_w , is required. In a practical situation where no information regarding the noise

characteristics is available, the noise autocorrelation must be estimated. The effect of estimating the noise autocorrelation on the performance of the traditional communication system has been investigated [3]. The noise autocorrelation is estimated by a correlation estimator [3,4] which uses noise samples, \mathbf{w}_g , obtained from gaps between transmissions. Since there is a limit to the number of noise samples taken, the estimated autocorrelation sequence $\hat{\mathbf{r}}_w$, will deviate from the actual autocorrelation sequence \mathbf{r}_w [3]. The larger the number of noise samples taken, the slower the transmission rate becomes. Under ideal circumstances, the noise autocorrelation sequence used is the actual one, thus assuming that the correlation estimator is 100% accurate. The classical biased estimator is the correlation estimator that was shown by Becker [3] to be the best choice for this particular problem. It is, therefore, used in this thesis since it was shown to produce the highest mean SNRI and the smallest standard deviation among numerous estimators, and for white, bandpass, and lowpass noise. It is also a consistent estimator, which means that its estimates improve as the length of the data sequence increases.

Since a single MAMF can be designed for every encoding signal \mathbf{s}_j , L MAMF are needed. After the MAMF bank is designed, the measurement vector \mathbf{r} ($= \mathbf{s} + \mathbf{w}$) is processed and the Output Signal-to-Noise Ratio (OSNR) is measured at the output of each MAMF. The detector, then, based on the information exiting each MAMF, makes a decision on which signal vector was most likely transmitted and therefore which data bit was most probably communicated.

The performance of the entire system is then measured in terms of Signal-to-Noise Ratio Improvement (SNRI) which is the ratio of OSNR to ISNR. In order to maximize the SNRI, one needs to maximize the OSNR since the ISNR remains fixed for a particular signal vector and noise characteristics.

Up to this point many authors have completed work towards designing a signal vector which maximizes the OSNR of the traditional MAMF system for a particular noise color [4,5,24]. An undesirable situation can arise, though, if the noise characteristics change or the noise becomes non-stationary during the

transmission. This will render the signal vector non-optimal since it was designed for one specific noise color. As a result the performance of the communication system will suffer. Under these circumstances, the SNRI could actually reach a value less than 1 (negative in dB), an observation indicating that the MAMF receiver system degraded the performance of the communication system, rather than improving it.

The general structure of the proposed MAMF communication system is displayed in Figures 2 and 4. In this system each N-dimensional signal vector used for encoding the data \mathbf{d} , is composed of K linearly independent basis vectors spanning a signal vector subspace of dimension M (= N/K). Thus, the encoding signal vector set is $\{\mathbf{S}_0, \mathbf{S}_1, \dots, \mathbf{S}_{L-1}\}$. Each individual bit of data is now encoded by the matrix \mathbf{S}_j and sent through the transmission medium where it is subject to additive colored noise, \mathbf{w} (Figure 2). Again the ISNR is measured at the input of the receiver based on the N-dimensional received measurement vector \mathbf{r} . Also, the autocorrelation sequence is estimated after obtaining noise samples, \mathbf{w}_g , from the gaps between transmissions [3].

In an attempt to maximize the OSNR, which is measured at the output of each MAMF, the K linearly independent basis vectors of dimension M in the matrix \mathbf{S}_j are linearly combined in the following manner:

$$\tilde{\mathbf{s}}_j = c_{j1}\mathbf{s}_{j1} + c_{j2}\mathbf{s}_{j2} + \dots + c_{jK}\mathbf{s}_{jK} \quad j = 0, 1, \dots, L-1$$

where the coefficient vector \mathbf{c}_j is designed in such a fashion so as to ensure maximum signal energy and thus maximum OSNR. The resulting combined signal vector, $\tilde{\mathbf{s}}_j$, is of dimension M and is used in conjunction with the autocorrelation sequence - the actual \mathbf{r}_w , under ideal conditions or the estimated $\hat{\mathbf{r}}_w$, under practical conditions - to design the j-th MAMF. In order to account for that shift in dimension - from N to M - the received vector \mathbf{r} is combined to produce:

$$\tilde{\mathbf{r}}_j = c_{j1}\mathbf{r}_1 + c_{j2}\mathbf{r}_2 + \dots + c_{jK}\mathbf{r}_K \quad j = 0, 1, \dots, L-1$$

which is now M -dimensional. The combined received vector $\tilde{\mathbf{r}}_j$ is then processed by the j -th MAMF (Figure 4). The OSNR is computed at the output of the MAMF and the performance of the overall receiving system is measured in terms of SNRI. Next, the output of each of the L MAMF's is considered by the detector which determines which linearly independent basis vector set \mathbf{S}_j was most likely transmitted and thus which data bit was most probably communicated.

The difference between the two communication systems lies in the following: whereas in the receiver of the traditional MAMF system the signal vector remains constant, in the receiver of the proposed MAMF system, any signal vector in the M -dimensional subspace can be formed by combining the linearly independent basis vectors of the signal space in order to maximize the OSNR. In that way undesirable situations, like the one described for the traditional MAMF system, are less likely to surface, thus ensuring a more robust data communication.

The flexibility to adapt to different noise environments, as introduced by the proposed system, creates the expectation that a more robust system than the traditional MAMF can be implemented, in the sense that the proposed system will deteriorate to a lesser degree than the traditional system when used under practical conditions, where the noise autocorrelation is a priori unknown and must be estimated. The final goal of this thesis is to design a selector which will decide which receiving MAMF system is to be used for each individual bit transmission, based on the estimation of the noise characteristics as well as the detector design.

The concern of the primary goal of the thesis is the detection and discrimination of the transmitted signal vectors. Other than the estimation of the noise autocorrelation, which represents work already completed, as seen previously, there is no emphasis placed on the explicit determination of the signal and noise parameters. Nevertheless, the second goal of the thesis requires the knowledge of the noise parameters in order for the selector to be able to make a correct decision. Parameter estimation is one more field that has been

the object of frenzied research activity during the last decades [2,5,7,8,9,10,21]. Due to the special nature of the noise - colored - modern spectral estimation techniques are used to estimate frequency and bandwidth parameters of the essentially narrowband noise [6]. It is shown that, based on this information, the selector can identify the communication system that on average performs better, or has the highest SNRI, under those noise conditions.

The theoretical development of both MAMF communication systems will be reviewed in Chapter 2. In addition the detector design as well as the estimation of the noise characteristics will be discussed. Chapter 3 presents the incorporation of the overall design in the two MAMF communication systems. Chapter 4 contains the presentation and evaluation of both communication systems in terms of SNRI results obtained by computer simulations. The noise used for the simulations has a Gaussian distribution. Different noise characteristics and encoding signal vector sets are used and both ideal and practical conditions are examined. An absolute measure of performance is also evaluated in Chapter 4 by measuring Bit Error Rates (BER's) as a function of ISNR, again for both ideal and practical conditions. Chapter 5 presents BER results with the communication system selector incorporated in the design, and its overall performance is assessed. The overall findings and evaluation of the system is discussed in the Conclusions, Chapter 6.

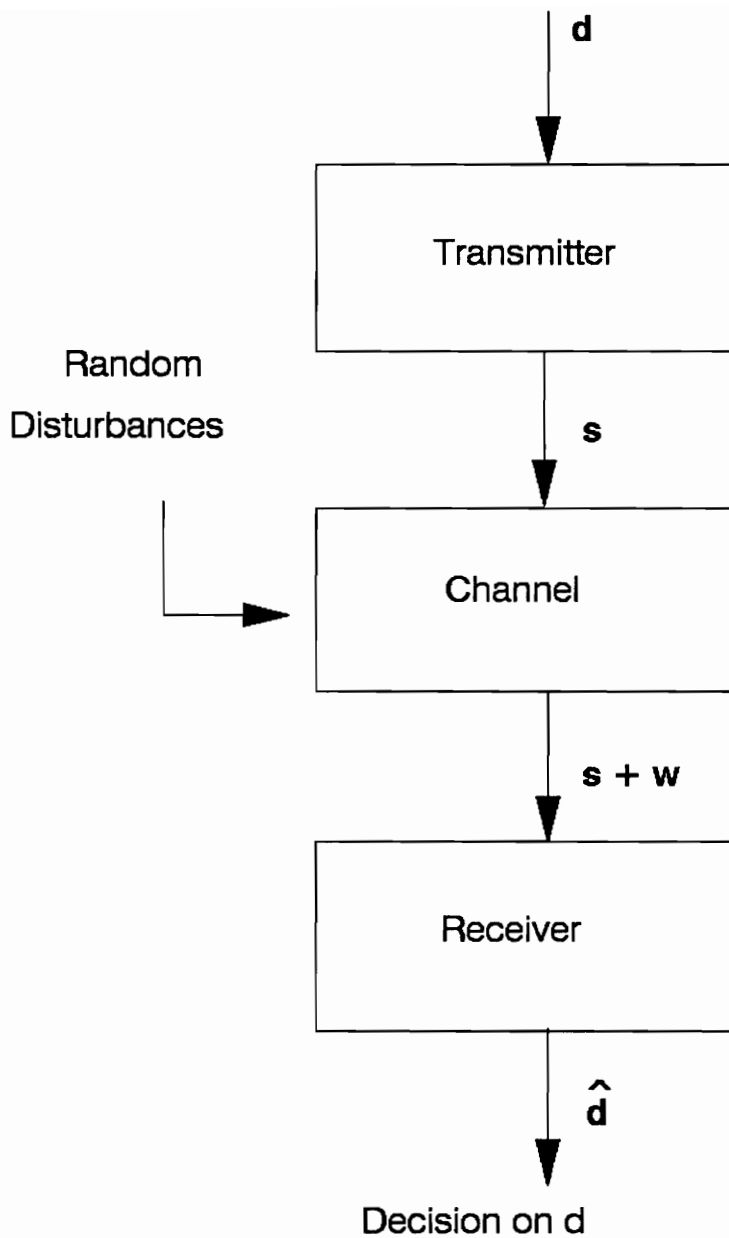


FIGURE 1. A GENERAL DIGITAL COMMUNICATION SYSTEM

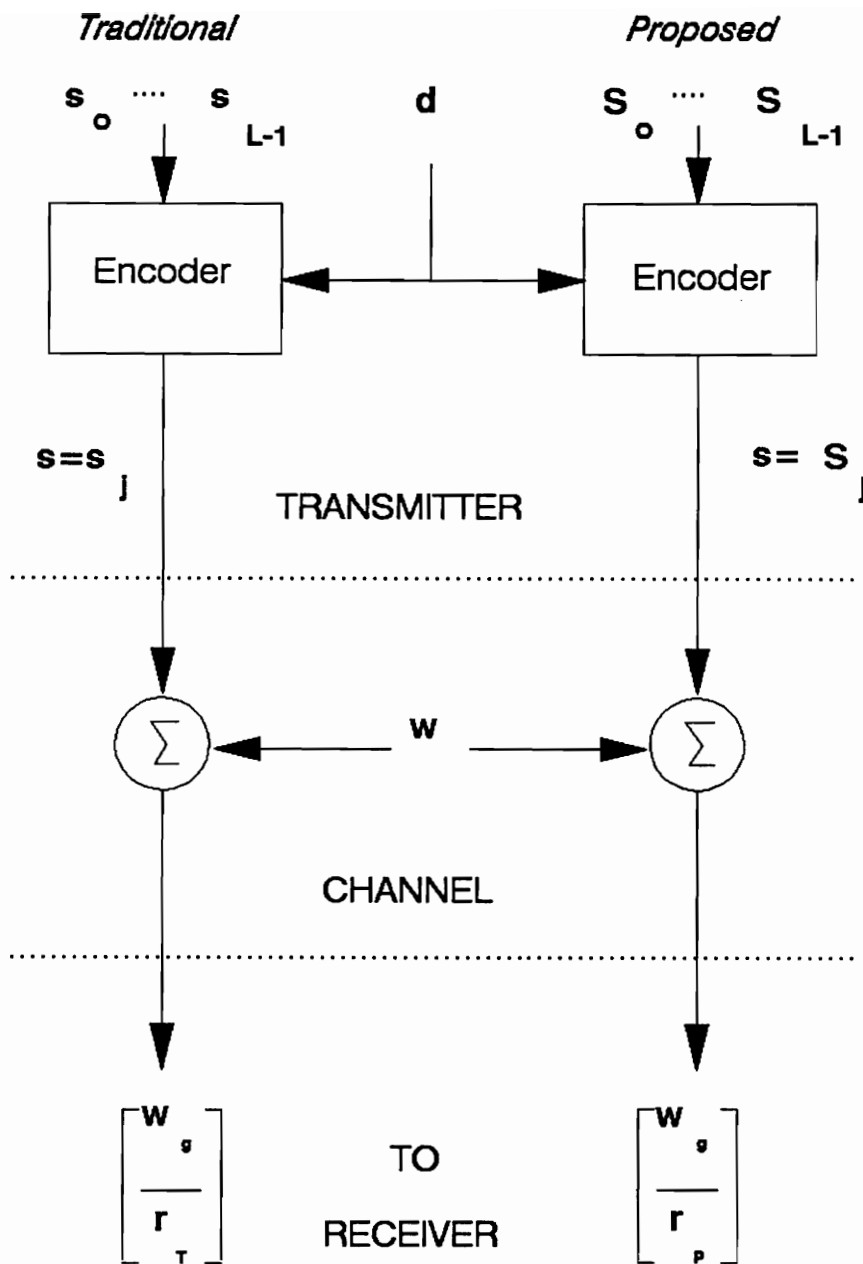


FIGURE 2. TRADITIONAL MAMF COMMUNICATION SYSTEM TRANSMITTER
vs.
PROPOSED MAMF COMMUNICATION SYSTEM TRANSMITTER

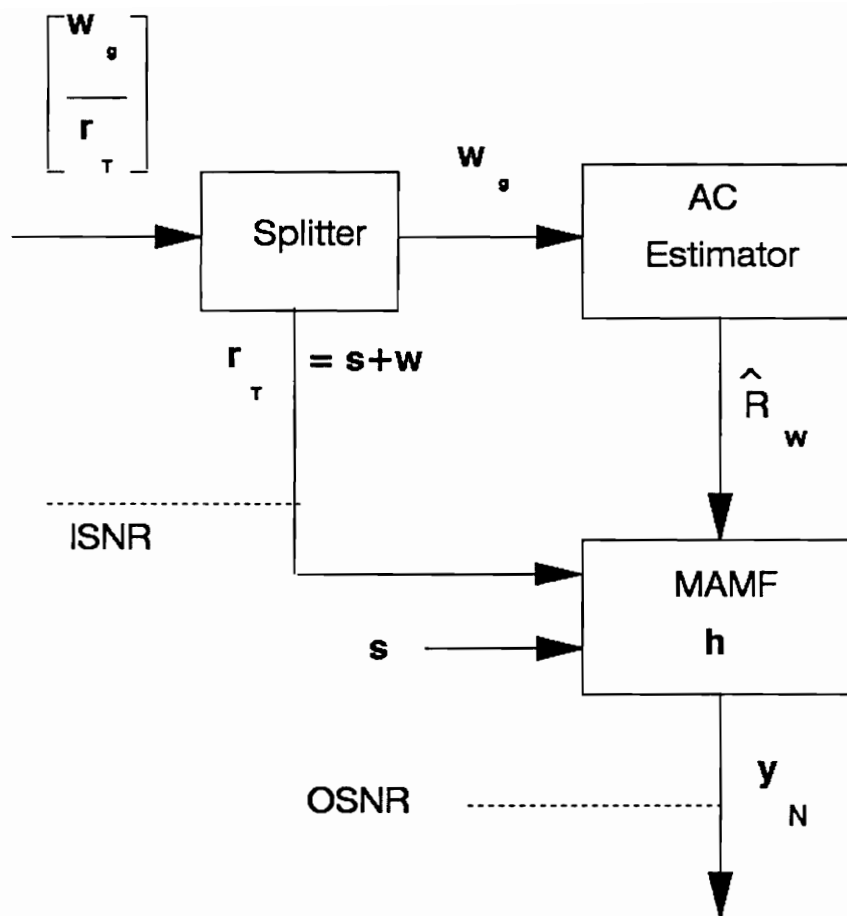


FIGURE 3. TRADITIONAL MAMF COMMUNICATION SYSTEM RECEIVER

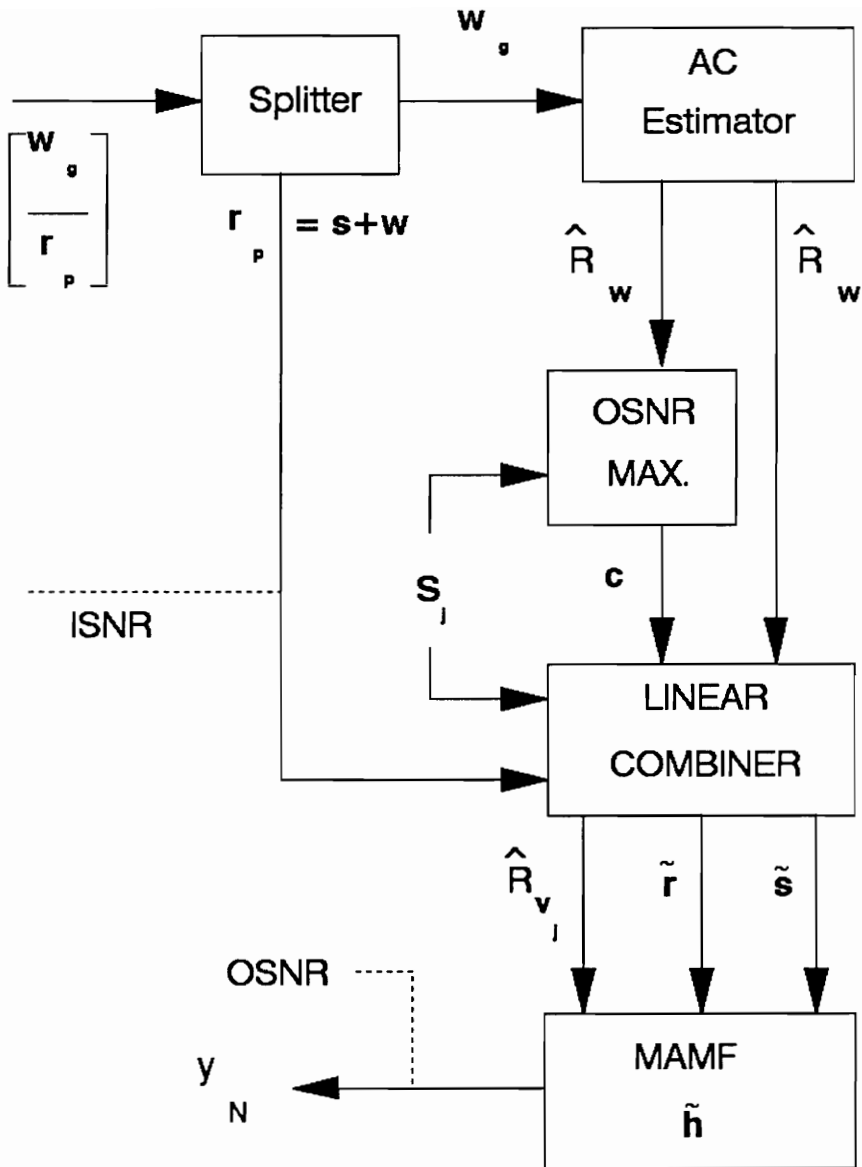


FIGURE 4. PROPOSED MAMF COMMUNICATION SYSTEM RECEIVER

2.0 THEORETICAL DEVELOPMENT

In this chapter the theory behind both the traditional and the proposed MAMF communication systems will be developed. Specifically, this chapter will first present the characteristics of the colored noise. Next, the properties of the MAMF and the correlation estimator, which are essential to the communication systems examined, will be investigated. Meanwhile, the properties and form of the traditional communication system will be discussed followed by those of the proposed communication system. The latter will include a presentation of the structure of the transmitted signal vector as well as the structure and linear combination of the received signal. In addition, the design of the optimal detector will be presented.

2.1 NOISE CHARACTERISTICS

The noise which corrupts the transmitted signals in the channel is assumed to be Gaussian, zero-mean with a noise autocorrelation sequence r_w , which is defined as follows:

$$r_w(\tau) = E\{w_{i+\tau} w_i^*\} \quad \tau = 0, \dots, N-1 \quad (2.1)$$

Furthermore, the noise is assumed to be wide-sense stationary only for the duration of the observation interval. Since the noise is colored and wide-sense stationary, the autocorrelation sequence is non-negative definite and well-behaved [7]. The vector form of (2.1) defines the Toeplitz colored noise autocorrelation matrix R_w as,

$$R_w = E\{\mathbf{w} \mathbf{w}^H\} = \begin{bmatrix} r_w(0) & r_w(-1) & \dots & r_w(-N+1) \\ r_w(1) & \ddots & & \vdots \\ \vdots & & \ddots & \vdots \\ r_w(N-1) & \dots & \dots & r_w(0) \end{bmatrix} \quad (2.2)$$

where $()^H$ indicates the Hermitian transpose. Since the noise is assumed to be wide-sense stationary, $r_w(-\tau) = r_w^*(\tau)$ [7] and thus R_w is also Hermitian.

Thus, the noise autocorrelation matrix R_w ($N \times N$) has the following properties which are used extensively for the detector design as well as the MAMF receiver system design:

1. $R_w = (R_w^*)^T = (R_w^T)^* = R_w^H$ by the definition of Hermitian matrices.
2. $R_w^{-1} = (R_w^{-1})^H$ by the definition of Hermitian matrices.

Proof. Assume that the inverse of R_w exists and is designated R_w^{-1} . Then,

$$R_w R_w^{-1} = I \Rightarrow (R_w R_w^{-1})^H = I$$

$$\Rightarrow (R_w^{-1})^H R_w = I$$

$$\Rightarrow R_w^{-1} = (R_w^{-1})^H$$

□

3. $R_w = F \Lambda F^{-1}$, where F is the transformation matrix containing the eigenvectors f_i of the matrix R_w as its columns, and Λ is the Jordan canonical form containing the eigenvalues λ_i of R_w [1]. In other words, R_w and Λ are similar matrices ($R_w \approx \Lambda$).

- (a) If R_w has rank N , it has N distinct eigenvalues. Then, its eigenvectors are independent and orthogonal, can be constructed as orthonormal, and F is unitary, where

$$F^H F = F F^H = I \quad (2.3)$$

Thus, R_w has a diagonal matrix representation, with Λ being a diagonal matrix containing the eigenvalues of R_w [1], or $\Lambda = \text{diag} \{\lambda_i\}_{i=1}^N$. Then,

$$R_w = F \Lambda F^{-1} = F \Lambda F^H \quad (2.4)$$

Note that (2.4) can be written as,

$$R_w F = F \Lambda \Rightarrow \quad (2.5.a)$$

$$F^H R_w^H = \Lambda^H F^H \quad (2.5.b)$$

Since R_w is Hermitian, right multiplication of (2.5.b) by F yields

$$F^H R_w F = \Lambda^H F^H F \Rightarrow F^H R_w F = \Lambda^H \quad (2.6)$$

Left multiplication of (2.5.a) by F^H yields

$$F^H R_w F = F^H F \Lambda = \Lambda \quad (2.7)$$

Thus $\Lambda = \Lambda^H$ and therefore the eigenvalues λ_i are real.

(b) If R_w has rank $\leq N$, it has at least one repeated eigenvalue. In this case, the eigenvectors are not necessarily orthogonal. Such eigenvectors may nevertheless be made orthogonal or orthonormal, for example by the Gram-Schmidt orthogonalization procedure [9] (Appendix A).

Therefore, all the properties of (a) also apply for (b).

Thus, R_w has N orthogonal / orthonormal eigenvectors and its eigenvalues are real.

4. $R_w \geq 0$, or the noise autocorrelation sequence is non-negative definite. Therefore its eigenvalues are greater than or equal to zero.

Proof. Since R_w is a non-negative definite matrix then, for any arbitrary vector \mathbf{x} ,

$$\mathbf{x}^H R_w \mathbf{x} \geq 0 \quad (2.8)$$

In addition, since Λ is diagonal and $\lambda_i \in \mathbb{R}$, then (2.5.a) becomes,

$$R_w \mathbf{f}_i = \lambda_i \mathbf{f}_i \quad (2.9)$$

where \mathbf{f}_i is the i -th eigenvector associated with the i -th eigenvalue λ_i of the noise autocorrelation matrix R_w . Since (2.8) holds for any vector \mathbf{x} , then it must hold for any of the eigenvectors $\mathbf{f}_1, \mathbf{f}_2, \dots, \mathbf{f}_N$. Hence according to (2.8),

$$\mathbf{f}_i^H R_w \mathbf{f}_i \geq 0$$

and by considering (2.9),

$$\mathbf{f}_i^H \lambda_i \mathbf{f}_i \geq 0$$

Finally from (2.3),

$$\lambda_i \geq 0 \quad i = 1, 2, \dots, N \quad \square.$$

2.2 TRANSMISSION AND RECEPTION OF SIGNALS

2.2.1 Transmission of signals

The thesis investigates two MAMF communication systems. In the traditional system, as seen from Figure 2, every individual bit of data to be communicated is encoded in a fixed N-dimensional signal vector \mathbf{s}_j :

$$\mathbf{s}_j = [s_{j1} \ s_{j2} \ \dots \ s_{jN}]^T \quad j = 0, 1, \dots, L-1 \quad (2.10)$$

where L depends upon the type of communication used. For instance, for a binary communication system $L = 2$ so that \mathbf{s}_0 would encode a "0" and \mathbf{s}_1 would encode a "1". In the channel, every signal element is corrupted by a colored noise vector \mathbf{w} ,

$$\mathbf{w} = [w_1 \ w_2 \ \dots \ w_N]^T \quad (2.11)$$

to produce the received or observed vector \mathbf{r}_T :

$$\mathbf{r}_T = [s_{j1}+w_1 \ s_{j2}+w_2 \ \dots \ s_{jN}+w_N]^T \quad \forall j \quad (2.12)$$

In the proposed system, as seen from Figure 2, the data bit to be transmitted is encoded by a matrix which has as its columns K linearly independent signal basis vectors of dimension M ($=N/K$). The signal matrix is designated \mathbf{S}_j :

$$\mathbf{S}_j = [s_{j1} \ s_{j2} \ \dots \ s_{jK}] \quad j = 0, 1, \dots, L-1 \quad (2.13)$$

where

$$\mathbf{s}_{ji} = [s_{ji1} \ s_{ji2} \ \dots \ s_{jiM}]^T \quad \forall j \quad (2.14)$$

Similarly, for the proposed system, the colored noise matrix \mathbf{W} , displays the following format:

$$\mathbf{W} = [\mathbf{w}_1 \ \mathbf{w}_2 \ \dots \ \mathbf{w}_K] \quad (2.15)$$

where

$$\mathbf{w}_i = [w_{i1} \ w_{i2} \ \dots \ w_{iM}]^T \quad (2.16)$$

The colored noise matrix \mathbf{W} , which has $N (=K \times M)$ elements, corrupts the transmitted signal matrix to produce the received or observed matrix \mathbf{R}_P :

$$\mathbf{R}_P = [s_{j1} + \mathbf{w}_1 \ s_{j2} + \mathbf{w}_2 \ \dots \ s_{jK} + \mathbf{w}_K] \quad \forall j \quad (2.17)$$

The K linearly independent basis vectors span a signal vector subspace of dimension K , within an M -dimensional space. Since any vector in the subspace can be represented by a linear combination of its basis vectors, the whole signal vector subspace is effectively transmitted rather than a single signal vector. By linearly combining the basis vectors, one can create the signal vector that ensures maximum probability of detection and discrimination of the transmitted signal vectors. This flexibility introduced by the proposed communication system is a solution to the problem of non-stationary noise where the noise characteristics vary with every bit transmission [4].

The purpose of the proposed MAMF receiver system is to detect and distinguish which set of basis vectors is transmitted. In order to accomplish this, one must ensure that a linear combination of the basis vectors of the j -th signal subspace will not result in a vector which belongs to the i -th signal subspace. In other words, the signal vector subspaces must not overlap. Thus each set of basis vectors must be orthogonal to every other set of basis vectors, in order to minimize the probability of error [4,25].

The two designations \mathbf{r}_T and \mathbf{R}_P , are theoretically created to represent the noise corrupted signals that enter the receiver of the traditional and the

proposed communication system respectively, as observed data sequences of finite length. Although \mathbf{r}_T is an N-dimensional vector and it is capable of the aforementioned representation, \mathbf{R}_P is an $M \times K$ matrix and it is not. Evidently, \mathbf{R}_P has to be converted to an N-dimensional vector, in order to truly represent an observed data sequence of finite length. One way to accomplish this is to transmit the linearly independent basis vectors sequentially [4,25], thus resulting in:

$$\mathbf{r}_P = [(\mathbf{s}_{j1} + \mathbf{w}_1)^T \mid (\mathbf{s}_{j2} + \mathbf{w}_2)^T \mid \dots \mid (\mathbf{s}_{jK} + \mathbf{w}_K)^T]^T \quad \forall j \quad (2.18)$$

Now \mathbf{r}_P is a vector of dimension N ($=M \times K$). Additional methods of transmission for the proposed system, as well as their restrictions will be looked upon in Sections 2.2.3 and 2.2.4.

The colored noise is assumed stationary over every single data bit transmission, or every single N-dimensional signal vector transmission. Thus the colored noise characteristics must be estimated for every bit transmission. For this reason noise samples \mathbf{w}_g , are obtained from the gaps between bit transmissions to form the observed vector actually entering the MAMF communication receiver:

$$\mathbf{r}_a = [\mathbf{w}_g^T \mid \mathbf{r}_P^T] \quad (\text{Proposed system}) \quad (2.19.a)$$

$$\mathbf{r}_a = [\mathbf{w}_g^T \mid \mathbf{r}_T^T] \quad (\text{Traditional system}) \quad (2.19.b)$$

At this point, (2.19) represents a single data bit transmission for either the proposed or the traditional system as encoded by their respective transmission schemes.

2.2.2 Linear Combination

In the proposed MAMF communication system, a signal vector subspace of dimension K is transmitted rather than a single signal vector, because a linear

combination of the linearly independent basis vectors can result in the creation of any vector in the subspace defined by these basis vectors.

Since the transmitted signal vector, or subspace, is subject to additive colored noise in the channel, it is obvious that when the basis vectors are linearly combined, so are their associated additive noise vectors. The effects and restrictions of the linear combination of the received signal and noise vectors were investigated by Wilson [25]. Thus, if \mathbf{c}_j is the coefficient vector associated with the j -th signal basis vector set,

$$\mathbf{c}_j = [c_{j1} \ c_{j2} \ \dots \ c_{jK}]^T \quad j = 0, 1, \dots, L-1 \quad (2.20)$$

the linear combination of the linearly independent basis vectors (2.13) is:

$$\begin{aligned} \tilde{\mathbf{s}}_j &= \mathbf{S}_j \mathbf{c}_j \\ &= [\mathbf{s}_{j1} \ \mathbf{s}_{j2} \ \dots \ \mathbf{s}_{jK}] \mathbf{c}_j \\ &= c_{j1}\mathbf{s}_{j1} + c_{j2}\mathbf{s}_{j2} + \dots + c_{jK}\mathbf{s}_{jK} \quad \forall j \end{aligned} \quad (2.21)$$

The coefficients c_{ji} are computed in such a way so as to maximize the signal energy out of the MAMF. The coefficients must be restricted in such a way so that the energy of the linearly combined signal vector $\tilde{\mathbf{s}}_j$ equals the energy of the transmitted signal matrix \mathbf{S}_j . If the linearly independent basis vectors are chosen such that each basis vector within a particular set is orthonormal to the others,

$$\mathbf{s}_{jm}^T \mathbf{s}_{jn} = \begin{cases} 0 & \text{for } m \neq n \\ 1 & \text{for } m = n \end{cases} \quad \forall j \quad (2.22)$$

then the following relation holds [25]:

$$\sum_{i=1}^K c_{ji}^2 = K \quad \forall j \quad (2.23)$$

From the linear combiner action upon the noise represented by (2.15), the linearly combined noise vector $\tilde{\mathbf{w}}_j$ is,

$$\tilde{\mathbf{w}}_j = \sum_{i=1}^K c_{ji} \mathbf{w}_i \quad \forall j \quad (2.24)$$

Notice that after the linear combiner action has been performed for the proposed MAMF communication system, $\tilde{\mathbf{s}}_j$ and $\tilde{\mathbf{w}}_j$ are M-dimensional vectors. Hence an analysis on the effects of the linear combiner action on the colored noise autocorrelation matrix follows.

2.2.3 Effects of linear combination on the noise autocorrelation matrix

As seen from the previous section in (2.17), the \mathbf{w}_i vector is the noise vector which corresponds to the \mathbf{s}_{ji} signal vector. Let us define,

$$\mathbf{R}_{\mathbf{w}_i \mathbf{w}_k} = \mathbf{E}\{\mathbf{w}_i \mathbf{w}_k^H\} \quad (2.25)$$

From the linear combiner action upon the noise as in (2.24), it is evident that,

$$\begin{aligned} \mathbf{R}_{\tilde{\mathbf{w}}_j} &= \mathbf{E}\{\tilde{\mathbf{w}}_j \tilde{\mathbf{w}}_j^H\} \\ &= \mathbf{E}\left\{ \sum_{l=1}^K c_{jl} \mathbf{w}_l \sum_{m=1}^K c_{jm}^* \mathbf{w}_m^H \right\} \\ &= \mathbf{E}\left\{ \sum_{l=1}^K \sum_{m=1}^K c_{jl} c_{jm}^* \mathbf{w}_l \mathbf{w}_m^H \right\} \\ &= \sum_{l=1}^K \sum_{m=1}^K c_{jl} c_{jm}^* \mathbf{E}\{\mathbf{w}_l \mathbf{w}_m^H\} \\ &= \sum_{l=1}^K \sum_{m=1}^K c_{jl} c_{jm}^* \mathbf{R}_{\mathbf{w}_l \mathbf{w}_m} \quad \forall j \end{aligned} \quad (2.26)$$

where c^* is the complex conjugate of c .

To preserve the idea of local stationarity (within a symbol transmission interval) the combiner noise autocorrelation matrix, $R_{\tilde{w}_j}$, should be Toeplitz. Thus, according to (2.26), each one of the above $R_{w_l w_m}$ matrices has to be Toeplitz. Furthermore, since the $R_{w_l w_m}$ matrices are $M \times M$, the combined noise autocorrelation matrix $R_{\tilde{w}_j}$ is also $M \times M$. By considering these restrictions, a few methods of transmission of signals can be investigated.

2.2.4 Methods of transmission of signals

As was mentioned in Section 2.2.1 there are several methods of transmitting the signal matrix for the proposed MAMF communication system. One of these methods is represented by (2.18) where the transmitted signal vector is constructed by concatenating the K linearly independent basis vectors. In order to simplify the presentation of this section consider the approach wherein an 8-dimensional signal vector is used to encode the transmitted data, and is composed of 2, 4-dimensional linearly independent basis vectors (thus $N=8$, $K=2$, and $M=4$.)

In the above, the transmitted signal vector is constructed by concatenating the two linearly independent basis vectors, and consequently all previous results [4,25] are based on the assignment:

$$\mathbf{s}_j = [\mathbf{s}_{j1}^T \mid \mathbf{s}_{j2}^T]^T \quad \forall j \quad (2.27)$$

Since the two vectors are of length 4, the component sequence is as follows:

$$\mathbf{s}_j = [s_{j11} \ s_{j12} \ s_{j13} \ s_{j14} \ s_{j21} \ s_{j22} \ s_{j23} \ s_{j24}]^T \quad \forall j$$

We have investigated possibilities with other assignments such as alternating the components of the two basis vectors, as well as other random assignments. For instance, the alternating element sequence is as follows:

$$\mathbf{s}_j = [s_{j11} \ s_{j21} \ s_{j12} \ s_{j22} \ s_{j13} \ s_{j23} \ s_{j14} \ s_{j24}]^T \quad \forall j$$

It is evident that the noise samples would follow the same sequence. Therefore, in the alternating element sequence:

$$\mathbf{w} = [w_{11} \ w_{21} \ w_{12} \ w_{22} \ w_{13} \ w_{23} \ w_{14} \ w_{24}]^T$$

The w_i element is the noise element which corresponds to the s_i signal element. Consequently, (2.18) becomes

$$\mathbf{r}_P = [(s_{j11}+w_{11}) \ (s_{j21}+w_{21}) \ \dots \ (s_{j24}+w_{24})]^T \quad \forall j$$

From the linear combiner action upon the noise (2.24),

$$\tilde{\mathbf{w}}_j = c_{j1}\mathbf{w}_1 + c_{j2}\mathbf{w}_2 \quad \forall j \quad (2.28)$$

it is evident that,

$$R_{\tilde{\mathbf{w}}_j} = E\{(c_{j1}\mathbf{w}_1 + c_{j2}\mathbf{w}_2)(c_{j1}^*\mathbf{w}_1^H + c_{j2}^*\mathbf{w}_2^H)\} \quad \forall j \quad (2.29)$$

After expanding, we have

$$R_{\tilde{\mathbf{w}}_j} = |c_{j1}|^2 E\{\mathbf{w}_1\mathbf{w}_1^H\} + c_{j1}c_{j2}^* E\{\mathbf{w}_1\mathbf{w}_2^H\} + c_{j2}c_{j1}^* E\{\mathbf{w}_2\mathbf{w}_1^H\} + |c_{j2}|^2 E\{\mathbf{w}_2\mathbf{w}_2^H\} \quad (2.30)$$

which is,

$$R_{\tilde{\mathbf{w}}_j} = |c_{j1}|^2 R_{\mathbf{w}_1\mathbf{w}_1} + c_{j1}c_{j2}^* R_{\mathbf{w}_1\mathbf{w}_2} + c_{j2}c_{j1}^* R_{\mathbf{w}_2\mathbf{w}_1} + |c_{j2}|^2 R_{\mathbf{w}_2\mathbf{w}_2} \quad (2.31)$$

which is the expanded form of (2.26) with $K=2$, $\forall j$. By setting an index of position for the noise vector,

$$\mathbf{w} = [w_0 \ w_1 \ w_2 \ w_3 \ w_4 \ w_5 \ w_6 \ w_7]^T$$

$$= [w_{11} \ w_{12} \ w_{13} \ w_{14} \ w_{21} \ w_{22} \ w_{23} \ w_{24}]^T$$

the concatenated vector assignment produces

$$\begin{aligned} R_{\mathbf{w}} &= \begin{bmatrix} R_{\mathbf{w}_1 \mathbf{w}_1} & | & R_{\mathbf{w}_1 \mathbf{w}_2} \\ - & - & - \\ R_{\mathbf{w}_2 \mathbf{w}_1} & | & R_{\mathbf{w}_2 \mathbf{w}_2} \end{bmatrix} \\ &= \begin{bmatrix} r_{\mathbf{w}}(0) \ r_{\mathbf{w}}(1) \ r_{\mathbf{w}}(2) \ r_{\mathbf{w}}(3) & | & r_{\mathbf{w}}(4) \ r_{\mathbf{w}}(5) \ r_{\mathbf{w}}(6) \ r_{\mathbf{w}}(7) \\ r_{\mathbf{w}}(-1) \ r_{\mathbf{w}}(0) \ r_{\mathbf{w}}(1) \ r_{\mathbf{w}}(2) & | & r_{\mathbf{w}}(3) \ r_{\mathbf{w}}(4) \ r_{\mathbf{w}}(5) \ r_{\mathbf{w}}(6) \\ r_{\mathbf{w}}(-2) \ r_{\mathbf{w}}(-1) \ r_{\mathbf{w}}(0) \ r_{\mathbf{w}}(1) & | & r_{\mathbf{w}}(2) \ r_{\mathbf{w}}(3) \ r_{\mathbf{w}}(4) \ r_{\mathbf{w}}(5) \\ r_{\mathbf{w}}(-3) \ r_{\mathbf{w}}(-2) \ r_{\mathbf{w}}(-1) \ r_{\mathbf{w}}(0) & | & r_{\mathbf{w}}(1) \ r_{\mathbf{w}}(2) \ r_{\mathbf{w}}(3) \ r_{\mathbf{w}}(4) \\ \hline r_{\mathbf{w}}(-4) \ r_{\mathbf{w}}(-3) \ r_{\mathbf{w}}(-2) \ r_{\mathbf{w}}(-1) & | & r_{\mathbf{w}}(0) \ r_{\mathbf{w}}(1) \ r_{\mathbf{w}}(2) \ r_{\mathbf{w}}(3) \\ r_{\mathbf{w}}(-5) \ r_{\mathbf{w}}(-4) \ r_{\mathbf{w}}(-3) \ r_{\mathbf{w}}(-2) & | & r_{\mathbf{w}}(-1) \ r_{\mathbf{w}}(0) \ r_{\mathbf{w}}(1) \ r_{\mathbf{w}}(2) \\ r_{\mathbf{w}}(-6) \ r_{\mathbf{w}}(-5) \ r_{\mathbf{w}}(-4) \ r_{\mathbf{w}}(-3) & | & r_{\mathbf{w}}(-2) \ r_{\mathbf{w}}(-1) \ r_{\mathbf{w}}(0) \ r_{\mathbf{w}}(1) \\ r_{\mathbf{w}}(-7) \ r_{\mathbf{w}}(-6) \ r_{\mathbf{w}}(-5) \ r_{\mathbf{w}}(-4) & | & r_{\mathbf{w}}(-3) \ r_{\mathbf{w}}(-2) \ r_{\mathbf{w}}(-1) \ r_{\mathbf{w}}(0) \end{bmatrix} \end{aligned} \quad (2.32)$$

This results from identifying elements of the assignment with elements of \mathbf{w} , i.e. $w_{22} = w_5$ and $w_{12} = w_1$, so that $E\{w_{22}w_{12}^*\} = E\{w_5w_1^*\} = r_{\mathbf{w}}(-4) = r_{\mathbf{w}}^*(4)$, because of the assumed stationarity of the noise.

Note that each of the four submatrices of $R_{\mathbf{w}}$ in (2.32) is Toeplitz, so that $R_{\tilde{\mathbf{w}}_j}$ in (2.26) is automatically Toeplitz. For every j ,

$$r_{\tilde{\mathbf{w}}_j}(0) = |c_{j1}|^2 r_{\mathbf{w}}(0) + |c_{j2}|^2 r_{\mathbf{w}}(0) + c_{j1}c_{j2}^* r_{\mathbf{w}}(4) + c_{j2}c_{j1}^* r_{\mathbf{w}}(-4) \quad (2.33.a)$$

$$r_{\tilde{\mathbf{w}}_j}(1) = |c_{j1}|^2 r_{\mathbf{w}}(1) + |c_{j2}|^2 r_{\mathbf{w}}(1) + c_{j1}c_{j2}^* r_{\mathbf{w}}(5) + c_{j2}c_{j1}^* r_{\mathbf{w}}(-3) \quad (2.33.b)$$

$$r_{\tilde{\mathbf{w}}_j}(2) = |c_{j1}|^2 r_{\mathbf{w}}(2) + |c_{j2}|^2 r_{\mathbf{w}}(2) + c_{j1}c_{j2}^* r_{\mathbf{w}}(6) + c_{j2}c_{j1}^* r_{\mathbf{w}}(-2) \quad (2.33.c)$$

$$r_{\tilde{w}_j}(3) = |c_{j1}|^2 r_w(3) + |c_{j2}|^2 r_w(3) + c_{j1}c_{j2}^* r_w(7) + c_{j2}c_{j1}^* r_w(-1) \quad (2.33.d)$$

Using the same procedure for evaluating R_w , the alternating element sequence yields,

$$R_w = \begin{bmatrix} R_{w_1 w_1} & | & R_{w_1 w_2} \\ - & - & - \\ R_{w_2 w_1} & | & R_{w_2 w_2} \end{bmatrix}$$

$$= \begin{bmatrix} r_w(0) & r_w(2) & r_w(4) & r_w(6) & | & r_w(1) & r_w(3) & r_w(5) & r_w(7) \\ r_w(-2) & r_w(0) & r_w(2) & r_w(4) & | & r_w(-1) & r_w(1) & r_w(3) & r_w(5) \\ r_w(-4) & r_w(-2) & r_w(0) & r_w(2) & | & r_w(-3) & r_w(-1) & r_w(1) & r_w(3) \\ r_w(-6) & r_w(-4) & r_w(-2) & r_w(0) & | & r_w(-5) & r_w(-3) & r_w(-1) & r_w(1) \\ \hline r_w(-1) & r_w(1) & r_w(3) & r_w(5) & | & r_w(0) & r_w(2) & r_w(4) & r_w(6) \\ r_w(-3) & r_w(-1) & r_w(1) & r_w(3) & | & r_w(-2) & r_w(0) & r_w(2) & r_w(4) \\ r_w(-5) & r_w(-3) & r_w(-1) & r_w(1) & | & r_w(-4) & r_w(-2) & r_w(0) & r_w(2) \\ r_w(-7) & r_w(-5) & r_w(-3) & r_w(-1) & | & r_w(-6) & r_w(-4) & r_w(-2) & r_w(0) \end{bmatrix} \quad (2.34)$$

Again the four submatrices are Toeplitz.

For the split vector assignment,

$$\mathbf{w} = [w_{23} \ w_{24} \ w_{11} \ w_{12} \ w_{13} \ w_{14} \ w_{21} \ w_{22}]^T$$

we get however,

$$\mathbf{R}_w = \left[\begin{array}{cccc|cccc} r_w(0) & r_w(1) & r_w(2) & r_w(3) & r_w(4) & r_w(5) & r_w(-2) & r_w(-1) \\ r_w(-1) & r_w(0) & r_w(1) & r_w(2) & r_w(3) & r_w(4) & r_w(-3) & r_w(-2) \\ r_w(-2) & r_w(-1) & r_w(0) & r_w(1) & r_w(2) & r_w(3) & r_w(-4) & r_w(-3) \\ r_w(-3) & r_w(-2) & r_w(-1) & r_w(0) & r_w(1) & r_w(2) & r_w(-5) & r_w(-4) \\ \hline r_w(-4) & r_w(-3) & r_w(-2) & r_w(-1) & r_w(0) & r_w(1) & r_w(-6) & r_w(-5) \\ r_w(-5) & r_w(-4) & r_w(-3) & r_w(-2) & r_w(-1) & r_w(0) & r_w(-7) & r_w(-6) \\ r_w(2) & r_w(3) & r_w(4) & r_w(5) & r_w(6) & r_w(7) & r_w(0) & r_w(1) \\ r_w(1) & r_w(2) & r_w(3) & r_w(4) & r_w(5) & r_w(6) & r_w(-1) & r_w(0) \end{array} \right] \quad (2.35)$$

In this case, the four submatrices are not all Toeplitz. In addition, no non-trivial linear combination of the four, as in (2.26), results in a Toeplitz $\mathbf{R}_{\tilde{w}_j}$. From the random assignments tried, only the concatenated vector and alternating bit sequences resulted in a Toeplitz combiner noise autocorrelation matrix $\mathbf{R}_{\tilde{w}_j}$. Unless otherwise stated, the concatenated vector assignment is used throughout this work.

2.3 AUTOCORRELATION ESTIMATOR

As was mentioned in Section 2.2.1, the noise autocorrelation sequence must be estimated for every data bit transmission due to the noise non-stationarity assumption. A noise sample vector \mathbf{w}_g is obtained from gaps between transmissions and used to estimate the autocorrelation sequence.

The estimator used in the simulations of this work is the classical biased estimator. The CB estimator is a moving-average estimator which computes estimates directly from the data samples. It has been shown to produce the smallest standard deviation among the unbiased, exponential, triangular, diagonal, and minimum norm MA estimators under white, bandpass, and lowpass noise [3]. The estimated autocorrelation sequence produced by the CB estimator is,

$$\hat{r}_{\mathbf{w}}(k) = \frac{1}{I} \sum_{i=0}^{I-k-1} \mathbf{w}_i \mathbf{w}_{i+k} \quad (2.36)$$

where I is the length of the data sequence or the dimension of the vector \mathbf{w}_g , and $0 \leq k \leq I-1$. Furthermore, the estimator is biased. Thus,

$$E\{\hat{r}_{\mathbf{w}}(k)\} - r_{\mathbf{w}}(k) \neq 0 \quad k = 0, 1, \dots, N-1 \quad (2.37)$$

Equation (2.37) indicates that the average deviation of the estimator from the true value is non-zero. This introduction of low-level bias, achieved by the scaling performed in (2.36), results in a significant reduction of the induced variance of the estimates.

Also, the Toeplitz autocorrelation matrix produced is non-negative definite (NND) which ensures that the wide-sense stationarity assumption on the noise is not contradicted [3].

The actual finite length sequences that enter the MAMF communication receiver are given in (2.19). The vector \mathbf{w}_g is of a finite dimension I , which implies that there exists a limit to the number of noise samples taken. As the

number of noise samples obtained increases, the estimated autocorrelation sequence $\hat{\mathbf{r}}_{\mathbf{w}}$ tends to match the actual autocorrelation sequence $\mathbf{r}_{\mathbf{w}}$. However the transmission rate decreases. Hence, there exists a trade-off between accuracy and speed.

2.4 MAMF-BASED RECEIVER SYSTEM

In modern digital communication systems, the problem of the receiving system is to determine, at a particular instant in time, which signal vector is present, if any. For these purposes a *receiver* is a mathematical description of the operation to be performed on the noise corrupted signal.

For such a problem, reason indicates that the ability to correctly determine which is true will improve for a large Signal-to-Noise Ratio (SNR). For a given signal vector, it is conceivable that some filter may exist that will amplify the signal energy while simultaneously reducing the noise energy as much as possible so that the SNR becomes a maximum. Such a time invariant filter which yields the maximum SNR is called a *matched filter*.

One class of matched filters is the class of Moving-Average Matched Filters (MAMF). The MAMF is a Finite Impulse Response (FIR) filter which performs a weighted sum over a finite portion of the data at a particular time instant (Moving-Average). The MAMF is designed to maximize OSNR for a given ISNR, at the time instant τ . Since the signal vectors received by the communication system are N-dimensional, the time instant τ is equal to N (N time instants for $\tau = 1, 2, \dots, N$). The goal of the MAMF is to produce a SNRI which is greater than 1 (positive on the dB scale) so as to really improve the ability to correctly distinguish between the transmitted signal vectors.

For this reason the MAMF constitutes the first of the two important stages of the *receiver* (Figures 3 and 4). It pre-conditions the noise corrupted signal by producing a high SNRI so as to prepare it for entrance to the second stage, the detector. The detector is the stage of the *receiver* that decides which signal was transmitted. The absolute measure of the performance of the detector is provided through the computation of Bit Error Rates (BER).

2.4.1 MAMF Characteristics

Let h designate the impulse response of the filter,

$$\mathbf{h} \triangleq [h_1 \ h_2 \ \dots \ h_N]^T$$

and \mathbf{r} the received N -dimensional vector which contains the signal vector information corrupted with additive colored noise,

$$\mathbf{r} = \begin{cases} \mathbf{J} \mathbf{r}_P & \text{(for the proposed system as in (2.18))} \\ \mathbf{J} \mathbf{r}_T & \text{(for the traditional system as in (2.12))} \end{cases}$$

where \mathbf{J} is the $N \times N$ exchange matrix,

$$\mathbf{J} = \begin{bmatrix} \mathbf{0} & & & 1 \\ & & \ddots & \\ & 1 & & \\ 1 & & & \mathbf{0} \end{bmatrix} \quad (2.38)$$

Thus \mathbf{r} designates the inverse of the received vectors \mathbf{r}_T or \mathbf{r}_P , according to the communication system used. The output of the MAMF at time instant $\tau = N$, y_N , due to the vector \mathbf{r} is:

$$\begin{aligned} y_N &= \sum_{k=1}^N r_{N+1-k} h_k \\ &= \mathbf{h}^T \mathbf{r} \end{aligned} \quad (2.39)$$

Due to the operation of the filter on a finite number of data points, the filter is a stable FIR digital filter.

The MAMF are designed efficiently by using the Levinson algorithm (Appendix B) as will be shown in the next section. The MAMF are also easy to implement and are guaranteed to be stable. These properties of the MAMF provide a reason for its use.

2.4.2 MAMF Theoretical Performance

The performance of the MAMF receiver system is measured in terms of Signal-to-Noise Ratio Improvement (SNRI). The SNRI is the ratio of the OSNR, which is measured at the output of the receiver, to the ISNR, which is measured at its input.

The ISNR is the ratio of the signal energy to the average power of the noise of the received vector \mathbf{r} . If

$$\mathbf{r} = \mathbf{s} + \mathbf{w}$$

where $\mathbf{s} = [s_N \ s_{N-1} \ \dots \ s_1]^T$ and $\mathbf{w} = [w_N \ w_{N-1} \ \dots \ w_1]^T$ then,

$$E_{s,i} = \mathbf{s}^H \mathbf{s} \quad (2.40.a)$$

$$E_{w,i} = E\{\mathbf{w}^H \mathbf{w}\} = r_w(0) \quad (2.40.b)$$

Thus,

$$\text{ISNR} = \frac{E_{s,i}}{E_{w,i}} = \frac{\mathbf{s}^H \mathbf{s}}{r_w(0)} \quad (2.41)$$

By considering (2.39), the output of the MAMF is given by,

$$\begin{aligned} y_N &= \sum_{k=1}^N r_{N+1-k} h_k \\ &= \mathbf{h}^T \mathbf{r} \\ &= \mathbf{h}^T (\mathbf{s} + \mathbf{w}) \\ &= \mathbf{h}^T \mathbf{s} + \mathbf{h}^T \mathbf{w} \\ &\triangleq y_{N,signal} + y_{N,noise} \end{aligned} \quad (2.42)$$

where $y_{N,signal}$ and $y_{N,noise}$ represent the signal component and the noise component of the output of the filter respectively. Thus the signal energy and average power of the noise at $\tau = N$ are,

$$\begin{aligned} E_{s,o} &= |y_{N,signal}|^2 \\ &= |(\mathbf{h}^T \mathbf{s})|^2 \end{aligned} \quad (2.43.a)$$

$$\begin{aligned} E_{w,o} &= E\{|y_{N,noise}|^2\} \\ &= E\{(y_{N,noise})(y_{N,noise})^*\} \\ &= E\{(\mathbf{h}^H \mathbf{w}^*)(\mathbf{h}^T \mathbf{w})\} \end{aligned} \quad (2.43.b)$$

Since $\mathbf{a}^H \mathbf{b} = \mathbf{b}^T \mathbf{a}^*$, (2.43.b) becomes,

$$\begin{aligned} E_{w,o} &= E\{(\mathbf{h}^T \mathbf{w})(\mathbf{w}^H \mathbf{h}^*)\} \\ &= \mathbf{h}^T E\{\mathbf{w} \mathbf{w}^H\} \mathbf{h}^* \\ &= \mathbf{h}^H \mathbf{R}_w \mathbf{h} \end{aligned} \quad (2.43.c)$$

where \mathbf{R}_w is given by (2.2). Hence, by use of equations (2.43), the OSNR is,

$$\text{OSNR} = \frac{E_{s,o}}{E_{w,o}} = \frac{|(\mathbf{h}^T \mathbf{s})|^2}{\mathbf{h}^H \mathbf{R}_w \mathbf{h}} \quad (2.44)$$

The impulse response which maximizes OSNR, assuming the colored noise autocorrelation is known, can be found by minimizing $E_{w,o}$ while keeping $\sqrt{E_{s,o}}$ constant. Hence, by applying the Lagrangian multiplier technique, the Lagrangian equation $I(\mathbf{h})$ is constructed,

$$I(\mathbf{h}) = E_{\mathbf{w},o} - \mu[(\mathbf{h}^T \mathbf{s}) - \sqrt{E_{\mathbf{s},o}}] - \mu[(\mathbf{h}^T \mathbf{s}) - \sqrt{E_{\mathbf{s},o}}]^* \quad (2.45)$$

where μ is a Lagrangian multiplier. Taking the partial derivative of (2.45) with respect to \mathbf{h} and setting the result equal to zero yields,

$$\frac{\partial I(\mathbf{h})}{\partial \mathbf{h}} = 2\mathbf{R}_{\mathbf{w}} \mathbf{h} - 2\mu \mathbf{s}^* = 0 \quad (2.46)$$

Solving for \mathbf{h} produces,

$$\mathbf{h}_{opt} = \mathbf{R}_{\mathbf{w}}^{-1} \mathbf{s}^* \quad (2.47)$$

By substitution of (2.47) in (2.44), the optimal value or maximum OSNR is obtained:

$$\begin{aligned} \text{OSNR}_{opt} &= \mathbf{h}_{opt}^T \mathbf{s} \\ &= \mathbf{s}^T \mathbf{R}_{\mathbf{w}}^{-1} \mathbf{s}^* \end{aligned} \quad (2.48)$$

Therefore, the SNRI, from (2.41) and (2.44) is,

$$\text{SNRI} = \frac{\text{OSNR}}{\text{ISNR}} = \frac{|(\mathbf{h}^T \mathbf{s})|^2}{\mathbf{h}^H \mathbf{R}_{\mathbf{w}} \mathbf{h}} \times \frac{\mathbf{s}^H \mathbf{s}}{r_{\mathbf{w}}(0)} \quad (2.49)$$

whereas the SNRI_{opt} is obtained from (2.41) and (2.48),

$$\text{SNRI}_{opt} = \frac{\text{OSNR}_{opt}}{\text{ISNR}} = (\mathbf{s}^T \mathbf{R}_{\mathbf{w}}^{-1} \mathbf{s}^*) \times \frac{\mathbf{s}^H \mathbf{s}}{r_{\mathbf{w}}(0)} \quad (2.50)$$

Since the MAMF is designed to maximize OSNR for a given ISNR, its theoretical performance is characterized by (2.50).

2.4.3 MAMF Practical Performance

As mentioned in the previous section, the OSNR_{opt} in (2.48) and, hence, the SNRI_{opt} in (2.50) were obtained under the assumption that the colored noise autocorrelation was known. Obviously, under practical circumstances this is rarely the case. The colored noise autocorrelation is estimated for every data bit communicated as shown in Sections 2.2.1 and 2.3. Thus, the Toeplitz colored noise autocorrelation matrix formed is $\hat{\mathbf{R}}_{\mathbf{w}}$. Evidently, the MAMF impulse response \mathbf{h} is not optimal and,

$$\mathbf{h} = \hat{\mathbf{R}}_{\mathbf{w}}^{-1} \mathbf{s}^* \quad (2.51)$$

Hence, (2.44) becomes,

$$\begin{aligned} \text{OSNR} &= \frac{|(\mathbf{h}^T \mathbf{s})|^2}{\mathbf{h}^H \mathbf{R}_{\mathbf{w}} \mathbf{h}} \\ &= \frac{|(\mathbf{s}^T \hat{\mathbf{R}}_{\mathbf{w}}^{-1} \mathbf{s}^*)|^2}{(\mathbf{s}^H \hat{\mathbf{R}}_{\mathbf{w}}^{-1} \mathbf{R}_{\mathbf{w}} \hat{\mathbf{R}}_{\mathbf{w}}^{-1} \mathbf{s})} \end{aligned} \quad (2.52)$$

which is very different from OSNR_{opt} in (2.48). Notice, though, that if $\mathbf{R}_{\mathbf{w}} = \hat{\mathbf{R}}_{\mathbf{w}}$, then (2.52) becomes (2.48). Consequently, the SNRI changes accordingly.

The general MAMF receiver system layouts for the traditional and the proposed communication systems are presented in Figures 3 and 4.

2.4.4 Optimal Detector Design

Once the noise corrupted signal has been processed by the MAMF, the ability to make a decision on which signal was most likely transmitted appears quite improved. At this point the design of an optimal detector can be presented whose main responsibility would be to make the aforementioned decision. Many authors have dealt with this particular problem [5,9,10,13,16,18,21-23] but this section presents the discrete-time version of detection of signals suited for use for this work.

Thus the goal of this section is to introduce a theoretically sound detector for use in the MAMF communication system under consideration. A binary type of communication will be used so $L=2$ (Section 2.2.1). Therefore, a receiver must be determined which chooses between hypotheses,

$$\begin{aligned} H_1 &: r_n = s_{1n} + w_n & n = 1, \dots, N \\ H_0 &: r_n = s_{0n} + w_n & n = 1, \dots, N \end{aligned}$$

where r_n is the received or measured element, s_{jn} is the element sent from signal vector $j(=0,1)$, w_n is the noise element which is added to the signal bit and N is the length of the signal vector.

According to the discussion presented in Section 2.1, the following relationship always holds,

$$R_w \mathbf{f}_i = \lambda_i \mathbf{f}_i \quad (2.53)$$

where λ_i are the real non-negative eigenvalues and \mathbf{f}_i are the corresponding orthonormal eigenvectors of the Toeplitz noise autocorrelation matrix R_w . Defining F to be the matrix ($N \times N$) whose columns are the orthonormal eigenvectors \mathbf{f}_i of the noise autocorrelation matrix R_w , then,

$$R_w F = F \Lambda \quad (2.54)$$

where

$$FF^H = F^H F = I \quad (2.55)$$

Hence, an expansion of the received signal vector \mathbf{r} is desirable in terms of a set of orthonormal eigenvectors \mathbf{f}_k with weighting coefficients \tilde{r}_k . With the eigenvectors, or columns of F , as a basis,

$$\mathbf{r} = \sum_{k=1}^N \tilde{r}_k \mathbf{f}_k = F \tilde{\mathbf{r}} \quad (2.56)$$

or,

$$\tilde{\mathbf{r}} = \mathbf{F}^H \mathbf{r} \quad (2.57)$$

$$= \mathbf{F}^H (\mathbf{s}_j + \mathbf{w})$$

$$= \mathbf{F}^H \mathbf{s}_j + \mathbf{F}^H \mathbf{w} \quad (2.58)$$

So when we take the mean under each hypothesis,

$$\mathbf{E}_1\{ \tilde{\mathbf{r}} \} = \mathbf{F}^H \mathbf{s}_1 \triangleq \boldsymbol{\mu}_1$$

$$\mathbf{E}_0\{ \tilde{\mathbf{r}} \} = \mathbf{F}^H \mathbf{s}_0 \triangleq \boldsymbol{\mu}_0$$

or in general,

$$\mathbf{E}_j\{ \tilde{\mathbf{r}} \} = \mathbf{F}^H \mathbf{s}_j \triangleq \boldsymbol{\mu}_j \quad (2.59)$$

where \triangleq denotes 'is defined as'.

By using (2.58), (2.59) and the initial assumptions on the noise presented in Section 2.1, the covariance of the coefficient vector under each hypothesis is,

$$\begin{aligned} \mathbf{E}_j\{(\tilde{\mathbf{r}} - \boldsymbol{\mu}_j)(\tilde{\mathbf{r}} - \boldsymbol{\mu}_j)^H\} &= \mathbf{E}_j\{ \tilde{\mathbf{r}} \tilde{\mathbf{r}}^H - \tilde{\mathbf{r}} \boldsymbol{\mu}_j^H - \boldsymbol{\mu}_j \tilde{\mathbf{r}}^H + \boldsymbol{\mu}_j \boldsymbol{\mu}_j^H \} \\ &= \mathbf{E}_j\{ \tilde{\mathbf{r}} \tilde{\mathbf{r}}^H \} - \mathbf{E}_j\{ \mathbf{F}^H \mathbf{r} \mathbf{s}_j^H \mathbf{F} \} - \mathbf{E}_j\{ \mathbf{F}^H \mathbf{s}_j \mathbf{r}^H \mathbf{F} \} + \mathbf{E}_j\{ \mathbf{F}^H \mathbf{s}_j \mathbf{s}_j^H \mathbf{F} \} \\ &= \mathbf{E}_j\{ \tilde{\mathbf{r}} \tilde{\mathbf{r}}^H \} - \mathbf{E}_j\{ \mathbf{F}^H \mathbf{s}_j \mathbf{s}_j^H \mathbf{F} \} - \mathbf{E}_j\{ \mathbf{F}^H \mathbf{s}_j \mathbf{s}_j^H \mathbf{F} \} + \mathbf{E}_j\{ \mathbf{F}^H \mathbf{s}_j \mathbf{s}_j^H \mathbf{F} \} \\ &= \mathbf{E}_j\{ \tilde{\mathbf{r}} \tilde{\mathbf{r}}^H \} - \mathbf{E}_j\{ \mathbf{F}^H \mathbf{s}_j \mathbf{s}_j^H \mathbf{F} \} \\ &= \mathbf{E}_j\{ \mathbf{F}^H \mathbf{s}_j \mathbf{s}_j^H \mathbf{F} \} + \mathbf{E}_j\{ \mathbf{F}^H \mathbf{w} \mathbf{w}^H \mathbf{F} \} - \mathbf{E}_j\{ \mathbf{F}^H \mathbf{s}_j \mathbf{s}_j^H \mathbf{F} \} \end{aligned}$$

$$\begin{aligned}
&= E_j\{ \mathbf{F}^H \mathbf{w} \mathbf{w}^H \mathbf{F} \} \\
&= \mathbf{F}^H \mathbf{R}_{\mathbf{w}} \mathbf{F}
\end{aligned} \tag{2.60}$$

In addition, from hypothesis testing theory [5],

$$E\{(\tilde{\mathbf{r}} - \boldsymbol{\mu})(\tilde{\mathbf{r}} - \boldsymbol{\mu})^H\} = E_1\{(\tilde{\mathbf{r}} - \boldsymbol{\mu}_1)(\tilde{\mathbf{r}} - \boldsymbol{\mu}_1)^H\} P(H_1) + E_0\{(\tilde{\mathbf{r}} - \boldsymbol{\mu}_0)(\tilde{\mathbf{r}} - \boldsymbol{\mu}_0)^H\} P(H_0)$$

where $P(H_1)$, $P(H_0)$ are the a priori probabilities of H_1 , H_0 being true respectively. Since the variance is the same under each of the disjoint hypotheses, we have

$$E\{(\tilde{\mathbf{r}} - \boldsymbol{\mu})(\tilde{\mathbf{r}} - \boldsymbol{\mu})^H\} = \mathbf{F}^H \mathbf{R}_{\mathbf{w}} \mathbf{F} \tag{2.61}$$

Because of (2.54) and (2.55), (2.61) becomes,

$$\begin{aligned}
E\{(\tilde{\mathbf{r}} - \boldsymbol{\mu})(\tilde{\mathbf{r}} - \boldsymbol{\mu})^H\} &= \mathbf{F}^H \mathbf{F} \boldsymbol{\Lambda} \\
&= \boldsymbol{\Lambda}
\end{aligned} \tag{2.62}$$

Consequently, when (2.54) holds, the coefficients \tilde{r}_k are uncorrelated and their variance is equal to λ_i . Thus it is reasonable to say that the received, or observed, vector \mathbf{r} has been 'whitened' by the transformation $\mathbf{F}^H \mathbf{r}$.

With the above derivation it is now possible to handle the problem of detection of signals in colored Gaussian noise by considering the transformed measurements $\tilde{\mathbf{r}}$. The likelihood ratio will be used to determine the optimum receiver.

The coefficient vector $\tilde{\mathbf{r}}$ results from a linear operation on a Gaussian process. Hence, $\tilde{\mathbf{r}}$ has a Gaussian distribution, and because the coefficients are uncorrelated, they are also independent. Using the mean and the variance of the coefficient vector, as derived in (2.59) and (2.62), the conditional density

functions can be expressed as follows:

$$p_1(\tilde{\mathbf{r}}) = \frac{1}{(2\pi)^{N/2}|\Lambda|} \exp \left\{ -\frac{1}{2} (\tilde{\mathbf{r}} - \boldsymbol{\mu}_1)^H \Lambda^{-1} (\tilde{\mathbf{r}} - \boldsymbol{\mu}_1) \right\} \quad (2.63.a)$$

$$p_0(\tilde{\mathbf{r}}) = \frac{1}{(2\pi)^{N/2}|\Lambda|} \exp \left\{ -\frac{1}{2} (\tilde{\mathbf{r}} - \boldsymbol{\mu}_0)^H \Lambda^{-1} (\tilde{\mathbf{r}} - \boldsymbol{\mu}_0) \right\} \quad (2.63.b)$$

Taking the log-likelihood ratio,

$$\begin{aligned} \ln \rho(\tilde{\mathbf{r}}) &= \frac{p_1(\tilde{\mathbf{r}})}{p_0(\tilde{\mathbf{r}})} \\ &= -\frac{1}{2} (\tilde{\mathbf{r}} - \boldsymbol{\mu}_1)^H \Lambda^{-1} (\tilde{\mathbf{r}} - \boldsymbol{\mu}_1) + \frac{1}{2} (\tilde{\mathbf{r}} - \boldsymbol{\mu}_0)^H \Lambda^{-1} (\tilde{\mathbf{r}} - \boldsymbol{\mu}_0) \\ &\triangleq G_1 - G_0 \end{aligned} \quad (2.64)$$

where

$$G_1 = \frac{1}{2} (\boldsymbol{\mu}_1^H \Lambda^{-1} \tilde{\mathbf{r}} + \tilde{\mathbf{r}}^H \Lambda^{-1} \boldsymbol{\mu}_1 - \boldsymbol{\mu}_1^H \Lambda^{-1} \boldsymbol{\mu}_1) \quad (2.65.a)$$

$$G_0 = -\frac{1}{2} (\boldsymbol{\mu}_0^H \Lambda^{-1} \tilde{\mathbf{r}} + \tilde{\mathbf{r}}^H \Lambda^{-1} \boldsymbol{\mu}_0 - \boldsymbol{\mu}_0^H \Lambda^{-1} \boldsymbol{\mu}_0) \quad (2.65.b)$$

when expanded. Using (2.58) and (2.59), G_1 can be written as,

$$\begin{aligned} G_1 &= \frac{1}{2} (\mathbf{s}_1^H \mathbf{F} \Lambda^{-1} \mathbf{F}^H \mathbf{r} + \mathbf{r}^H \mathbf{F} \Lambda^{-1} \mathbf{F}^H \mathbf{s}_1 - \mathbf{s}_1^H \mathbf{F} \Lambda^{-1} \mathbf{F}^H \mathbf{s}_1) \\ &= \frac{1}{2} (\mathbf{s}_1^H \mathbf{R}_w^{-1} \mathbf{r} + \mathbf{r}^H \mathbf{R}_w^{-1} \mathbf{s}_1 - \mathbf{s}_1^H \mathbf{R}_w^{-1} \mathbf{s}_1) \end{aligned} \quad (2.66)$$

Let us define the following for $j=0,1$,

$$\bar{\mathbf{h}}_j = \mathbf{R}_w^{-1} \mathbf{s}_j \quad (2.67)$$

This equation must not be confused with the optimal impulse response \mathbf{h}_{opt} , of a MAMF as shown in Section 2.4.2. Nevertheless, it will be shown later that a

relation exists between the two. In addition, since $R_w = R_w^H$ then $R_w^{-1} = (R_w^{-1})^H$, as proved in Section 2.1. Thus,

$$\bar{h}_j^H = s_j^H R_w^{-1} \quad (2.68)$$

Using the three last equations,

$$G_1 = \frac{1}{2} (\bar{h}_1^H r + r^H \bar{h}_1 - s_1^H \bar{h}_1) \quad (2.69.a)$$

Similarly,

$$G_0 = \frac{1}{2} (\bar{h}_0^H r + r^H \bar{h}_0 - s_0^H \bar{h}_0) \quad (2.69.b)$$

Therefore, the maximum likelihood decision rule becomes,

$$G \triangleq \ln \rho(\tilde{r}) = G_1 - G_0 \underset{H_0}{\overset{H_1}{>}} \ln \rho_0 \quad (2.70)$$

where ρ_0 is determined by the most suitable criterion for the application at hand. The most desirable detector is the one with maximum probability of detection and minimum probability of error. Under these circumstances the Bayes Criterion can be used. In this criterion, costs are assigned to each type of error to account for difference in importance [5,9]. Next, the average cost or risk is minimized. As a result the test threshold ρ_0 , is defined as

$$\rho_0 \triangleq \frac{P(H_0) (C_{10} - C_{00})}{P(H_1) (C_{01} - C_{11})} \quad (2.71)$$

where $P(H_1)$, $P(H_0)$ are the a priori probabilities of H_1 , H_0 being true respectively. C_{ij} is defined as the cost associated with choosing H_i when actually H_j is true. So, in general,

$$C_{10} - C_{00} > 0 \text{ and } C_{01} - C_{11} > 0$$

Obviously, no cost should be assigned when the correct decision is made so that $C_{00} = C_{11} = 0$. On the other hand, for communication all errors are equally significant and undesirable and thus equal cost is assigned so that $C_{10} = C_{01}$. Thus (2.71) becomes,

$$\rho_0 = \frac{P(H_0)}{P(H_1)} \quad (2.72)$$

In case the probability of transmitting the "0" bit is equal to the probability of transmitting the "1" bit as in $P(H_0) = P(H_1) = \frac{1}{2}$, then $\rho_0 = 1$ and $\ln \rho_0 = 0$. So the decision rule becomes,

$$\ln \rho(\tilde{\mathbf{r}}) = G = G_1 - G_0 \underset{H_0}{\overset{H_1}{>}} 0 \quad (2.73)$$

Now, it is time to determine the relation between the $\bar{\mathbf{h}}_j$ which was defined as the solution to the equation $\mathbf{R}_w \bar{\mathbf{h}}_j = \mathbf{s}_j$ and the MAMF unit pulse response \mathbf{h}_j . It is known that the unit pulse response of the MAMF which maximizes OSNR for a given \mathbf{R}_w and \mathbf{s}_j (Section 2.4.2), is the solution to the equation,

$$\mathbf{R}_w \mathbf{h}_j = [s_{jN} \ s_{j(N-1)} \ \dots \ s_{j1}]^H \quad j = 0, 1 \quad (2.74)$$

when
$$\mathbf{h}_j = [h_{j1} \ h_{j2} \ \dots \ h_{jN}]^T \quad j = 0, 1$$

Since for the detector design presented herein,

$$\mathbf{s}_j = [s_{j1} \ s_{j2} \ \dots \ s_{jN}]^T \quad j = 0, 1$$

then
$$\mathbf{R}_w \mathbf{h}_j = \mathbf{J} \mathbf{s}_j^* \quad (2.75)$$

where \mathbf{J} has been defined as the $N \times N$ exchange matrix and repeated here,

$$\mathbf{J} = \begin{bmatrix} \mathbf{0} & & & 1 \\ & & \ddots & \\ & 1 & & \\ 1 & & & \mathbf{0} \end{bmatrix}$$

From (2.75), using $\mathbf{J}\mathbf{J} = \mathbf{I}$,

$$\mathbf{R}_{\mathbf{w}}^* \mathbf{h}_j^* = \mathbf{J} \mathbf{s}_j \Rightarrow \mathbf{J} \mathbf{R}_{\mathbf{w}}^* \mathbf{J} \mathbf{J} \mathbf{h}_j^* = \mathbf{J} \mathbf{J} \mathbf{s}_j \quad (2.76)$$

Since $\mathbf{J} \mathbf{R}_{\mathbf{w}}^* \mathbf{J} = (\mathbf{R}_{\mathbf{w}}^*)^T$, (2.76) becomes

$$\mathbf{R}_{\mathbf{w}} \mathbf{J} \mathbf{h}_j^* = \mathbf{s}_j \quad (2.77)$$

and thus, when comparing with (2.67), we have the relation

$$\bar{\mathbf{h}}_j = \mathbf{J} \mathbf{h}_j^* \quad (2.78)$$

which means that the $\bar{\mathbf{h}}_j$ defined in (2.67) is the reverse and complex conjugate of the unit pulse response of the MAMF associated with the signal vector \mathbf{s}_j . Now (2.69) can be manipulated further by considering the MAMF output equation given in (2.39),

$$\bar{\mathbf{h}}_j^H \mathbf{s}_j = \sum_{k=1}^N \mathbf{s}_{jk} \mathbf{h}_{\mathbf{i}(N+1-k)} \triangleq \text{MAMF output @ } N \text{ due to } \mathbf{s}_j$$

Since $\bar{\mathbf{h}}_j^H \mathbf{s}_j = \mathbf{s}_j^H \bar{\mathbf{h}}_j$, (2.69.a) becomes,

$$\begin{aligned} G_1 &= \frac{1}{2} (\bar{\mathbf{h}}_1^H \mathbf{r} - \frac{1}{2} \bar{\mathbf{h}}_1^H \mathbf{s}_1 + \mathbf{r}^H \bar{\mathbf{h}}_1 - \frac{1}{2} \mathbf{s}_1^H \bar{\mathbf{h}}_1) \\ &= \frac{1}{2} \{ \bar{\mathbf{h}}_1^H (\mathbf{r} - \frac{1}{2} \mathbf{s}_1) + (\mathbf{r} - \frac{1}{2} \mathbf{s}_1)^H \bar{\mathbf{h}}_1 \} \end{aligned}$$

$$= \text{Re}\{ \bar{\mathbf{h}}_1^H (\mathbf{r} - \frac{1}{2} \mathbf{s}_1) \} \quad (2.79.a)$$

which is the real part of the MAMF output @ N due to $(\mathbf{r} - \frac{1}{2} \mathbf{s}_1)$. Similarly,

$$G_0 = \text{Re}\{ \bar{\mathbf{h}}_0^H (\mathbf{r} - \frac{1}{2} \mathbf{s}_0) \} \quad (2.79.b)$$

The decision rule is to choose H_1 whenever $G \geq 0$.

2.4.5 Optimal Detector Performance

An error is made when H_1 is true and $G < 0$, as well as when H_0 is true and $G \geq 0$. In order to determine the probability of these errors and therefore the receiver performance, the density function of G must be determined. Since G results from a linear operation on a Gaussian process \mathbf{r} , it is itself Gaussian. From (2.73) and (2.79), G under H_1 becomes,

$$\begin{aligned} G^{(H_1)} &= \frac{1}{2} \text{Re}\{ \bar{\mathbf{h}}_1^H \mathbf{s}_1 + 2 \bar{\mathbf{h}}_1^H \mathbf{w} - 2 \bar{\mathbf{h}}_0^H \mathbf{s}_1 + \bar{\mathbf{h}}_0^H \mathbf{s}_0 - 2 \bar{\mathbf{h}}_0^H \mathbf{w} \} \\ &= \frac{1}{2} \text{Re}\{ \bar{\mathbf{h}}_1^H \mathbf{s}_1 \} - \frac{1}{2} \text{Re}\{ \bar{\mathbf{h}}_0^H (2 \mathbf{s}_1 - \mathbf{s}_0) \} + \text{Re}\{ (\bar{\mathbf{h}}_1 - \bar{\mathbf{h}}_0)^H \mathbf{w} \} \end{aligned} \quad (2.80.a)$$

Similarly,

$$G^{(H_0)} = -\frac{1}{2} \text{Re}\{ \bar{\mathbf{h}}_0^H \mathbf{s}_0 \} + \frac{1}{2} \text{Re}\{ \bar{\mathbf{h}}_1^H (2 \mathbf{s}_0 - \mathbf{s}_1) \} + \text{Re}\{ (\bar{\mathbf{h}}_1 - \bar{\mathbf{h}}_0)^H \mathbf{w} \} \quad (2.80.b)$$

Thus, the means of G under each hypothesis are,

$$E_1\{G\} = \frac{1}{2} \text{Re}\{ \bar{\mathbf{h}}_1^H \mathbf{s}_1 \} - \frac{1}{2} \text{Re}\{ \bar{\mathbf{h}}_0^H (2 \mathbf{s}_1 - \mathbf{s}_0) \} \quad (2.81.a)$$

$$E_0\{G\} = -\frac{1}{2} \text{Re}\{ \bar{\mathbf{h}}_0^H \mathbf{s}_0 \} + \frac{1}{2} \text{Re}\{ \bar{\mathbf{h}}_1^H (2 \mathbf{s}_0 - \mathbf{s}_1) \} \quad (2.81.b)$$

From a theoretical point of view, (2.67) can be used to replace $\bar{\mathbf{h}}_i$ in the above equations in order to reach a more convenient expression for the means. It is

obvious that from a computational point of view this is undesirable since $\bar{\mathbf{h}}_i$ is computed by the Levinson algorithm (Appendix B) and can be incorporated directly into the above equations to yield the means. Substituting (2.67), into (2.81.a) and (2.81.b), yields

$$E_1\{G\} = \frac{1}{2} \text{Re}\{ (\mathbf{s}_1 - \mathbf{s}_0)^H \mathbf{R}_w^{-1} (\mathbf{s}_1 - \mathbf{s}_0) \} \quad (2.82.a)$$

$$E_0\{G\} = -\frac{1}{2} \text{Re}\{ (\mathbf{s}_1 - \mathbf{s}_0)^H \mathbf{R}_w^{-1} (\mathbf{s}_1 - \mathbf{s}_0) \} \quad (2.82.b)$$

and if the following definition is made,

$$\sigma_G^2 \triangleq \text{Re}\{ (\mathbf{s}_1 - \mathbf{s}_0)^H \mathbf{R}_w^{-1} (\mathbf{s}_1 - \mathbf{s}_0) \} \quad (2.83)$$

then

$$E_1\{G\} = -E_0\{G\} = \frac{\sigma_G^2}{2} \quad (2.84)$$

From (2.80), and (2.81) we see that,

$$\begin{aligned} G^{(H_1)} - E_1\{G\} &= G^{(H_0)} - E_0\{G\} \\ &= \text{Re}\{(\bar{\mathbf{h}}_1 - \bar{\mathbf{h}}_0)^H \mathbf{w}\} \end{aligned} \quad (2.85)$$

Therefore, the variance of G is the same under each hypothesis and equals,

$$\begin{aligned} V\{G\} &= E\{|G - E_1\{G\}|^2\} \\ &= \frac{1}{4} E\left\{ \left((\bar{\mathbf{h}}_1 - \bar{\mathbf{h}}_0)^H \mathbf{w} + \mathbf{w}^H (\bar{\mathbf{h}}_1 - \bar{\mathbf{h}}_0) \right) \left((\bar{\mathbf{h}}_1 - \bar{\mathbf{h}}_0)^H \mathbf{w} + \mathbf{w}^H (\bar{\mathbf{h}}_1 - \bar{\mathbf{h}}_0) \right)^* \right\} \\ &= \frac{1}{4} E\left\{ (\bar{\mathbf{h}}_1 - \bar{\mathbf{h}}_0)^H \mathbf{w} (\bar{\mathbf{h}}_1 - \bar{\mathbf{h}}_0)^T \mathbf{w}^* + \mathbf{w}^H (\bar{\mathbf{h}}_1 - \bar{\mathbf{h}}_0) \mathbf{w}^T (\bar{\mathbf{h}}_1 - \bar{\mathbf{h}}_0)^* \right. \\ &\quad \left. + \mathbf{w}^H (\bar{\mathbf{h}}_1 - \bar{\mathbf{h}}_0) (\bar{\mathbf{h}}_1 - \bar{\mathbf{h}}_0)^T \mathbf{w}^* + (\bar{\mathbf{h}}_1 - \bar{\mathbf{h}}_0)^H \mathbf{w} \mathbf{w}^T (\bar{\mathbf{h}}_1 - \bar{\mathbf{h}}_0)^* \right\} \end{aligned}$$

Now since $(\bar{\mathbf{h}}_1 - \bar{\mathbf{h}}_0)^H \mathbf{w} = \mathbf{w}^T (\bar{\mathbf{h}}_1 - \bar{\mathbf{h}}_0)^*$, and according to (2.83),

$$\begin{aligned}
V\{G\} &= \frac{1}{4} \left\{ (\bar{\mathbf{h}}_1 - \bar{\mathbf{h}}_0)^H \mathbf{R}_{\mathbf{w}} (\bar{\mathbf{h}}_1 - \bar{\mathbf{h}}_0) + (\bar{\mathbf{h}}_1 - \bar{\mathbf{h}}_0)^T \mathbf{R}_{\mathbf{w}}^* (\bar{\mathbf{h}}_1 - \bar{\mathbf{h}}_0)^* \right. \\
&\quad \left. + (\bar{\mathbf{h}}_1 - \bar{\mathbf{h}}_0)^H \mathbf{E}\{\mathbf{w} \mathbf{w}^T\} (\bar{\mathbf{h}}_1 - \bar{\mathbf{h}}_0)^* + (\bar{\mathbf{h}}_1 - \bar{\mathbf{h}}_0)^T \mathbf{E}\{\mathbf{w}^* \mathbf{w}^H\} (\bar{\mathbf{h}}_1 - \bar{\mathbf{h}}_0) \right\} \\
&= \frac{1}{2} \text{Re}\{(\bar{\mathbf{h}}_1 - \bar{\mathbf{h}}_0)^H \mathbf{R}_{\mathbf{w}} (\bar{\mathbf{h}}_1 - \bar{\mathbf{h}}_0)\} + \frac{1}{2} \text{Re}\{(\bar{\mathbf{h}}_1 - \bar{\mathbf{h}}_0)^H \mathbf{E}\{\mathbf{w} \mathbf{w}^T\} (\bar{\mathbf{h}}_1 - \bar{\mathbf{h}}_0)^*\} \\
&= \frac{\sigma_G^2}{2} + \frac{1}{2} \text{Re}\{(\bar{\mathbf{h}}_1 - \bar{\mathbf{h}}_0)^H \mathbf{E}\{\mathbf{w} \mathbf{w}^T\} (\bar{\mathbf{h}}_1 - \bar{\mathbf{h}}_0)^*\} \quad (\text{complex case}) \\
&= \frac{\sigma_G^2}{2} + \frac{\sigma_G^2}{2} \\
&= \sigma_G^2 \quad (\text{real case}) \quad \square
\end{aligned}$$

Consider $V\{G\} \triangleq \eta^2$ as the variance of G for any case, complex or real. Thus, if the data is real $\eta^2 = \sigma_G^2$. Then, the probability density functions of G are (Figure 5),

$$P_1(G) = \frac{1}{(2\pi\eta^2)^{1/2}} \exp\left\{\frac{(G - \frac{1}{2}\sigma_G^2)^2}{-2\eta^2}\right\} \quad (2.86.a)$$

$$P_0(G) = \frac{1}{(2\pi\eta^2)^{1/2}} \exp\left\{\frac{(G + \frac{1}{2}\sigma_G^2)^2}{-2\eta^2}\right\} \quad (2.86.b)$$

Finally, the probability of error, denoted as P_e [5], is

$$P_e = P(D_1 | H_0)P(H_0) + P(D_0 | H_1)P(H_1) \quad (2.87)$$

where $P(D_i | H_j)$ represents the probability of choosing H_i when actually H_j is true. Thus, for equal a priori probabilities [5] where $\rho_0 = 1$ as seen in (2.72),

$$P_e = P(D_0 | H_1) = P(D_1 | H_0) \quad (2.88)$$

Therefore,

$$P_e = \int_0^\infty P_0(G) dG = \int_R^\infty \frac{1}{(2\pi)^{1/2}} e^{-z^2/2} dz \quad (2.89)$$

where $R = \frac{\eta}{2}$ (Figure 5).

The error probability in (2.89) decreases as η increases. Therefore in order to obtain the best performance η must be maximized for a given set of signal vectors $\mathbf{s}_1, \mathbf{s}_0$ with the following constraint on the signal energy,

$$\mathbf{s}_1^H \mathbf{s}_1 + \mathbf{s}_0^H \mathbf{s}_0 = 2E_s$$

where E_s is the transmitted signal energy. So for the purposes of this application the following must be maximized:

$$Q \triangleq \eta^2 - 2\mu E_s \quad (2.90)$$

Due to the irregularities presented by the variance of G η^2 , when it assumes complex values, only the real data case is considered where $\sigma_G^2 = \eta^2$. Thus (2.90) becomes,

$$Q \triangleq \sigma_G^2 - 2\mu E_s \quad (2.91)$$

where μ is an undetermined Lagrange multiplier. Thus Q is given by

$$Q \triangleq (\mathbf{s}_1 - \mathbf{s}_0)^T \mathbf{R}_w^{-1} (\mathbf{s}_1 - \mathbf{s}_0) - \mu(\mathbf{s}_1^H \mathbf{s}_1 + \mathbf{s}_0^H \mathbf{s}_0) \quad (2.92)$$

Let $\bar{\mathbf{s}}_1$ and $\bar{\mathbf{s}}_0$ represent the optimum signal vectors for \mathbf{s}_1 and \mathbf{s}_0 respectively. Then, let

$$\mathbf{s}_1 = \bar{\mathbf{s}}_1 + \alpha_1 \beta_1 \text{ and } \mathbf{s}_0 = \bar{\mathbf{s}}_0 + \alpha_0 \beta_0 \quad (2.93)$$

where α_1 and α_0 are arbitrary multipliers and β_1 and β_0 are arbitrary vectors. First maximize (2.92) for \mathbf{s}_1 holding \mathbf{s}_0 fixed and next maximize for \mathbf{s}_0 holding \mathbf{s}_1 fixed. Therefore, the two resulting equations are,

$$\left. \frac{\partial Q(\alpha_1)}{\partial \alpha_1} \right|_{\alpha_1=0} = 0 \text{ and } \left. \frac{\partial Q(\alpha_0)}{\partial \alpha_0} \right|_{\alpha_0=0} = 0$$

These lead to the following simultaneous equations,

$$\mathbf{R}_w^{-1}(\bar{\mathbf{s}}_1 - \mathbf{s}_0) = \mu \bar{\mathbf{s}}_1 \quad (2.94.a)$$

$$\mathbf{R}_w^{-1}(\mathbf{s}_1 - \bar{\mathbf{s}}_0) = -\mu \bar{\mathbf{s}}_0 \quad (2.94.b)$$

Since (2.94.a) was obtained with $\alpha_1 = 0$ and (2.94.b) with $\alpha_0 = 0$ then,

$$\mathbf{R}_w^{-1}(\mathbf{s}_1 - \mathbf{s}_0) = \mu \mathbf{s}_1 \quad (2.95.a)$$

$$\mathbf{R}_w^{-1}(\mathbf{s}_1 - \mathbf{s}_0) = -\mu \mathbf{s}_0 \quad (2.95.b)$$

From these equations it follows that the signal vectors satisfy the following restriction:

$$\mathbf{s}_1 = -\mathbf{s}_0 \quad (2.96)$$

which with $\alpha_1 = 0$ and $\alpha_0 = 0$ in (2.93) implies

$$\bar{\mathbf{s}}_1 = -\bar{\mathbf{s}}_0 \quad (2.97)$$

Substituting (2.96) into (2.95),

$$\mathbf{R}_w^{-1} \mathbf{s}_1 = \frac{\mu}{2} \mathbf{s}_1 \Rightarrow \mathbf{R}_w \mathbf{s}_1 = \frac{2}{\mu} \mathbf{s}_1 \quad (2.98)$$

Comparing this equation with (2.54) points out that the optimum signal vector \mathbf{s}_1 is the eigenvector of \mathbf{R}_w corresponding to the eigenvalue $\frac{2}{\mu}$. From Section 2.1, as $\mathbf{R}_w \geq 0$, then $\lambda \geq 0$, and thus $\mu \geq 0$. Applying (2.96) and (2.98) to (2.92) yields,

$$Q = 0 \Rightarrow \sigma_G^2 = 2\mu E_s$$

Therefore,

$$\sigma_G^2 = \frac{4E_s}{\lambda} \quad (2.99)$$

In order to maximize σ_G^2 , the eigenvalue λ must be the smallest eigenvalue of \mathbf{R}_w according to (2.54). Therefore, by choosing for \mathbf{s}_1 the eigenvector associated with the smallest eigenvalue λ , a maximum σ_G^2 and thus a minimum probability of error P_e , are ensured.

One might find the fact that minimum probability of error P_e , is the result of maximizing the variance of G σ_G^2 , hard to comprehend. Let us consider Figure 5, (2.84), and (2.86). A variance σ_G^2 of 9 results in Gaussian probability density functions of narrow width and close proximity (Figure 5A). When the variance σ_G^2 is set to 49, the width of the probability density functions increases and their relative proximity decreases (Figure 5B). However, $P_0(G)$ and $P_1(G)$ overlap less. From (2.84), the means of $P_0(G)$ and $P_1(G)$ are proportional to the variance. Hence, an increase in the variance of G will also increase the distance between the two density functions. In signal detection, the area of interest is the overlap area of the two density functions which identifies the P_e , as seen from Figure 5A and described by (2.89). The smallest overlap area of the two probability density functions results from a high variance which increases the distance between the two density functions in a faster rate than their width.

Up to this point many authors have completed work towards designing a

signal vector which maximizes the OSNR of the MAMF receiver system for a particular noise color [4,5,24]. The result presented in their work coincides with the result of the approach just presented, where the detector was placed as the primary stage of the receiver. The optimal signal vector was thus designed with the goal to minimize the probability of error P_e of the detector, whereas previous authors [4,24] designed the optimal signal vector by setting as a goal to maximize the OSNR of the whole receiver system. It is evident, then, that maximizing the OSNR - and hence the SNRI - and minimizing the P_e are equivalent concepts.

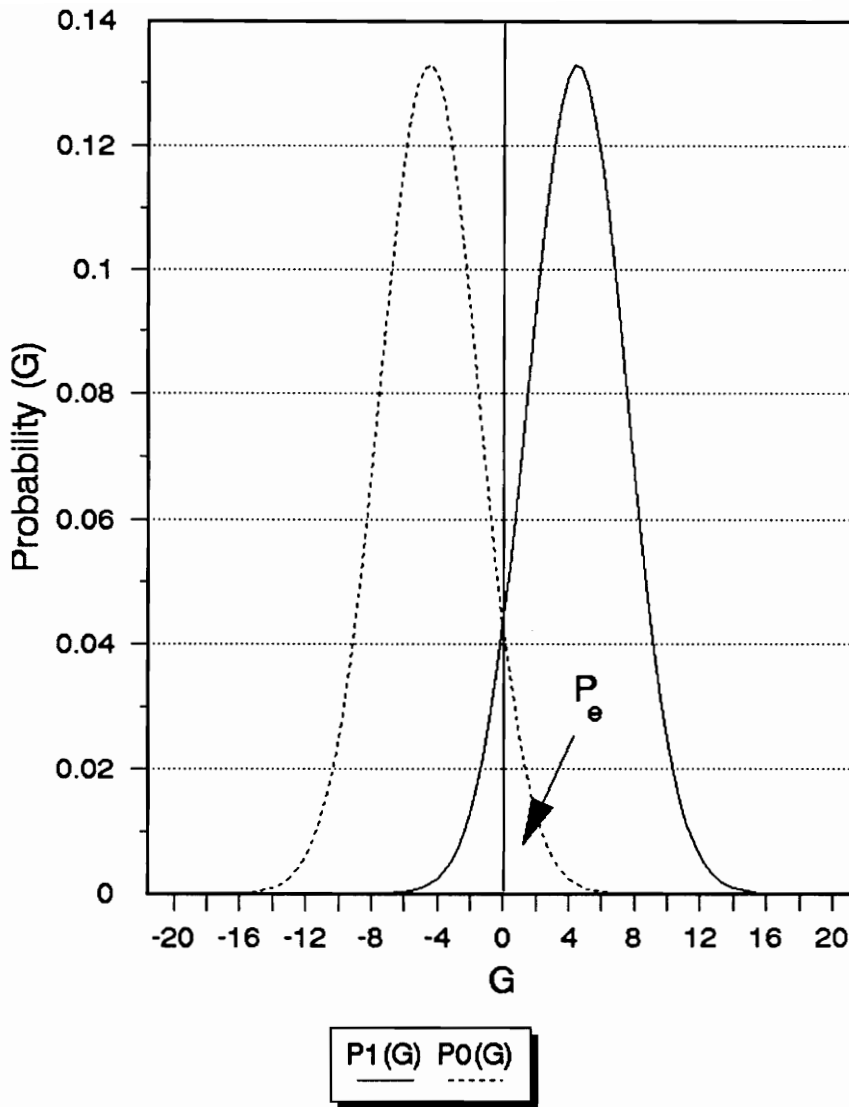


FIGURE 5A. CONDITIONAL PROBABILITY DENSITY FUNCTIONS &
DICHOTOMY OF SAMPLE SPACE [5]
 $\sigma_G^2 = 9$

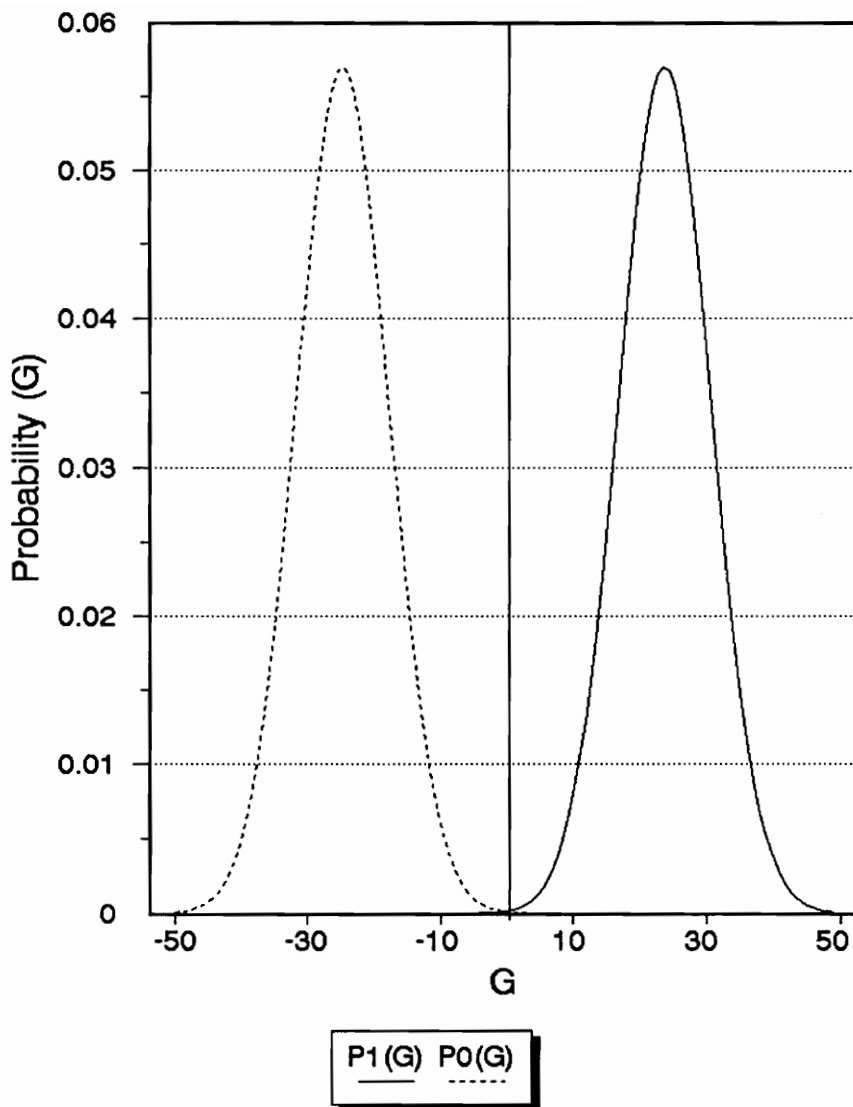


FIGURE 5B. CONDITIONAL PROBABILITY DENSITY FUNCTIONS & DICHOTOMY OF SAMPLE SPACE [5]
 $\sigma_G^2 = 49$

3.0 SIMULATION

This chapter presents the steps taken in order to fully simulate the behavior of both the traditional and the proposed MAMF communication systems. The simulation will be used as a tool for the detailed examination of both systems in terms of performance. It will also provide the flexibility to change with ease the conditions under which each communication system is examined, i.e. noise characteristics, method of transmission, duration of transmission, etc. The goal of an accurate and efficient simulation is to present a complete study that accounts for most, if not all, of the possible outcomes of the particular problem in question.

Specifically, the colored noise generation procedure is presented followed by the system descriptions of both MAMF communication systems. A **binary** communication system was chosen to be examined with **real** data.

3.1 COLORED NOISE GENERATION

The colored noise used in the simulations is generated by taking a Gaussian white noise process with zero mean and unity variance, and processing it with an Auto-Regressive (AR) digital filter of order 2 as seen in Figure 6. Hence, the coloring filter is an AR(2) filter with the following transfer function:

$$\begin{aligned}
 H(z) &= \frac{b_0 z^2}{(z - z_1)(z - z_2)} \\
 &= \frac{b_0}{1 - 2\rho \cos(\theta)z^{-1} + \rho^2 z^{-2}} \\
 &= \frac{b_0}{1 + a_1 z^{-1} + a_2 z^{-2}} \tag{3.1}
 \end{aligned}$$

where b_0 is defined such that the peak magnitude response is normalized to 1. Thus $b_0 = (1-\rho) |e^{j\theta} - \rho e^{-j\theta}|$. The transfer function $H(z)$ has two dominant poles at $z = \rho e^{\pm j\theta}$, and two non-contributing zeros at $z = 0$ (Figure 6). The variable ρ represents the distance of the complex conjugate poles from the origin of the unit circle and controls the bandwidth of the colored noise. For instance, when $\rho = 0.95$ the noise is narrowband, whereas when $\rho = 0.7$ the noise is more broadband (Figure 7). The angle θ determines where the narrowband noise is centered. Figure 7A presents the magnitude response of the coloring filter for $\rho = 0.95$ and $\theta = 60^\circ$ whereas Figure 7B presents the coloring filter magnitude response for $\rho = 0.7$ and $\theta = 60^\circ$.

The first points exiting the noise coloring filter are discarded to prevent transient effects from influencing the noise samples and hence the autocorrelation estimates. The *memory depth* of the specific filter is the range of points set from the first point exiting the filter to the point at which the impulse response reaches 1% of its maximum value. The memory depth of the filter described by

(3.1) depends on ρ and θ , and the maximum memory depth was found to be 220 points. If a second signal is transmitted, again the next 220 points are discarded so as to guarantee the stationarity of the noise and the independence of the subsequent noise vectors. Hence, for each data bit transmission the first 220 noise points are discarded, the next N points are used for the autocorrelation estimator as the vector \mathbf{w}_g , and the last N noise points are used as the noise vector \mathbf{w} , which corrupts the transmitted signal \mathbf{s}_j of dimension N .

In order to study the effects of estimating the colored noise autocorrelation sequence, the same experiments must be conducted with the actual autocorrelation sequence. The actual autocorrelation can be computed by using the method presented by Dugre, Beex, and Scharf [12].

The output of that algorithm consists of the first 3 points of the actual autocorrelation sequence \mathbf{r}_w , due to the 3 AR coefficients of the coloring filter. Since \mathbf{r}_w must be of the same dimension as the signal vectors, namely N , linear prediction is used to calculate the remaining points in the sequence. According to [12], the unit-pulse sequence corresponding to $H(z)$ is,

$$h_k = \begin{cases} 0, & k < 0 \\ b_k - \sum_{n=1}^R a_n h_{k-n}, & k \geq 0 \end{cases} \quad (3.2)$$

where R is the AR order of $H(z)$, namely 2. Obviously, b_k is assumed to be zero for $k \geq 1$. The autocorrelation sequence $\mathbf{r}_w(k)$ is related to the unit-pulse sequence h_n as follows:

$$\mathbf{r}_w(k) = \sum_{n=0}^{\infty} h_n h_{n+k} = \mathbf{r}_w(-k), \quad k \geq 0 \quad (3.3)$$

By substituting (3.2) into (3.3),

$$\sum_{n=1}^R a_n \mathbf{r}_w(k-n) = d_k, \quad k \geq 0 \quad (3.4)$$

where,

$$d_k = \sum_{n=0}^{Q-k} h_n b_{n+k} \quad (3.5)$$

where Q is the MA order of $H(z)$, namely 0. Thus, $d_k = 0$ for $k \geq 1$, in which case the autocorrelation sequence $r_w(k)$ satisfies a linear homogeneous difference equation. From (3.4) and (3.5) the remaining points of $r_w(k)$ can be found.

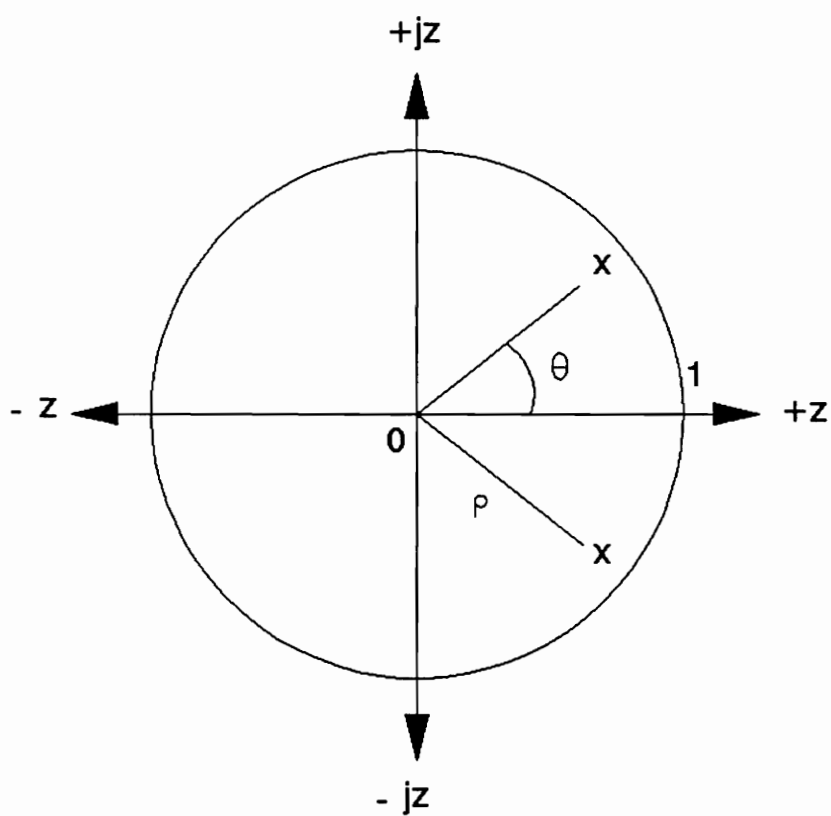
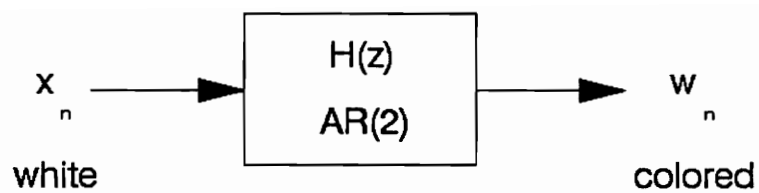


FIGURE 6. COLORED NOISE AR(2) FILTER CHARACTERISTICS [4]

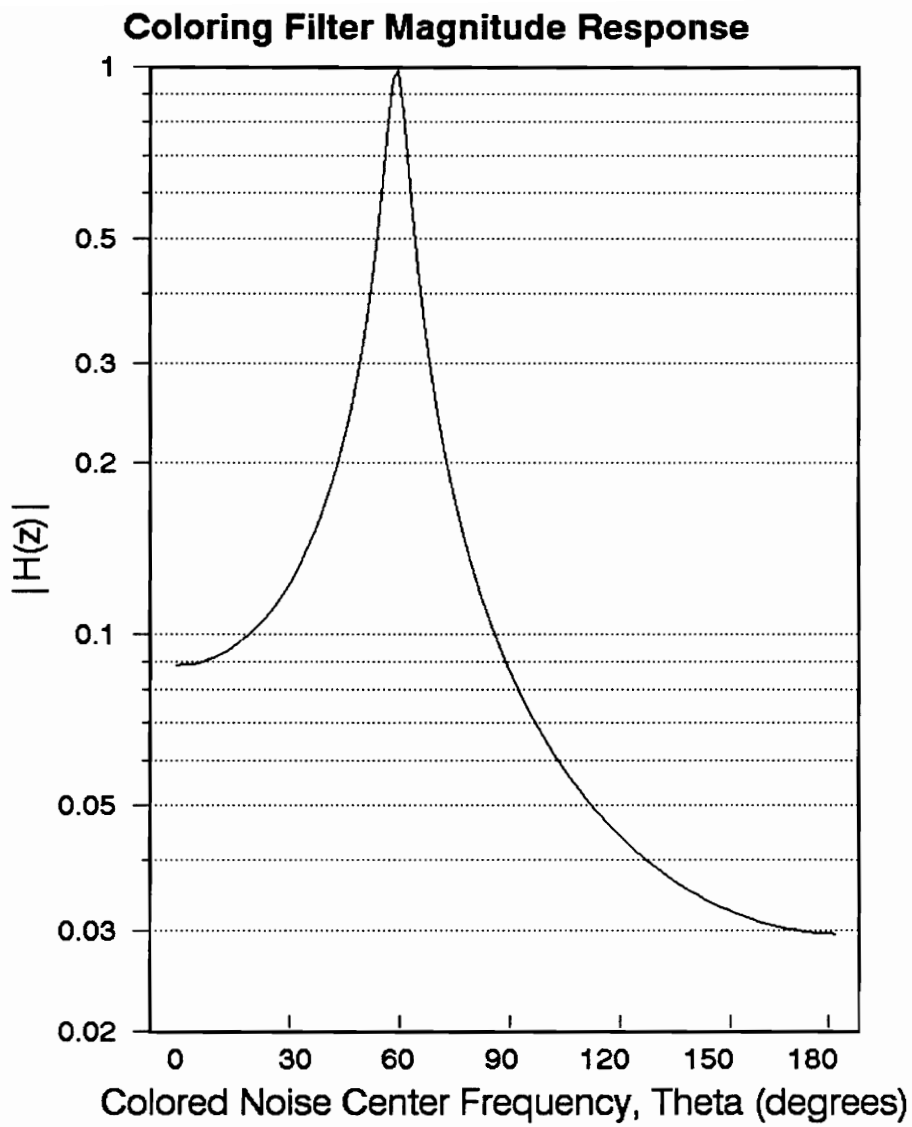


FIGURE 7A. COLORED NOISE AR(2) FILTER MAGNITUDE RESPONSE
 $\rho = 0.95$ AND $\theta = 60^\circ$

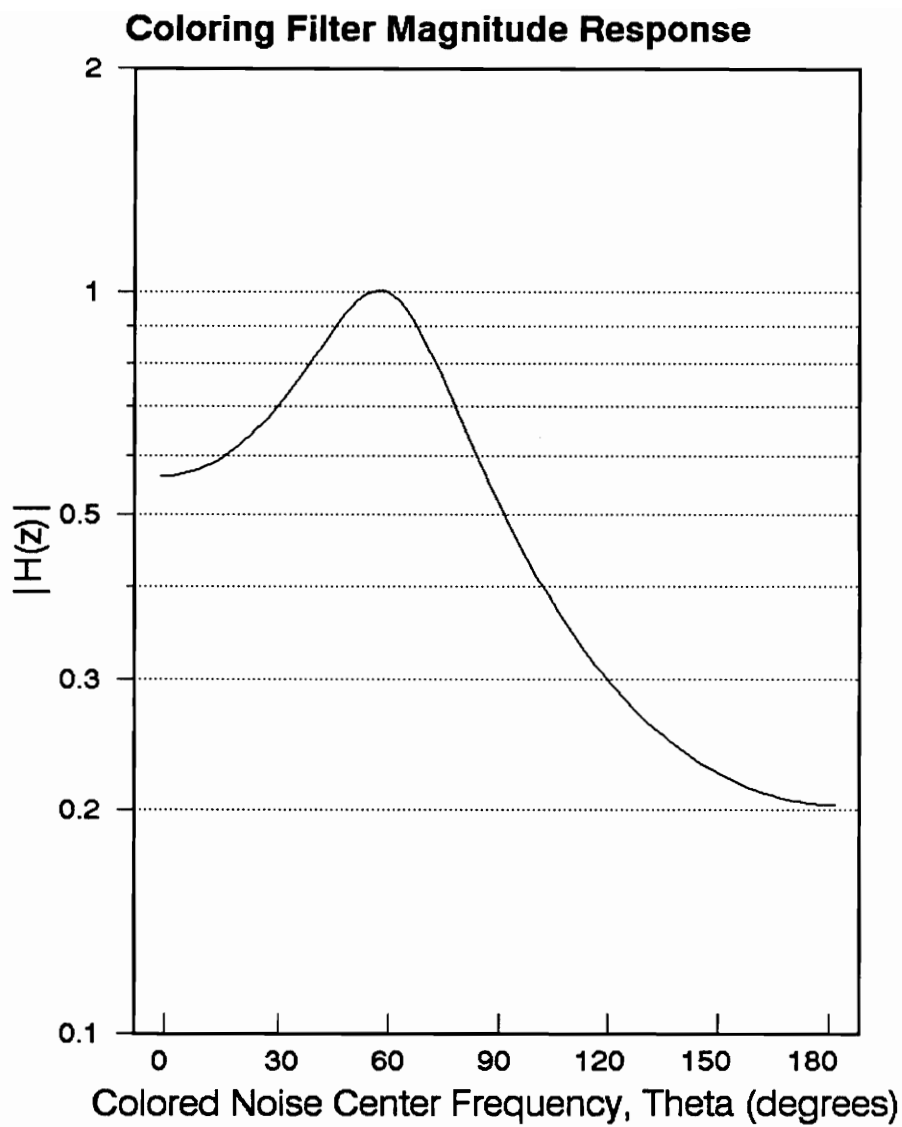


FIGURE 7B. COLORED NOISE AR(2) FILTER MAGNITUDE RESPONSE
 $\rho = 0.7$ AND $\theta = 60^\circ$

3.2 SYSTEM DESCRIPTIONS

3.2.1 Proposed System Description

Since a binary system of communication was chosen for the simulation then, by referring to Section 2.2, it is evident that $L = 2$. Hence, the signal matrix that encodes the data bit to be communicated is:

$$\mathbf{S}_j = [\mathbf{s}_{j1} \ \mathbf{s}_{j2} \ \dots \ \mathbf{s}_{jK}] \quad j = 0, 1 \quad (3.6)$$

where \mathbf{S}_0 is the signal matrix which represents the "0" and \mathbf{S}_1 is the signal matrix which represents the "1" (Figure 2). As discussed in Section 2.2.1, the minimum number of linearly independent basis vectors required to span a subspace is 2. Hence, $K = 2$. Furthermore, the signal vector subspaces defined by \mathbf{S}_j must not overlap so as to have minimum probability of error [4]. Thus, one set of basis vectors must be orthogonal to the other set of basis vectors. In order to ensure 2 orthogonal subspaces, a minimum length of $M = 2 \times 2 = 4$ is required for every basis vector [25]. Then (3.6) becomes,

$$\mathbf{S}_j = [\mathbf{s}_{j1} \ \mathbf{s}_{j2}] \quad j = 0, 1 \quad (3.7)$$

where

$$\mathbf{s}_{ji} = [s_{ji1} \ s_{ji2} \ s_{ji3} \ s_{ji4}]^T \quad \text{for } \begin{cases} j = 0, 1 \\ i = 1, 2 \end{cases} \quad (3.8)$$

The method of transmission chosen is the concatenated vector assignment. Thus the transmitted signal vector is of dimension $N = 8 (= K \times M)$ and is:

$$\mathbf{s}_j = [s_{j11} \ s_{j12} \ s_{j13} \ s_{j14} \ s_{j21} \ s_{j22} \ s_{j23} \ s_{j24}]^T \quad j = 0, 1 \quad (3.9)$$

Similarly, the colored noise matrix \mathbf{W} , is of the following format:

$$\mathbf{W} = [\mathbf{w}_1 \ \mathbf{w}_2] \quad (3.10)$$

where

$$\mathbf{w}_i = [w_{i1} \ w_{i2} \ w_{i3} \ w_{i4}]^T \quad i = 1, 2 \quad (3.11)$$

Following again the concatenated vector assignment, the colored noise vector \mathbf{w} that corrupts the transmitted signal is,

$$\mathbf{w} = [w_{11} \ w_{12} \ w_{13} \ w_{14} \ w_{21} \ w_{22} \ w_{23} \ w_{24}]^T \quad (3.12)$$

resulting in the received 8-dimensional vector \mathbf{r}_P ,

$$\mathbf{r}_P = [\mathbf{s}_j + \mathbf{w}] \quad j = 0, 1 \quad (3.13)$$

In addition, the autocorrelation sequence is of length $N = 8$, thus at least $N = 8$ noise samples are required from the gaps between transmissions. Therefore, the finite length sequence actually entering the proposed MAMF communication receiver (Figure 2), is the 16-dimensional vector \mathbf{r}_a :

$$\mathbf{r}_a = [\mathbf{w}_g^T \mid \mathbf{r}_P^T]^T \quad (3.14)$$

For the concatenated vector assignment, the 8×8 noise autocorrelation matrix \mathbf{R}_w is given by,

$$\mathbf{R}_w = \begin{bmatrix} \mathbf{R}_{w_1 w_1} & | & \mathbf{R}_{w_1 w_2} \\ - & - & - \\ \mathbf{R}_{w_2 w_1} & | & \mathbf{R}_{w_2 w_2} \end{bmatrix}$$

$$= \left[\begin{array}{cccc|cccc} r_w(0) & r_w(1) & r_w(2) & r_w(3) & r_w(4) & r_w(5) & r_w(6) & r_w(7) \\ r_w(-1) & r_w(0) & r_w(1) & r_w(2) & r_w(3) & r_w(4) & r_w(5) & r_w(6) \\ r_w(-2) & r_w(-1) & r_w(0) & r_w(1) & r_w(2) & r_w(3) & r_w(4) & r_w(5) \\ r_w(-3) & r_w(-2) & r_w(-1) & r_w(0) & r_w(1) & r_w(2) & r_w(3) & r_w(4) \\ \hline r_w(-4) & r_w(-3) & r_w(-2) & r_w(-1) & r_w(0) & r_w(1) & r_w(2) & r_w(3) \\ r_w(-5) & r_w(-4) & r_w(-3) & r_w(-2) & r_w(-1) & r_w(0) & r_w(1) & r_w(2) \\ r_w(-6) & r_w(-5) & r_w(-4) & r_w(-3) & r_w(-2) & r_w(-1) & r_w(0) & r_w(1) \\ r_w(-7) & r_w(-6) & r_w(-5) & r_w(-4) & r_w(-3) & r_w(-2) & r_w(-1) & r_w(0) \end{array} \right] \quad (3.15)$$

as discussed in Section 2.2.4.

The linearly independent basis vectors in (3.7) can be linearly combined to create any vector in the subspace spanned by them. Since $K = 2$, only two coefficients are required to linearly combine the basis vectors for each j . Thus, if \mathbf{c}_j is the coefficient vector associated with the j -th signal basis vector set,

$$\mathbf{c}_j = [c_{j1} \ c_{j2}]^T \quad j = 0, 1 \quad (3.16)$$

the linear combination of the linearly independent basis vectors (3.7) is:

$$\begin{aligned} \tilde{\mathbf{s}}_j &= \mathbf{S}_j \mathbf{c}_j \\ &= [\mathbf{s}_{j1} \ \mathbf{s}_{j2}] \mathbf{c}_j \\ &= c_{j1} \mathbf{s}_{j1} + c_{j2} \mathbf{s}_{j2} \quad j = 0, 1 \end{aligned} \quad (3.17)$$

Similarly, from (2.24), and the noise vectors represented by (3.10), the linearly combined noise vector $\tilde{\mathbf{w}}_j$ is,

$$\begin{aligned}
\tilde{\mathbf{w}}_j &= \mathbf{W} \mathbf{c}_j \\
&= [\mathbf{w}_1 \ \mathbf{w}_2] \mathbf{c}_j \\
&= c_{j1} \mathbf{w}_1 + c_{j2} \mathbf{w}_2 \quad j = 0, 1
\end{aligned} \tag{3.18}$$

Notice that $\tilde{\mathbf{s}}_j$ and $\tilde{\mathbf{w}}_j$ are 4-dimensional vectors. Then from (2.23), the signal energy of the transmitted signal is 2 and the following restrictions hold,

$$\begin{aligned}
c_{01}^2 + c_{02}^2 &= 2 \\
c_{11}^2 + c_{12}^2 &= 2
\end{aligned} \tag{3.19}$$

which denote that the points (c_{01}, c_{02}) and (c_{11}, c_{12}) satisfy the equations of a circle, with radius $\sqrt{2}$ in the c_1 - c_2 plane. Keep in mind that the coefficients c_{ji} are computed in such a way so as to maximize the OSNR.

After the combiner action has been performed, the combined colored noise autocorrelation matrix is given in (2.31) which is the expanded form of (2.26):

$$\mathbf{R}_{\tilde{\mathbf{w}}_j} = |c_{j1}|^2 \mathbf{R}_{\mathbf{w}_1 \mathbf{w}_1} + c_{j1} c_{j2}^* \mathbf{R}_{\mathbf{w}_1 \mathbf{w}_2} + c_{j2} c_{j1}^* \mathbf{R}_{\mathbf{w}_2 \mathbf{w}_1} + |c_{j2}|^2 \mathbf{R}_{\mathbf{w}_2 \mathbf{w}_2} \tag{3.20}$$

where the submatrices $\mathbf{R}_{\mathbf{w}_i \mathbf{w}_j}$ are given by (3.15). Thus, $\mathbf{R}_{\tilde{\mathbf{w}}_j}$ is a 4×4 matrix. Since real data is used, (3.20) is equivalent to,

$$\mathbf{R}_{\tilde{\mathbf{w}}_j} = c_{j1}^2 \mathbf{R}_{\mathbf{w}_1 \mathbf{w}_1} + c_{j1} c_{j2} (\mathbf{R}_{\mathbf{w}_1 \mathbf{w}_2} + \mathbf{R}_{\mathbf{w}_2 \mathbf{w}_1}) + c_{j2}^2 \mathbf{R}_{\mathbf{w}_2 \mathbf{w}_2} \tag{3.21}$$

When the actual autocorrelation is known, then (2.47) can be modified to accomodate the proposed system as,

$$\tilde{\mathbf{h}}_{j,opt} = \mathbf{R}_{\tilde{\mathbf{w}}_j}^{-1} \tilde{\mathbf{s}}_j \quad j = 0, 1 \tag{3.22}$$

Notice from the last five equations that since the optimal coefficients (c_{01}, c_{02}) for the "0" and (c_{11}, c_{12}) for the "1" are two different sets of points, the combined signal vector $\tilde{\mathbf{s}}_j$, the combined noise vector $\tilde{\mathbf{w}}_j$, and thus the combined

autocorrelation matrix $R_{\tilde{\mathbf{w}}_j}$ are different for the "0" and for the "1". Hence, the $OSNR_{opt}$ for the "1" does not necessarily equal that for the "0". From (2.48),

$$OSNR_{j,opt} = \tilde{\mathbf{s}}_j^T R_{\tilde{\mathbf{w}}_j}^{-1} \tilde{\mathbf{s}}_j \quad j = 0, 1 \quad (3.23)$$

The coefficients c_{j1} and c_{j2} are computed by maximizing $OSNR_{j,opt}$ in (3.23).

When the actual autocorrelation is unknown and must be estimated (Section 2.4.3), then (2.51) becomes,

$$\tilde{\mathbf{h}}_j = \hat{R}_{\tilde{\mathbf{w}}_j}^{-1} \tilde{\mathbf{s}}_j \quad j = 0, 1 \quad (3.24)$$

because $\hat{\mathbf{r}}_{\mathbf{w}}$ is used to form the $R_{\mathbf{w}}$ Toeplitz autocorrelation matrix in (3.15) from which $R_{\tilde{\mathbf{w}}_j}$ is derived. Furthermore, since $\hat{\mathbf{r}}_{\mathbf{w}}$ does not necessarily match the actual autocorrelation sequence $\mathbf{r}_{\mathbf{w}}$, the estimated combined autocorrelation matrix $\hat{R}_{\tilde{\mathbf{w}}_j}$ does not equal the actual combined autocorrelation matrix $R_{\tilde{\mathbf{w}}_j}$ and the estimated MAMF impulse response $\tilde{\mathbf{h}}_j$ is not optimal.

The estimated OSNR is the modification of (2.52),

$$\begin{aligned} OS\hat{N}R_j &= \frac{(\tilde{\mathbf{h}}_j^T \tilde{\mathbf{s}}_j)^2}{\tilde{\mathbf{h}}_j^T R_{\tilde{\mathbf{w}}_j} \tilde{\mathbf{h}}_j} \\ &= \frac{(\tilde{\mathbf{s}}_j^T \hat{R}_{\tilde{\mathbf{w}}_j}^{-1} \tilde{\mathbf{s}}_j)^2}{(\tilde{\mathbf{s}}_j^T \hat{R}_{\tilde{\mathbf{w}}_j}^{-1} R_{\tilde{\mathbf{w}}_j} \hat{R}_{\tilde{\mathbf{w}}_j}^{-1} \tilde{\mathbf{s}}_j)} \end{aligned} \quad (3.25)$$

Note that for the computation of $OS\hat{N}R_j$ knowledge of the actual combined autocorrelation matrix $R_{\tilde{\mathbf{w}}_j}$ is required. As a result, the $OS\hat{N}R_j$ cannot be maximized directly to yield the estimated optimal coefficients, \hat{c}_{j1} and \hat{c}_{j2} , required for the linear combination of the basis vectors. In an effort to overcome this problem, the signal energy at the output of the MAMF is maximized for each j ($=0, 1$). From (2.43.a),

$$\begin{aligned}
E_{\tilde{\mathbf{s}},o} &= (\tilde{\mathbf{h}}_j^T \tilde{\mathbf{s}}_j)^2 \\
&= (\tilde{\mathbf{s}}_j^T \hat{\mathbf{R}}_{\tilde{\mathbf{w}}_j}^{-1} \tilde{\mathbf{s}}_j)^2
\end{aligned} \tag{3.26}$$

As $\hat{\mathbf{R}}_{\tilde{\mathbf{w}}_j}$ approaches $\mathbf{R}_{\tilde{\mathbf{w}}_j}$, \hat{c}_{j1} and \hat{c}_{j2} approach c_{j1} and c_{j2} respectively. Thus, OSNR_j tends toward $\text{OSNR}_{j,opt}$. It is evident that the accuracy of the maximization procedure depends mainly on the accuracy of the autocorrelation estimator. The maximization of (3.23) (or (3.26)) is performed by varying c_{j1} (or \hat{c}_{j1}) from $-\sqrt{2}$ to $\sqrt{2}$ by increments of $(2\sqrt{2}/200)$ while satisfying the restrictions of (3.19).

Under any circumstances - actual or estimated noise autocorrelation sequence - since the signal energy of the transmitted signal is $K = 2$ then from (2.41),

$$\text{ISNR} = \frac{K}{r_{\mathbf{w}}(0)} \tag{3.27}$$

As far as the detector is concerned (Figure 8), the decision rule was given in (2.73) and is repeated here,

$$G = G_1 - G_0 \begin{matrix} H_1 \\ > \\ < \\ H_0 \end{matrix} 0 \tag{3.28}$$

where H_1 represents the hypothesis that a "1" was transmitted and H_0 represents the hypothesis that a "0" was transmitted. In addition, from (2.79),

$$G_1 = \tilde{\mathbf{h}}_1^T (\tilde{\mathbf{r}}_1 - \frac{1}{2} \tilde{\mathbf{s}}_1) \tag{3.29.a}$$

$$G_0 = \tilde{\mathbf{h}}_0^T (\tilde{\mathbf{r}}_0 - \frac{1}{2} \tilde{\mathbf{s}}_0) \tag{3.29.b}$$

where $\tilde{\mathbf{h}}_j$ is the reverse and complex conjugate of the MAMF impulse response $\tilde{\mathbf{h}}_j$ as described by (2.78). Also, $\tilde{\mathbf{r}}_j$ is the combined received vector described by,

$$\tilde{\mathbf{r}}_j = [\tilde{\mathbf{s}}_j + \tilde{\mathbf{w}}_j] \quad j = 0, 1 \tag{3.30}$$

The above operation is necessary to maintain the same dimension of $M = 4$ for the vector operations in (3.29). Notice that $\tilde{\mathbf{r}}_1$ does not necessarily equal $\tilde{\mathbf{r}}_0$ due to the different coefficient sets used for the respective linear combinations.

Equations (3.29), describe the detector operation for estimated noise autocorrelation. When the actual noise autocorrelation is used,

$$\tilde{\mathbf{h}}_j = \tilde{\mathbf{h}}_{j,opt} \quad j = 0, 1 \quad (3.31)$$

in (3.29).

In order to determine the optimal detector performance of the proposed MAMF receiver system, consider the discussion presented in Section 2.4.5. For optimal detection the signal vectors must satisfy the restriction of (2.96) which for the proposed system translates to:

$$\tilde{\mathbf{s}}_1 = -\tilde{\mathbf{s}}_0 \quad (3.32)$$

Also, the variance of $\mathbf{G}^T \mathbf{V}\{\mathbf{G}\}$, is the same under each hypothesis and for real data equals σ_G^2 which is given by (2.83). It, then, must satisfy (2.99) or,

$$\sigma_G^2 = \frac{4E_{\tilde{\mathbf{s}}}}{\lambda_{min}} \quad (3.33)$$

where $E_{\tilde{\mathbf{s}}} = K = 2$ and λ_{min} is the minimum eigenvalue of the combined colored noise autocorrelation matrix $\mathbf{R}_{\tilde{\mathbf{w}}_j}$. Since the restriction (3.32) holds,

$$\mathbf{R}_{\tilde{\mathbf{w}}_j} = \mathbf{R}_{\tilde{\mathbf{w}}_1} = \mathbf{R}_{\tilde{\mathbf{w}}_0} \quad (3.34)$$

The mean of \mathbf{G} under each hypothesis, $E_0\{\mathbf{G}\}$ or $E_1\{\mathbf{G}\}$, is given by (2.82) and repeated here,

$$E_0\{\mathbf{G}\} = -E_1\{\mathbf{G}\} = \frac{\sigma_G^2}{2} \quad (3.35)$$

Thus, the probability density functions of G are given by (2.86) as,

$$P_1(G) = \frac{1}{(2\pi\sigma_G^2)^{1/2}} \exp\left\{\frac{(G - \frac{1}{2}\sigma_G^2)^2}{-2\sigma_G^2}\right\} \quad (3.36.a)$$

$$P_0(G) = \frac{1}{(2\pi\sigma_G^2)^{1/2}} \exp\left\{\frac{(G + \frac{1}{2}\sigma_G^2)^2}{-2\sigma_G^2}\right\} \quad (3.36.b)$$

By setting the probability of transmitting either a "1" or a "0" equal and $P(H_1) = P(H_0) = \frac{1}{2}$ and the test threshold $\rho_0 = 1$, from (2.88) and (2.89) the probability of error is P_e (Figure 5),

$$P_e = \int_0^\infty P_0(G) dG = \int_R^\infty \frac{1}{(2\pi)^{1/2}} e^{-z^2/2} dz \quad (3.37)$$

where $R = \frac{\sigma_G}{2}$. Therefore, P_e can be evaluated for the optimal case, with known autocorrelation, from (3.37) and (3.33).

In order to accomodate the proposed system, (2.83) can be modified to,

$$\sigma_G^2 = (\tilde{s}_1 - \tilde{s}_0)^T R_{\tilde{w}_j}^{-1} (\tilde{s}_1 - \tilde{s}_0) \quad (3.38)$$

By applying (3.32), and (3.23) to (3.38),

$$\begin{aligned} \sigma_G^2 &= 4 (\tilde{s}_1)^T R_{\tilde{w}_1}^{-1} (\tilde{s}_1) \\ &= 4 \text{OSNR}_{1,opt} \\ &= 4 \text{OSNR}_{0,opt} \end{aligned} \quad (3.39)$$

By equating (3.39) and (3.33),

$$\text{OSNR}_{1,opt} = \text{OSNR}_{0,opt} = \frac{E_{\tilde{\mathbf{s}}}}{\lambda_{min}} \quad (3.40)$$

By considering the last two equations the ROC can be presented as the plot of the probability of error P_e vs. OSNR. Figure 9 presents the ROC for the proposed system.

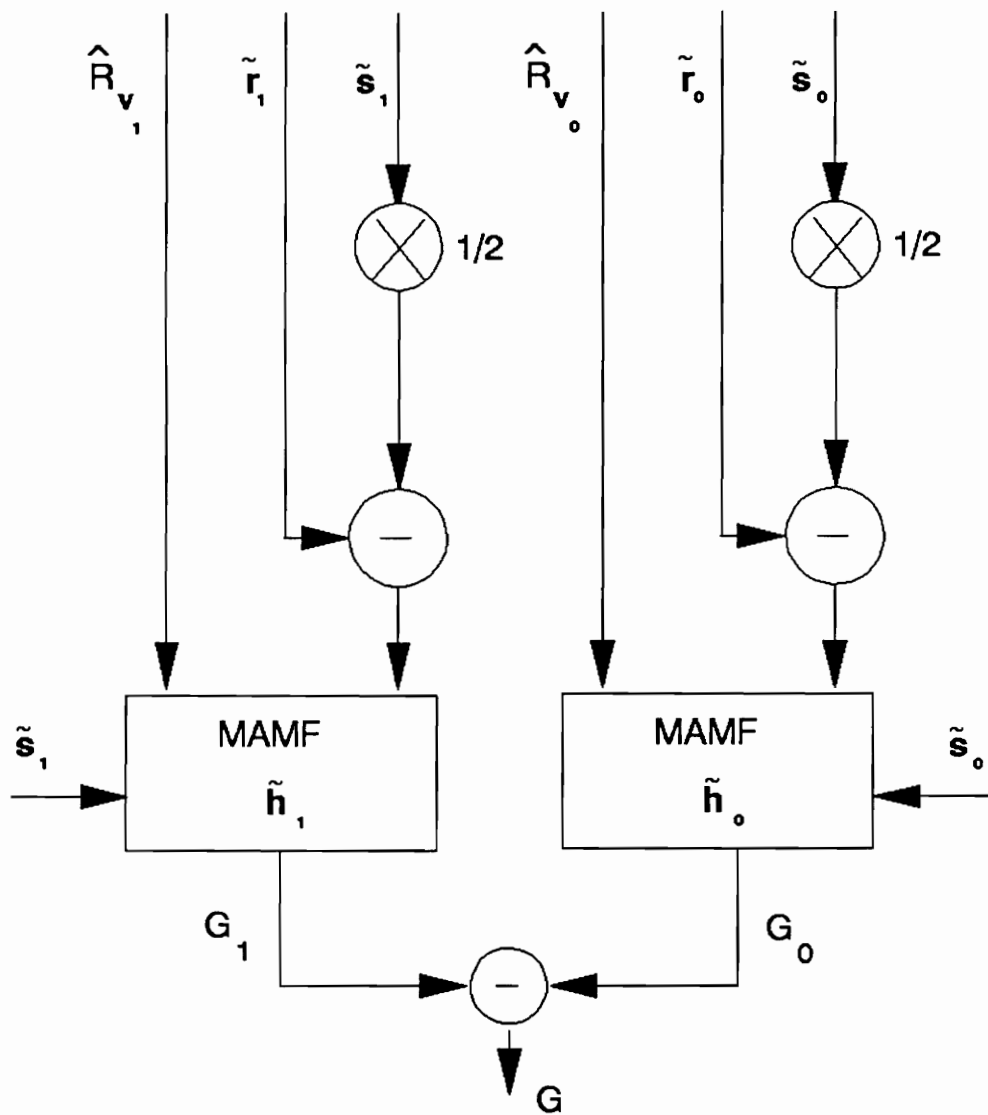


FIGURE 8. PROPOSED MAMF COMMUNICATION SYSTEM DETECTOR

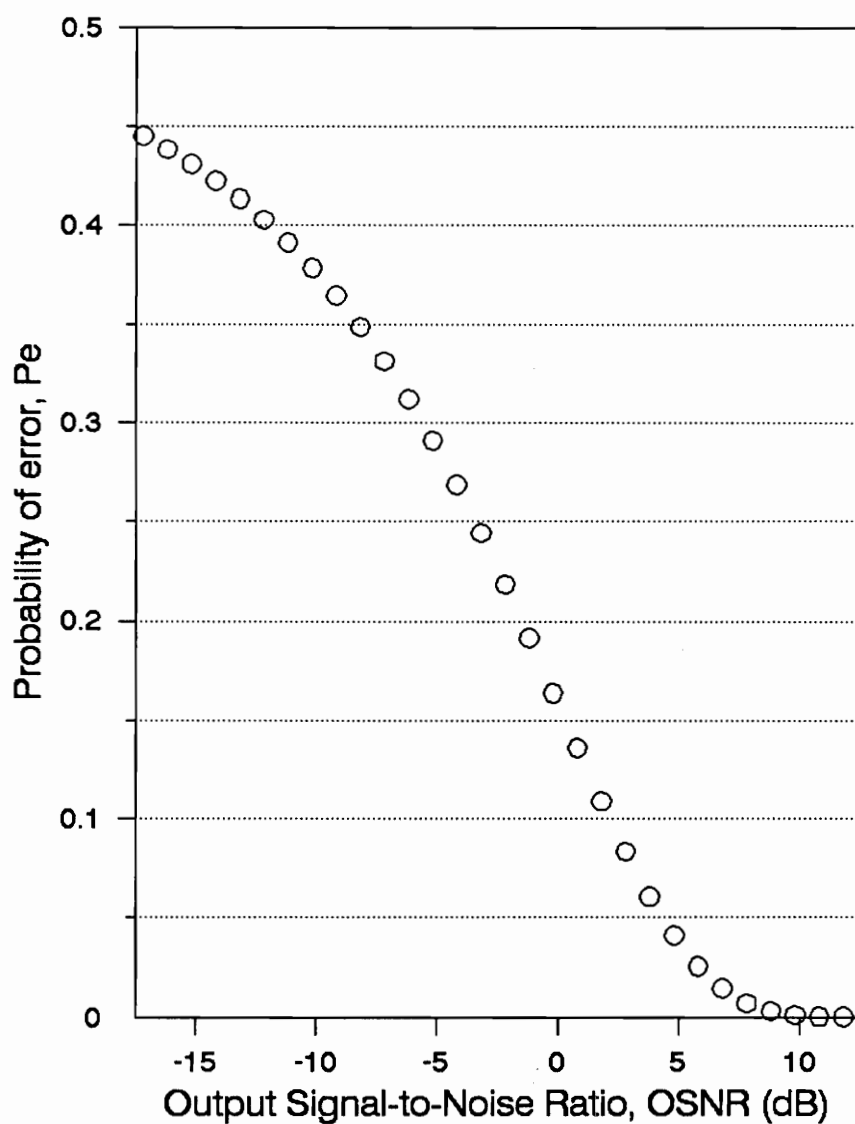


FIGURE 9. ROC FOR THE PROPOSED SYSTEM AS A FUNCTION OF OSNR

3.2.2 Traditional System Description

For a binary system of communication the transmitted signal vector in the proposed MAMF communication system is of dimension $N = 8$. Thus, in order to compare the two systems fairly, $N = 8$ should be the dimension of the transmitted signal vector in the traditional MAMF communication system as well. In the traditional system, as seen from Section 2.2.1 and Figure 2, every individual bit of data to be communicated is encoded in a fixed N -dimensional signal vector \mathbf{s}_j ,

$$\mathbf{s}_j = [s_{j1} \ s_{j2} \ \dots \ s_{j8}]^T \quad j = 0, 1 \quad (3.41)$$

so that \mathbf{s}_0 encodes a "0" and \mathbf{s}_1 encodes a "1". The colored noise vector \mathbf{w} , which corrupts the transmitted signal vector is,

$$\mathbf{w} = [w_1 \ w_2 \ \dots \ w_8]^T \quad (3.42)$$

to produce the received vector \mathbf{r}_T :

$$\mathbf{r}_T = [s_{j1}+w_1 \ s_{j2}+w_2 \ \dots \ s_{j8}+w_8]^T \quad j = 0, 1 \quad (3.43)$$

Therefore, the finite length sequence actually entering the traditional MAMF communication receiver, is the 16-dimensional vector \mathbf{r}_a :

$$\mathbf{r}_a = [\mathbf{w}_g^T \mid \mathbf{r}_T^T]^T \quad (3.44)$$

The 8×8 noise autocorrelation matrix \mathbf{R}_w is given by (3.15). When the actual colored noise autocorrelation is known, then the optimal impulse response of the MAMF which maximizes OSNR is (2.47), and is repeated here to accomodate each j ($=0, 1$),

$$\mathbf{h}_{j,opt} = \mathbf{R}_w^{-1} \mathbf{s}_j \quad j = 0, 1 \quad (3.45)$$

as well as the optimal value of the OSNR as presented in (2.48),

$$\text{OSNR}_{j,opt} = \mathbf{s}_j^T \mathbf{R}_w^{-1} \mathbf{s}_j \quad j = 0, 1 \quad (3.46)$$

As opposed to the combined colored noise autocorrelation matrix $\mathbf{R}_{\tilde{\mathbf{w}}_j}$ of the proposed system, \mathbf{R}_w is the same for every j ($=0, 1$).

In case the noise autocorrelation is estimated the MAMF impulse response is given by (2.51),

$$\mathbf{h}_j = \hat{\mathbf{R}}_w^{-1} \mathbf{s}_j \quad j = 0, 1 \quad (3.47)$$

whereas (2.52) becomes,

$$\begin{aligned} \text{OS}\hat{\text{NR}}_j &= \frac{(\mathbf{h}_j^T \mathbf{s}_j)^2}{\mathbf{h}_j^T \mathbf{R}_w \mathbf{h}_j} \\ &= \frac{(\mathbf{s}_j^T \hat{\mathbf{R}}_w^{-1} \mathbf{s}_j)^2}{(\mathbf{s}_j^T \hat{\mathbf{R}}_w^{-1} \mathbf{R}_w \hat{\mathbf{R}}_w^{-1} \mathbf{s}_j)} \end{aligned} \quad (3.48)$$

Note again that for the computation of $\text{OS}\hat{\text{NR}}_j$ knowledge of the actual autocorrelation matrix \mathbf{R}_w , is required.

Again, when either the actual or the estimated noise autocorrelation sequence is used,

$$\text{ISNR} = \frac{\mathbf{s}_j^T \mathbf{s}_j}{\mathbf{r}_w(0)} \quad (3.49)$$

Obviously, if system Bit Error Rate (BER) comparisons are to be performed and the encoding signal vectors of the proposed system are different from the encoding signal vectors of the traditional system, then the ISNR for the proposed system in (3.27) and the ISNR for the traditional system in (3.49) must be made equal by adjusting the transmitted signal energy. This action ensures a fair

comparison between the two systems.

The decision rule of the detector incorporated in the traditional MAMF communication system (Figure 10) is given by (3.28), whereas its operation is described by the following equations:

$$G_1 = \bar{\mathbf{h}}_1^T (\mathbf{r}_T - \frac{1}{2} \mathbf{s}_1) \quad (3.50.a)$$

$$G_0 = \bar{\mathbf{h}}_0^T (\mathbf{r}_T - \frac{1}{2} \mathbf{s}_0) \quad (3.50.b)$$

where $\bar{\mathbf{h}}_j$ is the reverse and complex conjugate of the MAMF impulse response \mathbf{h}_j . Also, \mathbf{r}_T is given in (3.43). The decision rule is to choose H_1 whenever $G_1 - G_0 \geq 0$.

The equations (3.50) present the behavior of the detector for estimated noise autocorrelation. In case the actual autocorrelation is used, the following relation holds,

$$\bar{\mathbf{h}}_j = \bar{\mathbf{h}}_{j,opt} \quad j = 0, 1 \quad (3.51)$$

for use in (3.50).

For optimal detection with the traditional MAMF receiver system, the signal vectors must satisfy (2.96) which for the traditional system becomes:

$$\mathbf{s}_1 = -\mathbf{s}_0 \quad (3.52)$$

The variance of G for real data equals σ_G^2 which is given by (2.83). Then, the variance must satisfy (2.99) or,

$$\sigma_G^2 = \frac{4E_s}{\lambda_{min}} \quad (3.53)$$

where $E_s = \mathbf{s}_1^T \mathbf{s}_1 = \mathbf{s}_0^T \mathbf{s}_0$ and λ_{min} is the minimum eigenvalue of the colored noise autocorrelation matrix \mathbf{R}_w .

The mean of G under each hypothesis, $E_0\{G\}$ or $E_1\{G\}$, is given by (2.82) and repeated here,

$$E_0\{G\} = -E_1\{G\} = \frac{\sigma_G^2}{2} \quad (3.54)$$

and the probability density functions of G are given by (2.86) as,

$$P_1(G) = \frac{1}{(2\pi\sigma_G^2)^{1/2}} \exp\left\{\frac{(G - \frac{1}{2}\sigma_G^2)^2}{-2\sigma_G^2}\right\} \quad (3.55.a)$$

$$P_0(G) = \frac{1}{(2\pi\sigma_G^2)^{1/2}} \exp\left\{\frac{(G + \frac{1}{2}\sigma_G^2)^2}{-2\sigma_G^2}\right\} \quad (3.55.b)$$

For equal probability of transmitting the "1" bit or the "0" bit $P(H_1) = P(H_0) = \frac{1}{2}$ and the test threshold $\rho_0 = 1$, from (2.88) and (2.89) the probability of error is P_e (Figure 5),

$$P_e = \int_0^\infty P_0(G) dG = \int_R^\infty \frac{1}{(2\pi)^{1/2}} e^{-z^2/2} dz \quad (3.56)$$

where $R = \frac{\sigma_G}{2}$. Therefore, P_e can be evaluated for the optimal case, with known autocorrelation, from (3.56) and (3.53).

For the traditional system, (2.83) can be modified to,

$$\sigma_G^2 = (\mathbf{s}_1 - \mathbf{s}_0)^T \mathbf{R}_w^{-1} (\mathbf{s}_1 - \mathbf{s}_0) \quad (3.57)$$

By applying (3.52), and (3.46) to (3.57),

$$\begin{aligned} \sigma_G^2 &= 4 (\mathbf{s}_1)^T \mathbf{R}_w^{-1} (\mathbf{s}_1) \\ &= 4 \text{OSNR}_{1,opt} \end{aligned}$$

$$= 4 \text{ OSNR}_{0,opt} \quad (3.58)$$

By equating (3.58) and (3.53),

$$\text{OSNR}_{1,opt} = \text{OSNR}_{0,opt} = \frac{E_s}{\lambda_{min}} \quad (3.59)$$

Again, with the last two equations the ROC can be presented as the plot of P_e vs. OSNR. Figure 11 presents the ROC for the traditional system. Note that Figures 9 and 11 are identical. This is because the detector is identical as developed in Section 2.4.5. It is only modified for incorporation in the two MAMF communication systems. Since the independent variable in the ROC curves is the OSNR, the P_e curve displays the behavior of the receiver itself.

Through the ROC curve, one can pinpoint the **ideal** probability of error for a specific OSNR. It will be used extensively in the next sections in order to confirm BER results which are obtained through a practical implementation of the detector. Since the derivation was developed for optimal detector performance, the actual noise autocorrelation sequence was used, resulting in the computation of **ideal** P_e . Note that as the OSNR decreases, P_e asymptotically reaches $\frac{1}{2}$, which represents the worst possible situation.

Nevertheless, since the ROC curve represents the detector under any circumstances, a \hat{P}_e can be obtained through an $\hat{\text{OSNR}}$, if the noise autocorrelation is estimated. In this way, the BER results obtained with estimated noise autocorrelation can also be confirmed, but with less certainty than the results obtained with the actual noise autocorrelation.

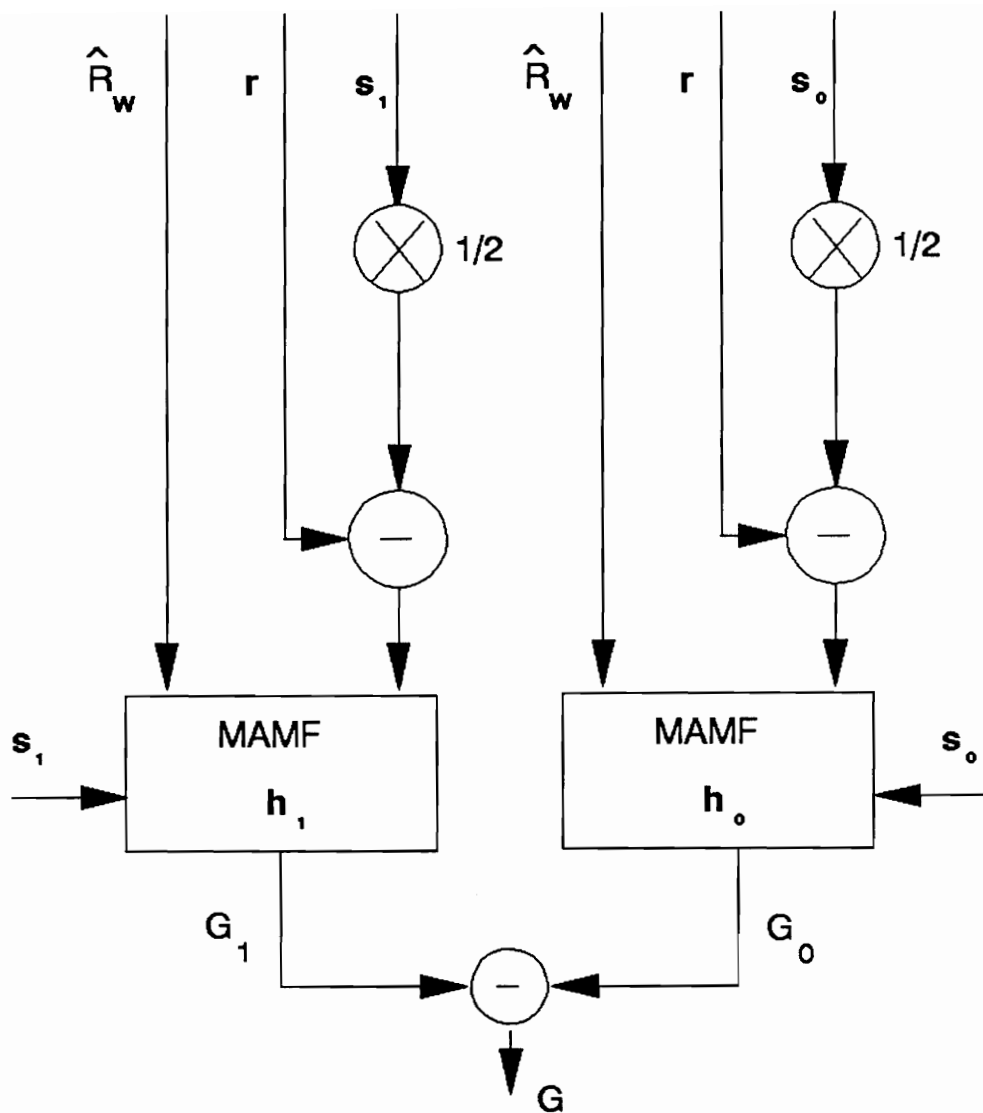


FIGURE 10. TRADITIONAL MAMF COMMUNICATION SYSTEM DETECTOR

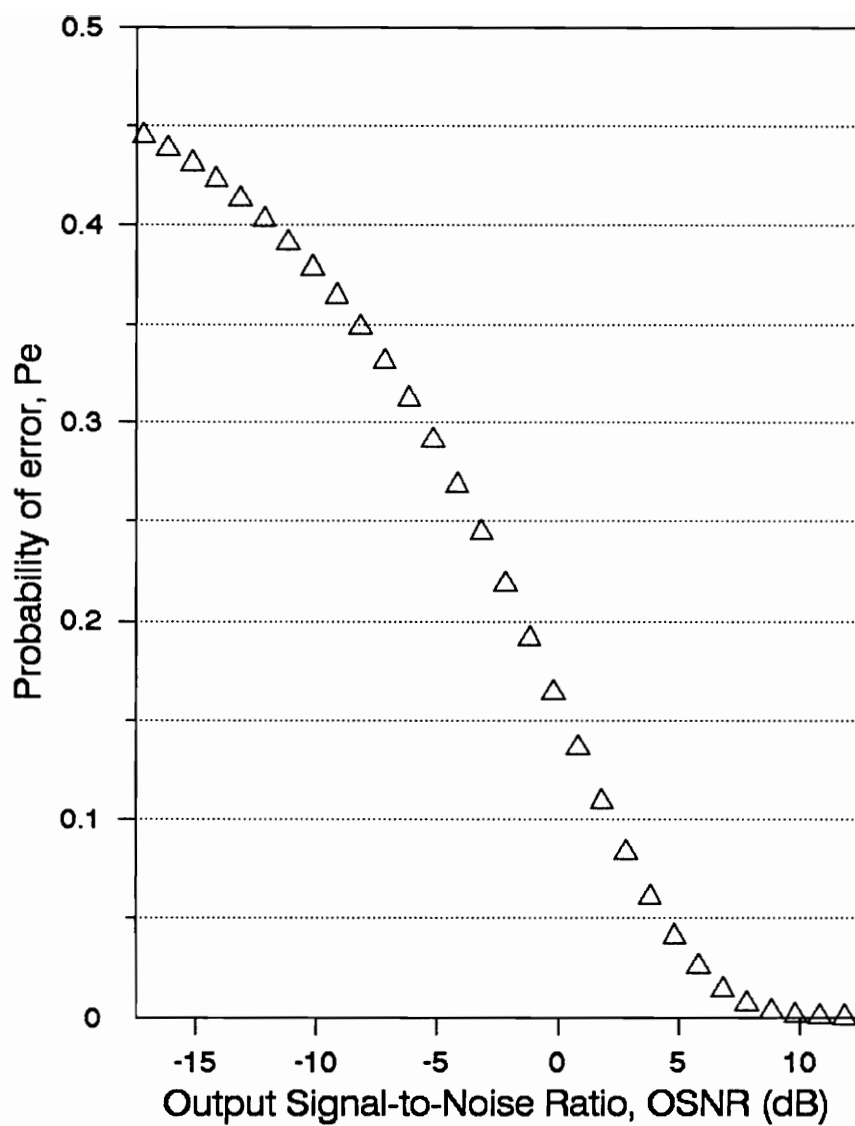


FIGURE 11. ROC FOR THE TRADITIONAL SYSTEM AS A FUNCTION OF OSNR

4.0 RESULTS ON MAMF RECEIVER PERFORMANCE

This chapter consists of the performance comparisons between the traditional and the proposed MAMF communication systems, in terms of SNRI as well as Bit Error Rates (BER). In other words, the two communication systems are examined prior to and following the incorporation of their detectors respectively. The effects of different colored noise characteristics, estimation of the colored noise autocorrelation sequence, and signal choice are studied for both systems. A number of experiments were conducted by Wilson [25], and some were repeated in this chapter in order to compare the results and check for consistency in the designs.

4.1 GENERAL SNRI COMPARISONS

The comparisons are displayed in terms of plots of SNRI vs. Colored Noise Center Frequency θ . The colored noise center frequency θ , is swept from 0° to 180° (or 0 to π in radians) and the maximum SNRI is plotted in decibels (dB). The center frequency range of π consists of $(\pi/50)$ points, and the SNRI is computed at each point. Initially, the colored noise used is narrowband ($\rho = 0.95$), followed by more broadband noise generated by decreasing ρ ($= 0.8, 0.5$) as explained in Section 3.1.

4.1.1 Maximum SNRI curves

The first SNRI comparisons between the two MAMF communication systems, consist of the maximum SNRI that can be attained for both systems. Since SNRI is maximum for maximum OSNR, the maximum OSNR is computed at each colored noise center frequency point. Theoretically, the maximum OSNR is found to be equal to the reciprocal of the smallest eigenvalue of the Toeplitz colored noise autocorrelation matrix R_w [4]. For R_w , the actual noise autocorrelation sequence is used (Section 3.1), which is computed at each θ .

As far as the traditional system is concerned, the maximum OSNR is computed, at each θ , as the inverse of the smallest eigenvalue of the 8×8 noise autocorrelation matrix R_w . The eigenvector associated with the smallest eigenvalue is chosen as the transmitted signal vector to compute the ISNR as in (3.40). Nevertheless, according to Section 2.1 the eigenvectors are orthonormal. Therefore, the ISNR is just the inverse of $r_w(0)$.

The maximum OSNR for the proposed system occurs when the reciprocal of the smallest eigenvalue of the 4×4 combined colored noise autocorrelation matrix $R_{\tilde{w}_j}$ is maximized. The autocorrelation matrix $R_{\tilde{w}_j}$ is computed based on information contained in R_w as in (3.21). For each colored noise center frequency θ , a new actual autocorrelation matrix R_w is produced. In addition, as the coefficients c_{j1} and c_{j2} vary according to (3.19), the combined

autocorrelation matrix $R_{\tilde{w}_j}$ changes in a similar manner. Meanwhile, its smallest eigenvalue is computed and saved. The eigenvalue selected for the maximum OSNR computation is the minimum of that sequence. Again, the ISNR is the inverse of $r_w(0)$.

The maximum SNRI is computed by taking the ratio of the maximum OSNR to ISNR and the results are presented graphically in Figures 12, 13, and 14 for different ρ 's. Notice that under ideal, theoretical conditions the traditional MAMF communication system always outperforms the proposed MAMF communication system. Theoretical or ideal conditions, of course, are not attainable in practice but the comparison does provide a theoretical upper envelope for SNRI performance as well as insight into the behavior of both communication systems.

Figure 12 is also presented by Beex and Wilson [4], and was used to check the consistency of the current implementation of the author.

4.1.2 Optimal Traditional System vs. Proposed System

These comparisons present the traditional MAMF communication system optimized to produce maximum OSNR at a specific colored noise center frequency θ , and the proposed system using various orthonormal basis vectors for its encoding signal matrix.

Figure 15 presents a comparison between the traditional system optimized for maximum OSNR, for a colored noise center frequency $\theta = 0^\circ$, and the proposed system using symmetric orthonormal basis vectors as its encoding signal vector set. Thus, for the traditional system, the signal vector was fixed to be the eigenvector associated with the smallest eigenvalue of R_w generated at that $\theta = 0^\circ$. In Figure 15, the signal vectors used in the proposed system are the following symmetric orthonormal basis vectors,

$$S = [s_1 \ s_2] \quad (4.1)$$

where

$$\mathbf{s}_1 = \left[\frac{\sqrt{2}}{2} \ 0 \ 0 \ \frac{\sqrt{2}}{2} \right]^T$$

$$\mathbf{s}_2 = \left[0 \ \frac{\sqrt{2}}{2} \ \frac{\sqrt{2}}{2} \ 0 \right]^T$$

Again the actual autocorrelation values were used. The colored noise center frequency θ was then swept from 0° to 180° in order to produce Figure 15.

Notice that the traditional system outperforms the proposed system in the vicinity of $\theta = 0^\circ$, since it is optimized for that θ . As soon as the colored noise center frequency deviates, indicating a different noise environment, the SNRI drops dramatically and actually reaches a negative decibel value in the vicinity of $\theta = 150^\circ$. A negative SNRI indicates degradation of receiver performance rather than improvement and is highly undesirable. The proposed system, on the other hand, presents a certain degree of robustness under different θ 's, clearly making it the more preferable system to use for $\theta \geq 105^\circ$, when the aforementioned signal vectors are used.

Figure 16 presents almost the same comparison with the exception of the signal vectors. The signal vectors used in the proposed system follow the assignment of (4.1) and are the following anti-symmetric orthonormal basis vectors,

$$\mathbf{s}_1 = \left[\frac{\sqrt{2}}{2} \ 0 \ 0 \ -\frac{\sqrt{2}}{2} \right]^T$$

$$\mathbf{s}_2 = \left[0 \ \frac{\sqrt{2}}{2} \ -\frac{\sqrt{2}}{2} \ 0 \right]^T$$

The same observations that were made for Figure 15 can be made for Figure 16 as well. The only difference appears in the behavior of the proposed system as a result of the different signal vectors used for the transmission.

Figures 17 and 18 differ from Figures 15 and 16 in that the traditional system is now optimized for a colored noise center frequency of $\theta = \pi$. It should

be noted that in this case, when the actual autocorrelation values are used, there exists a 2-dimensional eigenspace associated with the smallest eigenvalue of \mathbf{R}_w . Since any combination of independent eigenvectors is theoretically valid as a signal vector, a family of SNRI curves can be produced for these specific conditions. Nevertheless, a comparison can be made at the point for which the traditional system is optimized ($\theta = \pi$). There the SNRI is the same for every possible minimal eigenvector.

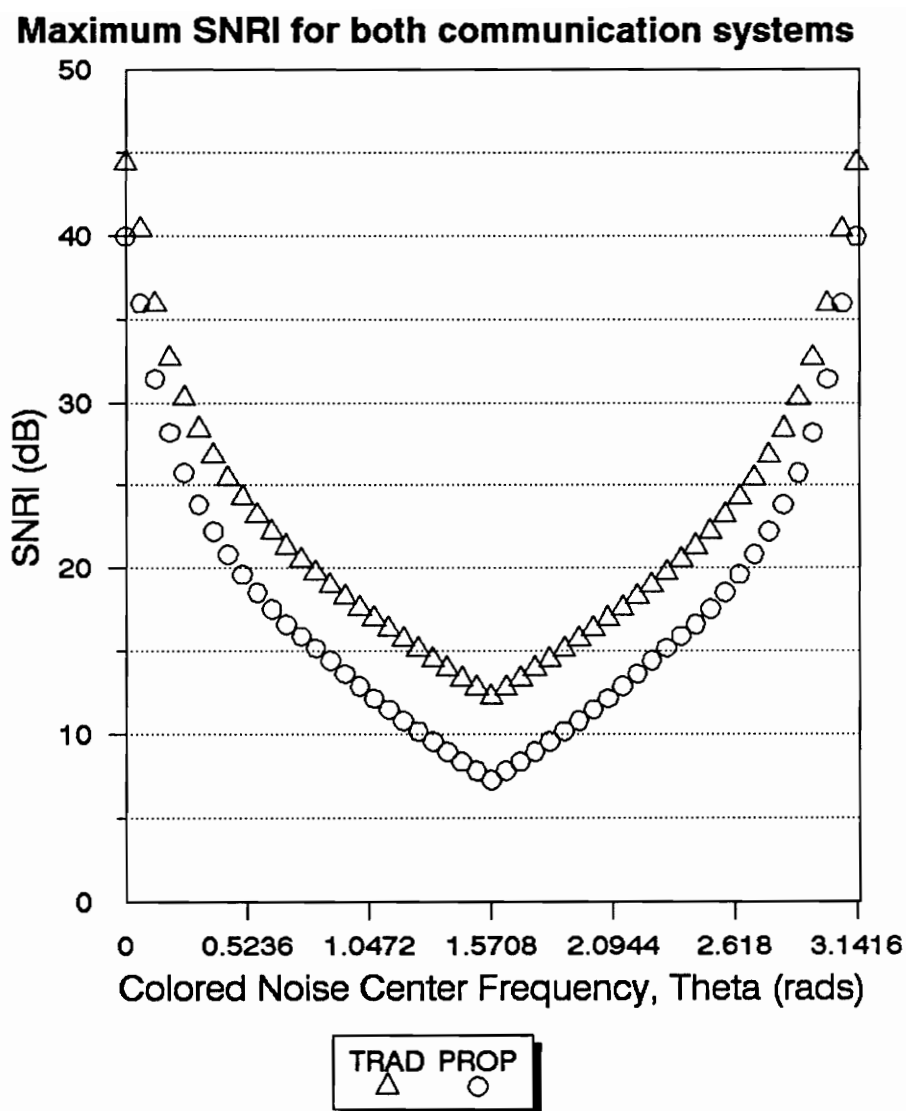


FIGURE 12. PLOT OF MAXIMUM SNRI vs. CENTER FREQUENCY θ FOR $\rho = 0.95$

Maximum SNRI for both communication systems

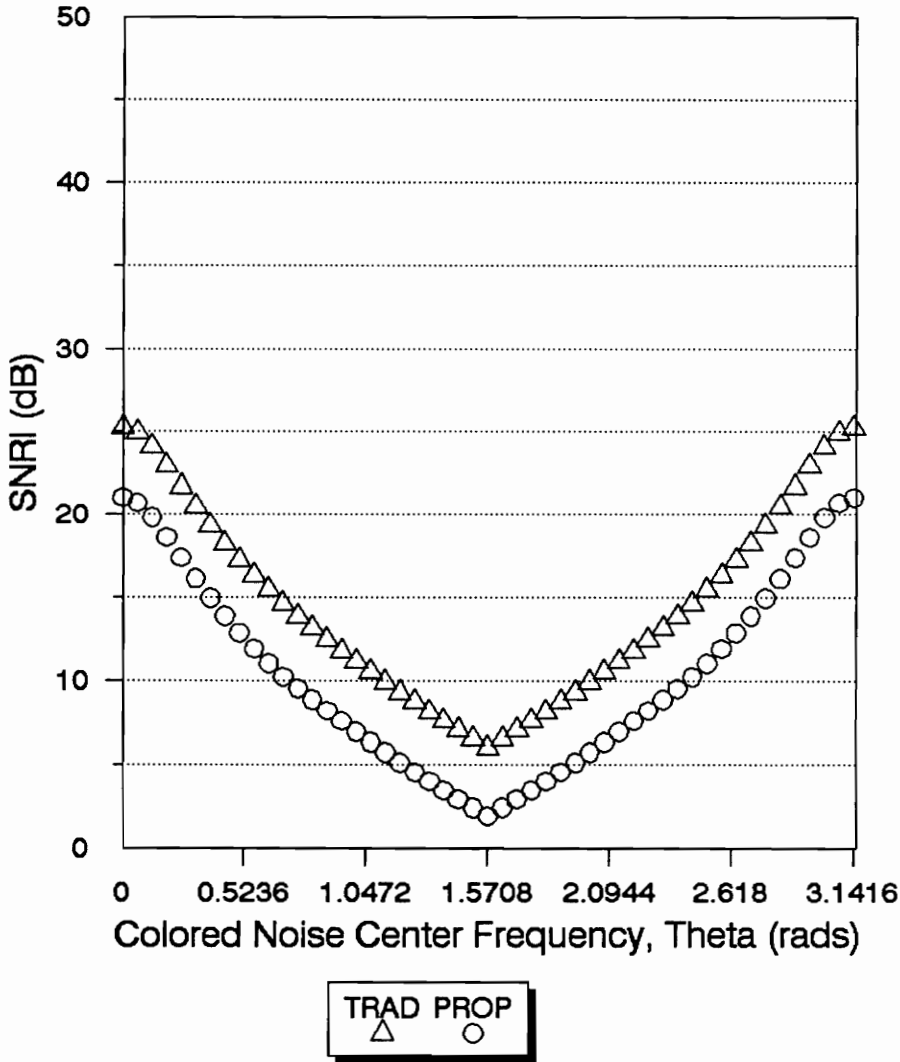


FIGURE 13. PLOT OF MAXIMUM SNRI vs. CENTER FREQUENCY θ FOR $\rho = 0.8$

Maximum SNRI for both communication systems

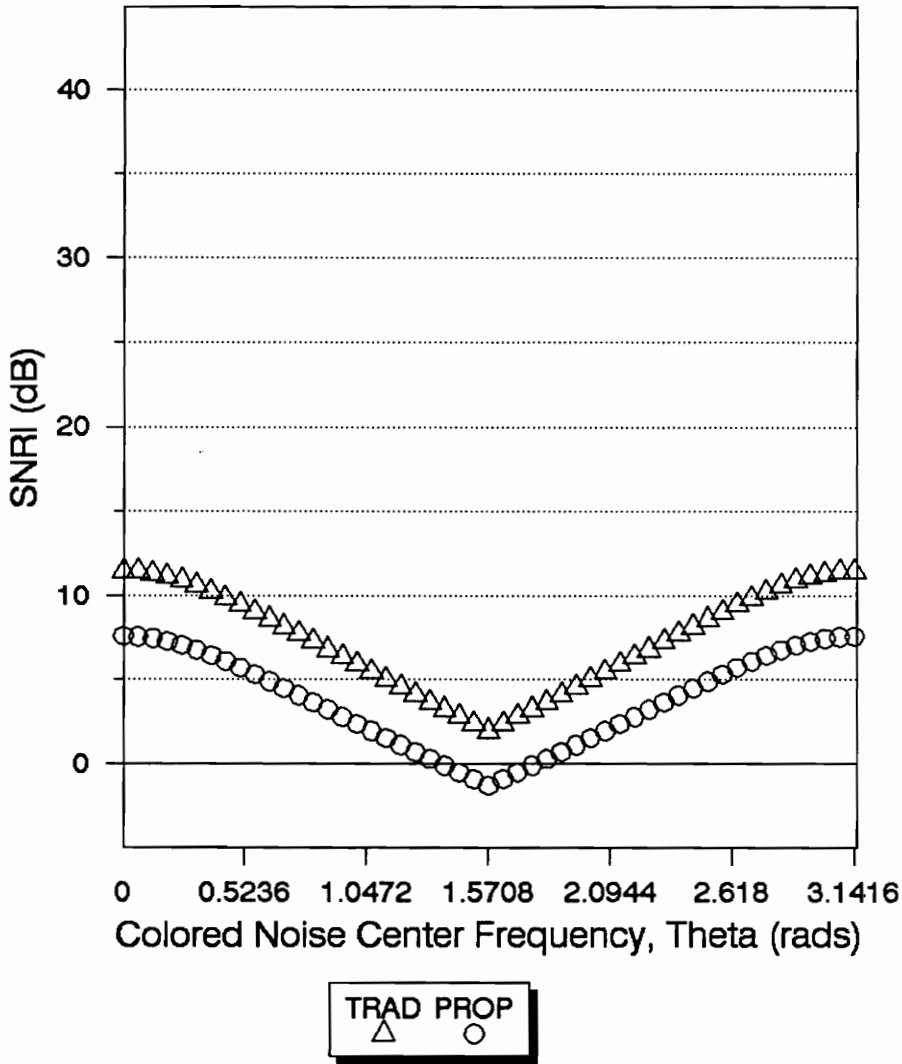


FIGURE 14. PLOT OF MAXIMUM SNRI vs. CENTER FREQUENCY θ FOR $\rho = 0.5$

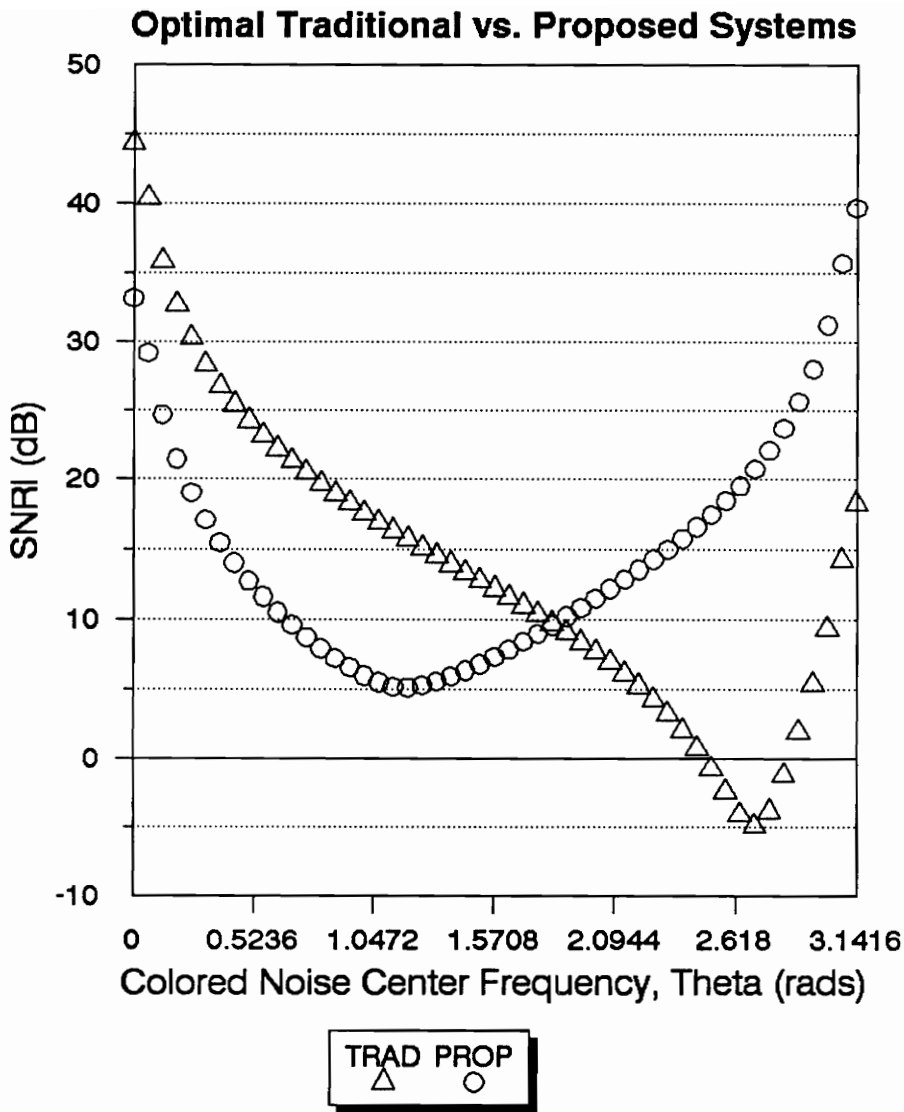


FIGURE 15. PLOT OF SNRI vs. CENTER FREQUENCY θ FOR $\rho = 0.95$
 TRADITIONAL SYSTEM IS OPTIMIZED AT $\theta = 0$
 PROPOSED SYSTEM SIGNAL VECTOR IS SYMMETRIC

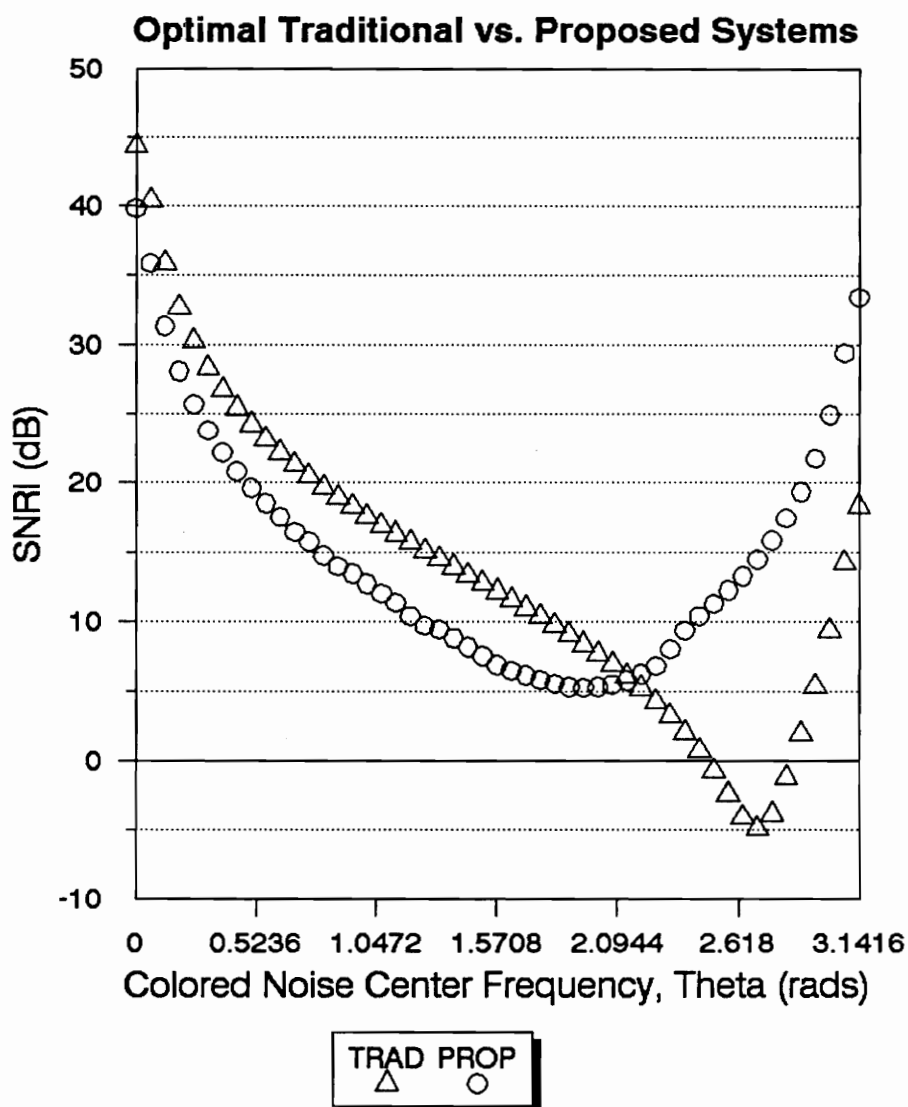


FIGURE 16. PLOT OF SNRI vs. CENTER FREQUENCY θ FOR $\rho = 0.95$
 TRADITIONAL SYSTEM IS OPTIMIZED AT $\theta = 0$
 PROPOSED SYSTEM SIGNAL VECTOR IS SKEW-SYMMETRIC

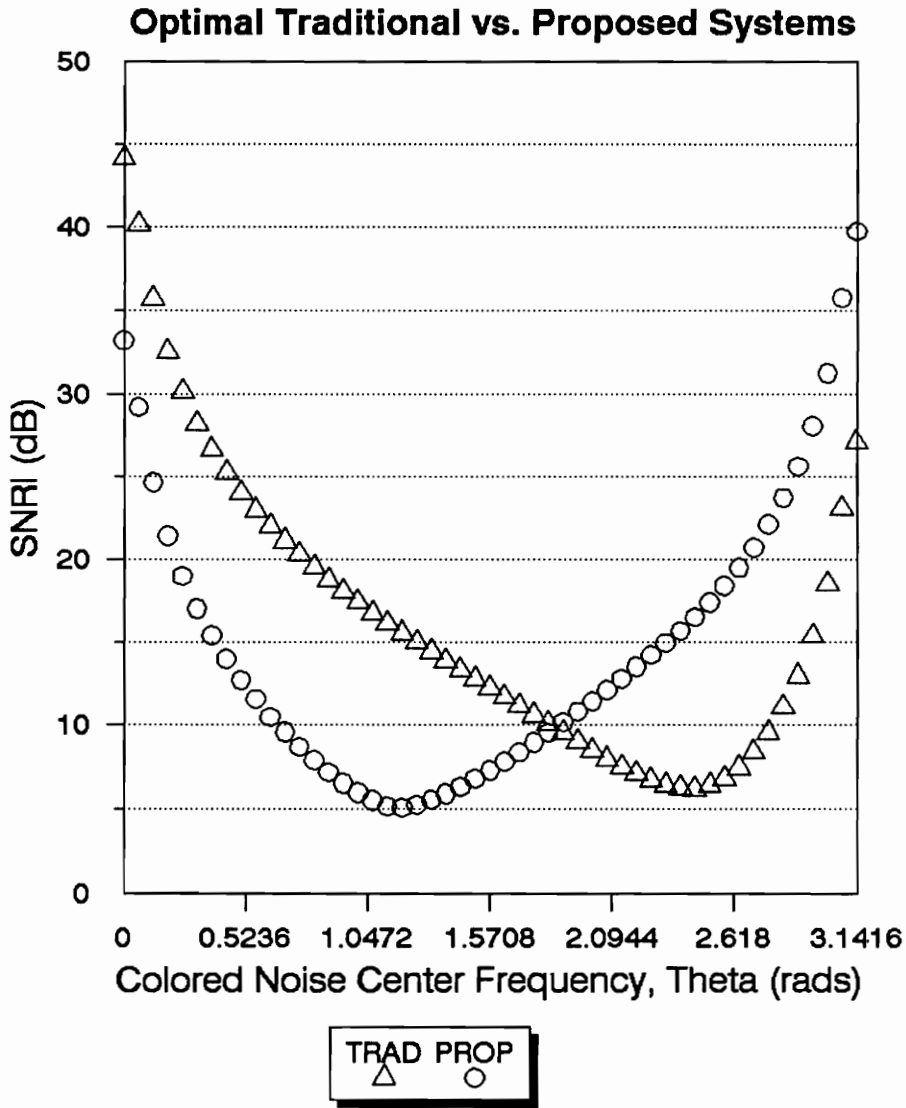


FIGURE 17. PLOT OF SNRI vs. CENTER FREQUENCY θ FOR $\rho = 0.95$
 TRADITIONAL SYSTEM IS OPTIMIZED AT $\theta = \frac{\pi}{2}$
 PROPOSED SYSTEM SIGNAL VECTOR IS SYMMETRIC

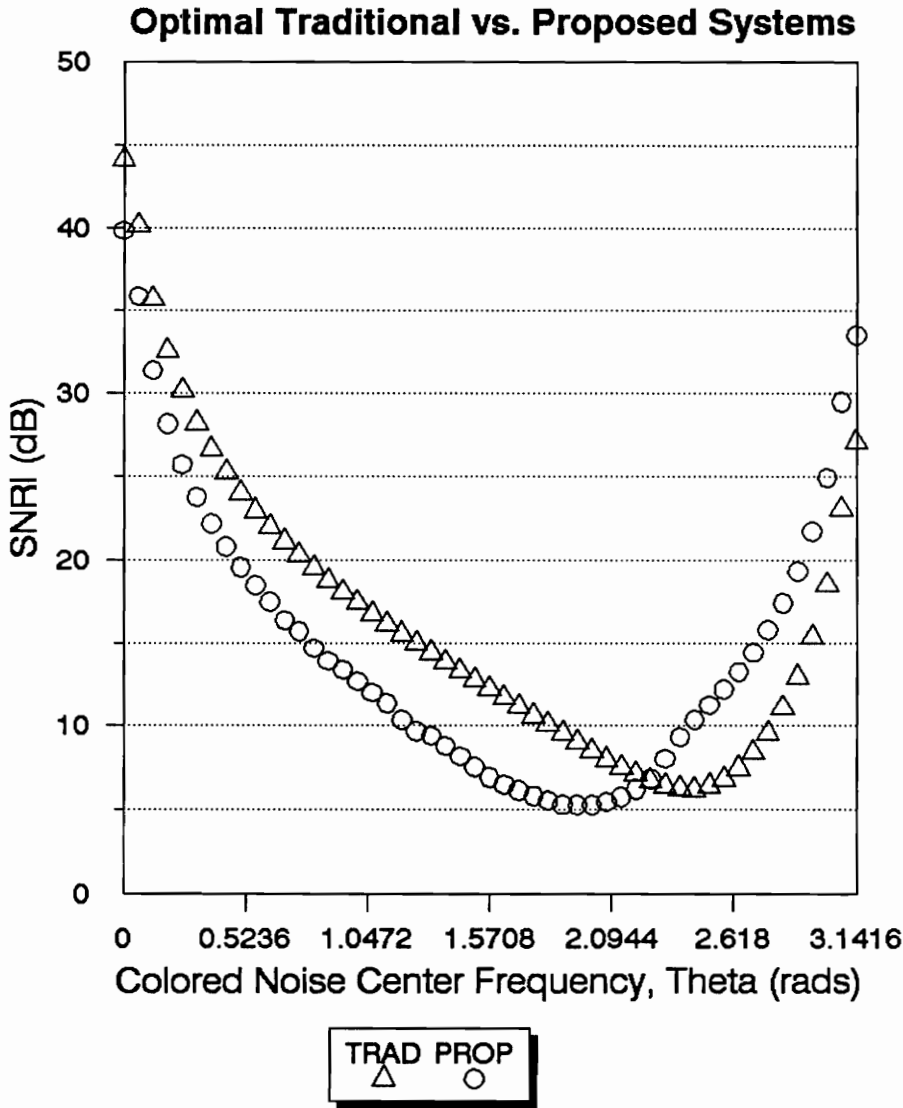


FIGURE 18. PLOT OF SNRI vs. CENTER FREQUENCY θ FOR $\rho = 0.95$
 TRADITIONAL SYSTEM IS OPTIMIZED AT $\theta = \frac{\pi}{2}$
 PROPOSED SYSTEM SIGNAL VECTOR IS SKEW-SYMMETRIC

4.2 SNRI AND BER RESULTS

This particular section presents the comparisons of the two MAMF communication systems in terms of SNRI, justified by BER results which represent the performance of their detectors.

4.2.1 Bit Error Rate (BER) Performance

With the detector design incorporated, the bit error rate (BER) performance for both the traditional and proposed MAMF communication systems can be determined. The BER is a statistical measure of the rate at which bit errors occur for a number of bits transmitted. The BER is dependent upon the ISNR and the SNRI provided by the system, and thus BER is presented as a function of ISNR.

The data to be communicated is random. Numbers are generated from a normal distribution with zero mean and unity variance. Therefore, if the random number is greater than or equal to 0 a "1" is communicated. A "0" is communicated otherwise. The transmitted signal energy is equal for both systems and the noise level is adjusted in order to obtain the desired ISNR according to,

$$r_w(0) = \frac{E_s}{ISNR} \quad (4.2)$$

In order to observe the performance of the system under ideal conditions the first runs were conducted using the actual autocorrelation values. In this way, for a particular colored noise center frequency, we can establish an upper bound of BER performance for both the traditional and the proposed MAMF communication systems.

The next runs were conducted with estimated autocorrelation values obtained from the Classical Biased Estimator (CBE). This results in the observation of a more practical situation through the effects of the estimator on

BER performance. The CBE was used since, as discussed in Section 2.3, it is the best estimator for this application.

Each run simulates the transmission of 1000 randomly generated binary bits. The transmitted signal vectors (which represent each bit) are corrupted by colored noise of a set center frequency, θ . The bit chosen by the detector is compared to the bit that was actually transmitted. If a "1" was transmitted but a "0" was selected then a "1|0" bit error occurs. Similarly, a "0|1" bit error occurs if a "0" was transmitted and a "1" was selected. When the actual autocorrelation is used, close correspondence between P_e and BER is expected. When the estimated autocorrelation is used, an increase of BER relative to that for using actual autocorrelations is expected.

4.2.2 Optimal Traditional System vs. Optimal Proposed System

After observing the performance of both MAMF communication systems for the conditions described in Section 4.1.2, it would be interesting to observe the effect of setting the proposed system at optimal conditions as well. Since this section also presents BER, it is necessary to identify the signal vectors that encode each bit.

For the proposed system, from (2.13), the following signal matrix was used to encode a "0":

$$\mathbf{S}_0 = [\mathbf{s}_{01} \ \mathbf{s}_{02}] \quad (4.3)$$

Since the concatenated vector assignment is used as the transmission scheme, (4.3) becomes,

$$\mathbf{s}_0^{(p)} = [\mathbf{s}_{01}^T \ | \ \mathbf{s}_{02}^T]^T \quad (4.4)$$

where $\mathbf{s}_{01} = [-.34506 \ 0 \ -.93858 \ 0]^T$ and $\mathbf{s}_{02} = [0 \ -.93858 \ 0 \ -.34506]^T$. For optimal detector performance the signal vector used to encode the "1" $\mathbf{s}_1^{(p)}$ satisfies (2.96), where

$$\mathbf{s}_1^{(p)} = -\mathbf{s}_0^{(p)} \quad (4.5)$$

The above signal vectors generate a SNRI curve that almost completely matched the theoretical maximum SNRI curve for the proposed system (Figure 12) as informed after private communication by J. R. Mitchell in October 1990.

The traditional system, as in the previous section, is optimized for $\theta = 0^\circ$. Therefore, the signal vector that encodes the "0" is,

$$\mathbf{s}_0^{(t)} = [.0693 \ .2454 \ -.4188 \ .5095 \ -.5095 \ .4188 \ -.2454 \ .0693]^T$$

which is the eigenvector associated with the smallest eigenvalue of the Toeplitz

noise autocorrelation matrix R_w at $\theta = 0^\circ$. In order to assure optimal detector performance,

$$\mathbf{s}_1^{(t)} = -\mathbf{s}_0^{(t)} \quad (4.6)$$

Notice that for the SNRI computations it is sufficient to use either the $\mathbf{s}_1^{(p)}$ signal vector or the $\mathbf{s}_0^{(p)}$ signal vector for the proposed system and either the $\mathbf{s}_1^{(t)}$ signal vector or the $\mathbf{s}_0^{(t)}$ signal vector for the traditional system. According to (4.5) and (4.6) the signal energy of the vector encoding the "1" is equal to the signal energy of the vector encoding the "0" for either system. Therefore, assuming that (4.5) and (4.6) hold, $\mathbf{s}_j^{(p)}$ and $\mathbf{s}_j^{(t)}$ ($j=0,1$) can be used for the proposed and the traditional systems respectively for SNRI calculations.

Figure 19 presents the SNRI curve for both the proposed and the traditional MAMF communication systems with the conditions described above.

The BER values presented in the next tables are the average of 5 statistically equivalent simulations, thus providing a better image of consistency in the results. Table 1 illustrates the fact that when the traditional system is optimized at $\theta = 0^\circ$ it cannot be outperformed when the colored noise center frequency is $\theta = 0^\circ$. From Figure 19, the actual SNRI for the proposed system is 39.95 dB and for the traditional system is 44.32 dB. Note from Figure 9, that for ISNR of -40 dB, the calculated P_e equals 0.05, which corresponds nicely to 53 (=27+26) bit errors out of 1000 (Table 1). Furthermore, when estimated autocorrelation values are used in the MAMF design, BER goes up. Note that for an ISNR of -40 dB there is an increase in the total BER of 8% and 17% for the proposed and the traditional systems respectively. This indicates that the proposed system is more robust since it degrades slower than the traditional system, for $\theta = 0^\circ$.

Table 2 presents the behavior of both systems at $\theta = 105.4^\circ$ where the actual SNRI for both communication systems is almost the same at 9.5 dB (Figure 19). From Figure 9, at ISNR of -10 dB, or at OSNR of -10+9.5 = -0.5 dB the P_e equals 0.178. Again this corresponds nicely to 173 (=87+86) out of

1000. Again, when estimated noise autocorrelation values are used, the total BER increases. At an ISNR of -10 dB, the total BER increases by 7% and 29% for the traditional and the proposed systems respectively. Hence, for $\theta = 105.4^\circ$, the traditional system is more robust than the proposed system.

When the center frequency is set at $\theta = 135^\circ$, the proposed system performs considerably better than the traditional one, as can be seen from Table 3. This is reasonable since the actual SNRI for the proposed system is 15.5 dB whereas the actual SNRI for the traditional system is 2.67 dB (Figure 19). The latter number shows that when the traditional system is optimized for $\theta = 0^\circ$ and is subject to a noise realization for $\theta = 135^\circ$, it produces very low SNRI. From Figure 9, at ISNR of -20 dB, or at OSNR of $-20.0 + 15.5 = -4.5$ dB the P_e equals 0.275. For the proposed system, the total BER is 276 ($=138+138$) out of 1000, which is in perfect agreement with the P_e . For the traditional system the OSNR is $-20.0 + 2.67 = -17.33$ dB. The P_e is 0.440 and the total BER is 437 ($=219+218$) out of 1000 which is again very close.

Figures 20 and 21 display the correlation between the theoretically derived and calculated probability of error P_e , and the practically calculated BER. Actual autocorrelation values were used and the results of two separate BER runs are overlaid on top of the ROC curves for both systems. The close correlation observed, gives an indication that evaluation of OSNR, when estimated autocorrelation values are used in the MAMF design, could also produce good correspondence of the probability of error and BER. In the next section, it will be shown that that is indeed the case.

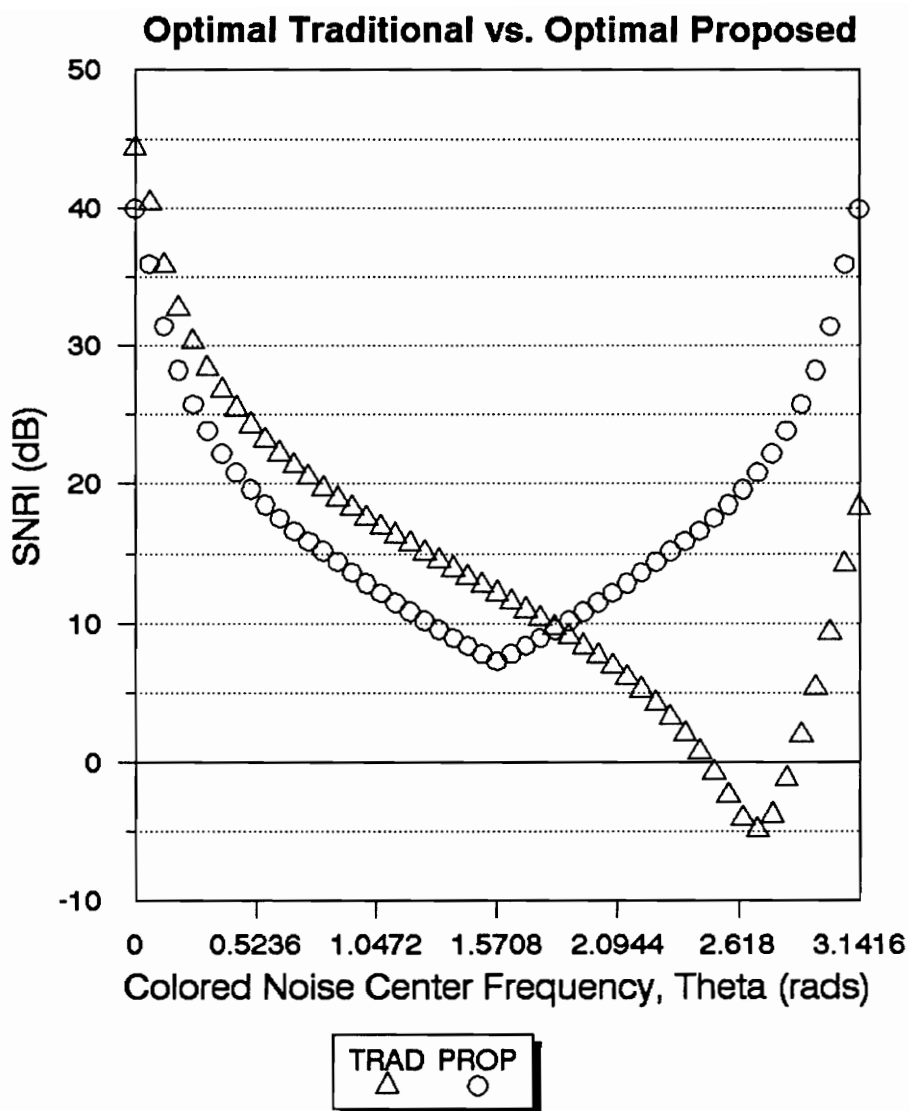


FIGURE 19. PLOT OF SNRI vs. CENTER FREQUENCY θ FOR $\rho = 0.95$
 TRADITIONAL SYSTEM IS OPTIMIZED AT $\theta = 0$
 PROPOSED SYSTEM OPTIMAL

Table 1. Bit Errors / 1000 Bits vs. ISNR, Run @ $\theta = 0^\circ$, with $\rho = 0.95$.
Traditional system: Optimized for $\theta = 0^\circ$
Proposed system: Optimal proposed signal vectors

System	Error Type	ISNR (dB)					
		0	-10	-20	-30	-40	-50
Trad.	1 0	0	0	0	0	27	150
	0 1	0	0	0	0	26	155
Prop.	1 0	0	0	0	0	76	196
	0 1	0	0	0	0	75	185
Trad.	1 0	0	0	0	0	30	148
	0 1	0	0	0	0	32	158
Prop.	1 0	0	0	0	2	87	181
	0 1	0	0	0	2	89	188

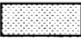
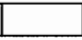
Actual AC values  Estimated AC values 

Table 2. Bit Errors / 1000 Bits vs. ISNR, Run @ $\theta = 105.4^\circ$, with $\rho = 0.95$.
Traditional system: Optimized for $\theta = 0^\circ$
Proposed system: Optimal proposed signal vectors

System	Error Type	ISNR (dB)					
		0	-10	-20	-30	-40	-50
Trad.	1 0	0	85	184	232	241	150
	0 1	1	87	194	232	241	250
Prop.	1 0	1	87	189	232	243	245
	0 1	1	86	196	232	240	252
Trad.	1 0	2	92	195	241	251	244
	0 1	2	92	196	229	250	248
Prop.	1 0	12	109	206	235	245	252
	0 1	12	114	208	233	243	248




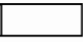
Actual AC values  Estimated AC values 

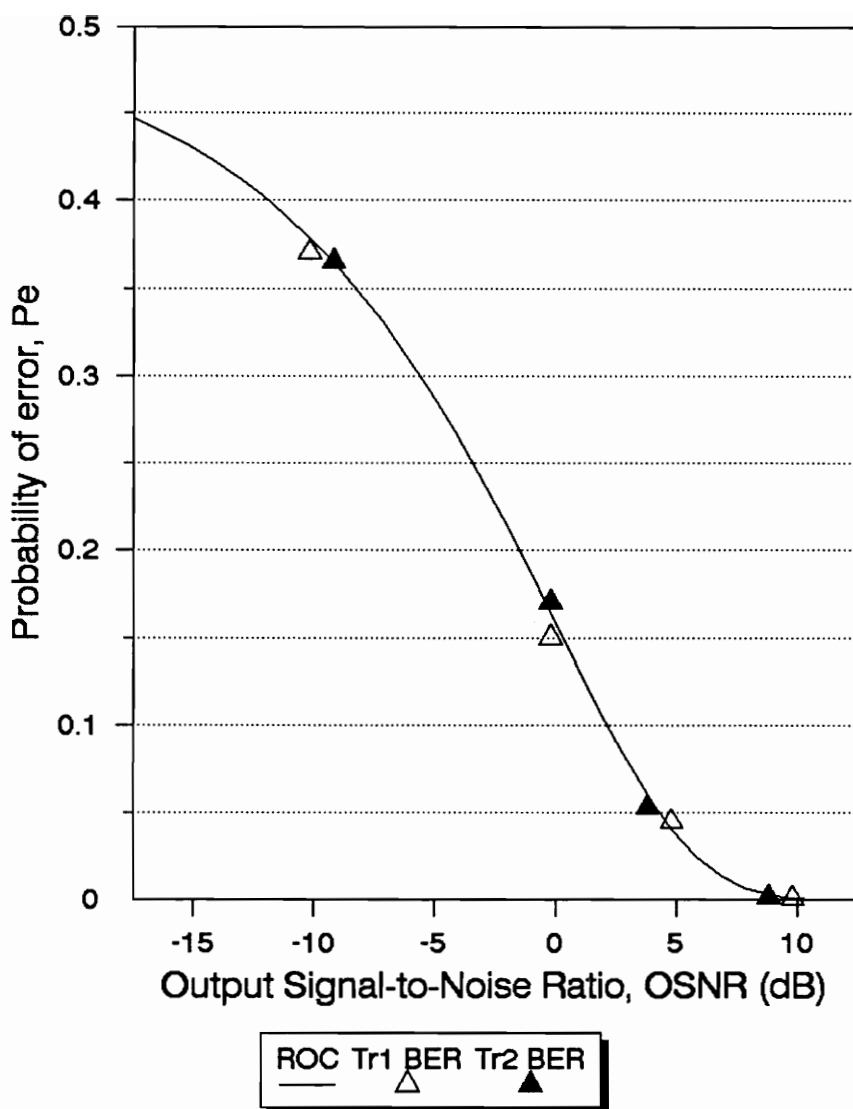
Table 3. Bit Errors / 1000 Bits vs. ISNR, Run @ $\theta = 135^\circ$, with $\rho = 0.95$.

Traditional system: Optimized for $\theta = 0^\circ$

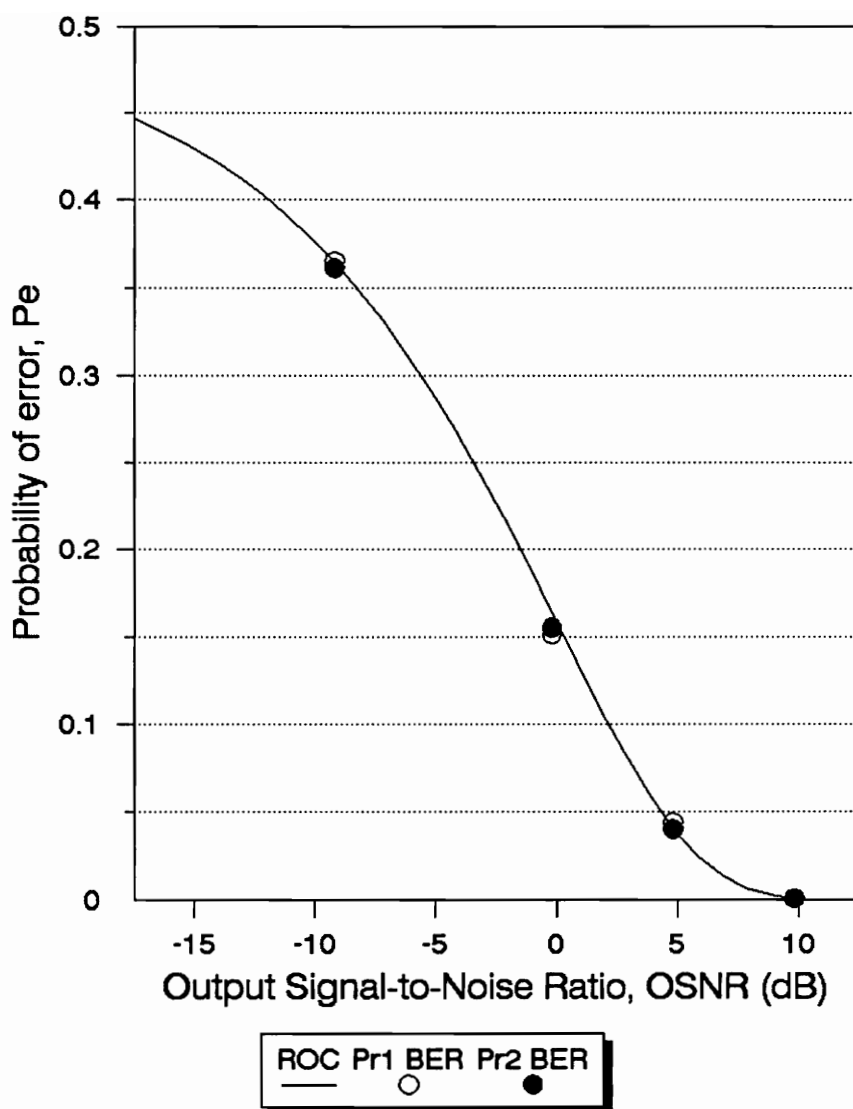
Proposed system: Optimal proposed signal vectors

System	Error Type	ISNR (dB)					
		0	-10	-20	-30	-40	-50
Trad.	1 0	46	167	219	245	247	241
	0 1	44	164	218	238	251	257
Prop.	1 0	0	13	138	217	234	247
	0 1	0	13	138	219	240	242
Trad.	1 0	53	174	232	233	247	249
	0 1	51	170	234	242	257	249
Prop.	1 0	0	20	144	208	246	252
	0 1	0	20	152	213	239	248

Actual AC values  Estimated AC values 



**FIGURE 20. COMPARISON BETWEEN ROC + BER RESULTS
TRADITIONAL SYSTEM
ACTUAL AUTOCORRELATION SEQUENCE USED**



**FIGURE 21. COMPARISON BETWEEN ROC + BER RESULTS
PROPOSED SYSTEM
ACTUAL AUTOCORRELATION SEQUENCE USED**

4.2.3 Optimal Proposed System vs. Traditional System

In an attempt to fairly compare the two MAMF communication systems the encoding signal vectors were chosen to be the same.

Thus, as in the previous section, the proposed system uses the optimal encoding signal vectors described by (4.4) and (4.5). Also, for a practical comparison of the two communication systems, the traditional system uses,

$$\mathbf{s}_0^{(t)} = [-.34506 \ 0 \ -.93858 \ 0 \ 0 \ -.93858 \ 0 \ -.34506]^T \quad (4.7)$$

to encode the "0" bit whereas the signal vector that encodes the "1" bit satisfies (4.6) for optimal detector performance.

First, the SNRI is computed for each system as a function of the colored noise center frequency θ , using actual autocorrelation values. The procedure is then repeated for estimated autocorrelation values. In this procedure, the $\hat{\text{SNRI}}$ (see Section 2.4.3) for each system is computed for a noise realization θ and the calculation is repeated 1000 times each time with a newly estimated autocorrelation sequence. The mean $\hat{\text{SNRI}}$ is then calculated and graphed.

This whole procedure is first followed for narrowband noise, where $\rho = 0.95$. It is then followed for more broadband noise, where $\rho = 0.8$ and $\rho = 0.5$, in order to obtain a more complete picture of the behavior of both communication systems.

Thus, Figure 22 presents the SNRI curves for both systems using actual autocorrelation values for $\rho = 0.95$, whereas Figure 23 presents the $\hat{\text{SNRI}}$ using estimated autocorrelation values. Figures 24 and 25 present the SNRI curves for actual and estimated autocorrelation values respectively for $\rho = 0.8$, while Figures 26 and 27 show the SNRI curves for $\rho = 0.5$.

Note that as ρ decreases and the noise becomes more broadband, the actual SNRI and mean $\hat{\text{SNRI}}$ values also decrease. This can be explained by looking at the signal spectrum. In this case, it is evident that the signal magnitude response is broadband since an increase in the bandwidth of the noise

makes the noise less distinctive, thus decreasing the SNRI.

Also notice that in Figures 22, 24, and 26 where actual autocorrelation values are used for different ρ , the traditional communication system outperforms the proposed system. This is an important observation when taking into consideration that the optimal proposed signal vectors described by (4.4) and (4.5) are used. From Figures 23, 25, and 27, where estimated autocorrelation values are used, the conclusion can be drawn that the proposed communication system is more robust in the sense that it deteriorates to a much lesser degree than the traditional system. For instance, the proposed system is clearly more desirable when θ is in the range of 0° - 30° , while the traditional system performs better in the 75° - 110° range.

Next, the BER are calculated for the aforementioned conditions. It should be mentioned that the BER values presented are the average of 5 statistically equivalent runs, thus providing a better image of consistency in the results. Tables 4, 5, and 6 present BER for both actual and estimated autocorrelation values for θ 's of 0° , 90° , and 180° respectively, for $\rho = 0.95$. Tables 7, 8, and 9 present the BER for $\rho = 0.8$ and Tables 10, 11, and 12 present the BER for $\rho = 0.5$. The BER corresponds directly to the behavior of the mean $\hat{\text{SNRI}}$ curves in the following manner.

Note from Figure 23 that the mean $\hat{\text{SNRI}}$ for the proposed system for 90° is about 6.3 dB and the mean $\hat{\text{SNRI}}$ for the traditional system is approximately 9.8 dB. From Table 5 for an ISNR of -10 dB, the BER total of 165 ($=84+81$) is computed for the traditional system, and the BER total of 266 ($=129+137$) is computed for the proposed system. The mean OSNR is -3.7 dB ($= -10+6.3$) for the proposed system and -0.2 dB ($= -10+9.8$) for the traditional system. By referring to the ROC curves given in Figures 9 or 11, one can find a $P_e = 0.260$ for the proposed system and a $P_e = 0.165$ for the traditional system, thus confirming the previous BER values.

For an additional example let us refer to Figure 27. For a noise realization at $\theta = 0^\circ$ and at $\rho = 0.5$ the mean $\hat{\text{SNRI}}$ is 7.1 dB for the proposed system, and 6.0 dB for the traditional system. Hence, for an ISNR of -20 dB, the

mean $\hat{\text{OSNR}}$ is -12.9 dB and -14.0 dB for the proposed and traditional systems respectively. By referring to the ROC curve in Figures 9 or 11, a $P_e = 0.41$ and a $P_e = 0.42$ is obtained for the proposed and the traditional system respectively. These values correspond nicely to the BER total of 400 ($=199+201$) for the proposed system and 427 ($= 212+215$) for the traditional system as taken from Table 10.

In an effort to display the correlation between the theoretically derived probability of error P_e , and the practically obtained BER when the noise autocorrelation is estimated, Figures 28 and 29 present the results of two separate BER simulations overlaid on the ROC curve for the traditional and the proposed communication system respectively. Figures 20 and 21 presented the same graphs when the actual noise autocorrelation was used for the BER. There is, of course, some deterioration of the OSNR, when the noise autocorrelation sequence is estimated. Since $\hat{\text{OSNR}}$ is an estimate, an estimate of the probability of error \hat{P}_e , is obtained. This deterioration is the result of the noise autocorrelation estimator. The BER values in Figures 28 and 29 will approach the ROC curve as the number of noise samples used by the estimator increases as seen from Section 2.3.

In summary, there are certain areas in the colored noise center frequency spectrum where the proposed system outperforms the traditional system and vice versa. Therefore, the need arises for a method which when implemented would be able to make a decision, based on the mean $\hat{\text{SNRI}}$ curves, about which system to use for better detection. This method is examined in the next chapter.

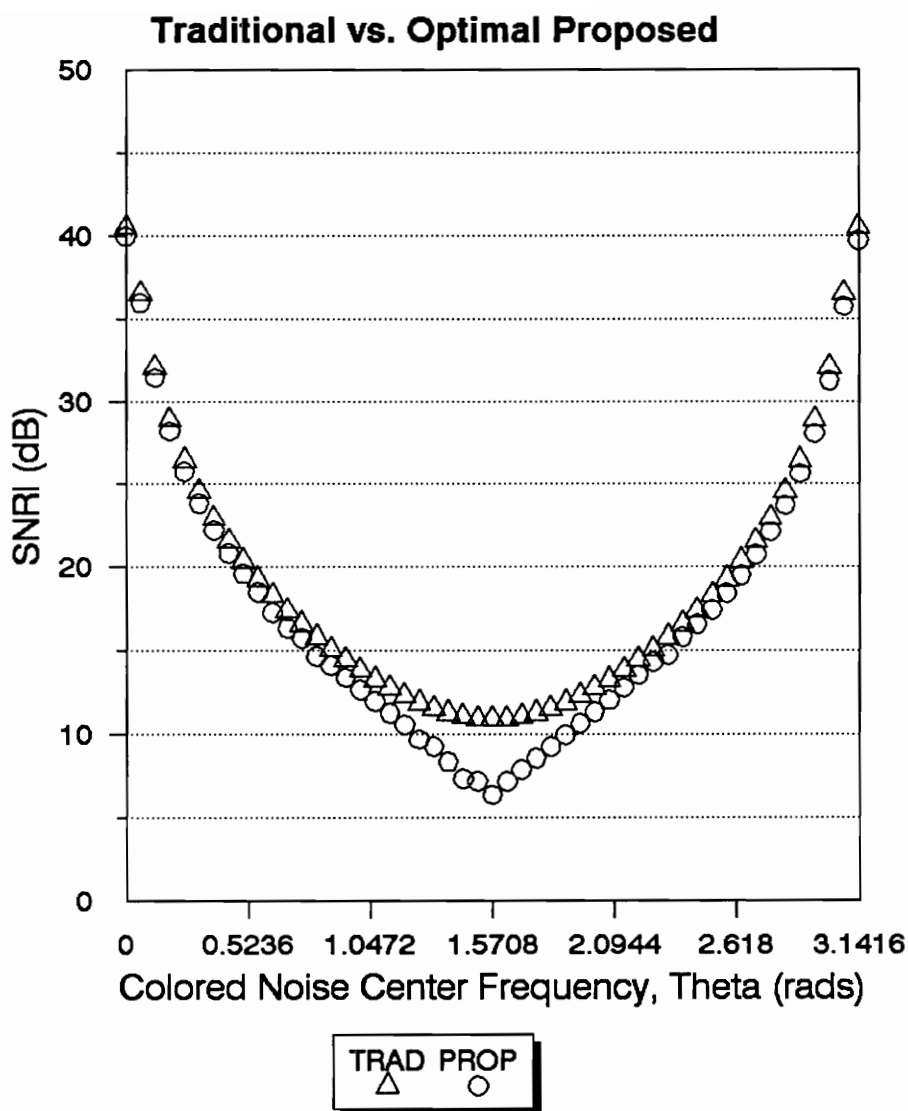


FIGURE 22. PLOT OF SNRI vs. CENTER FREQUENCY θ FOR $\rho = 0.95$
 TRAD. & PROP. SYSTEMS USE OPTIMAL PROPOSED VECTORS
 w/ ACTUAL AUTOCORRELATION SEQUENCE

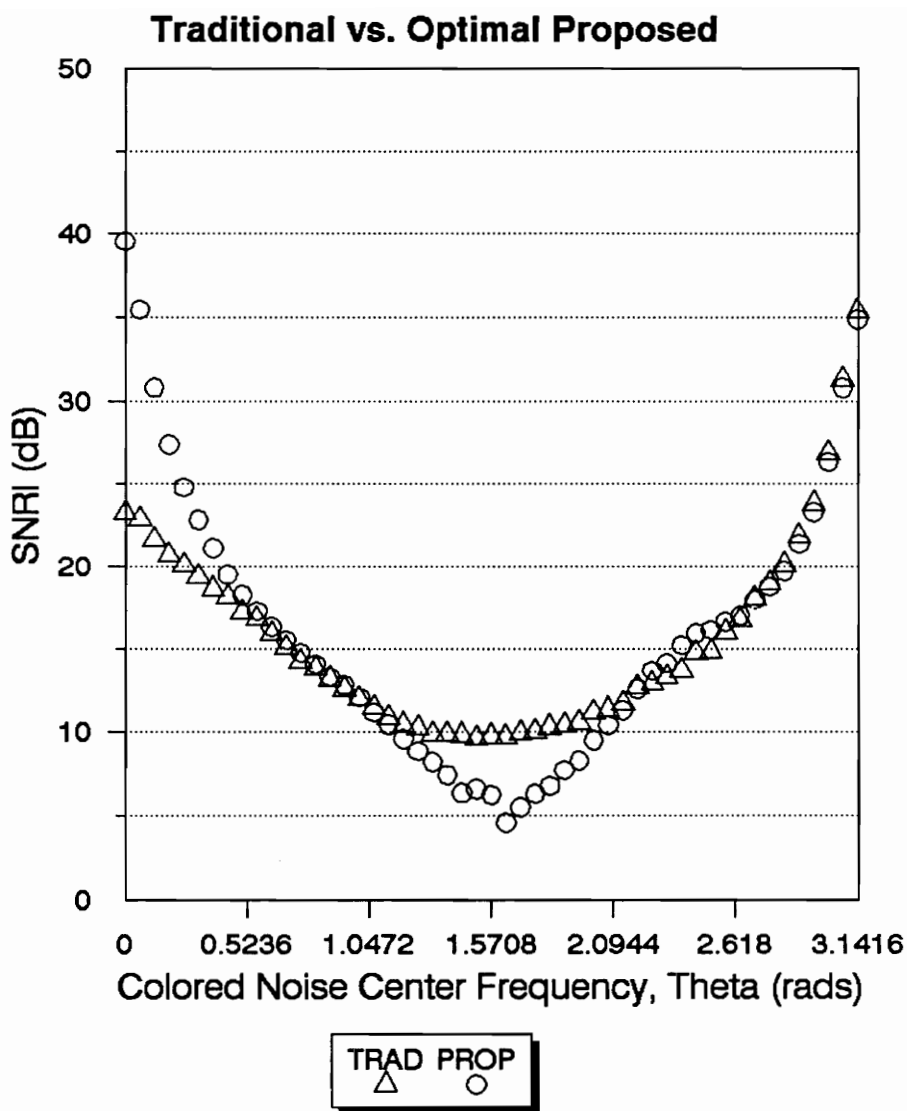


FIGURE 23. PLOT OF MEAN $\hat{\text{SNRI}}$ vs. CENTER FREQUENCY θ FOR $\rho = 0.95$
 TRAD. & PROP. SYSTEMS USE OPTIMAL PROPOSED VECTORS
 w/ ESTIMATED AUTOCORRELATION SEQUENCE

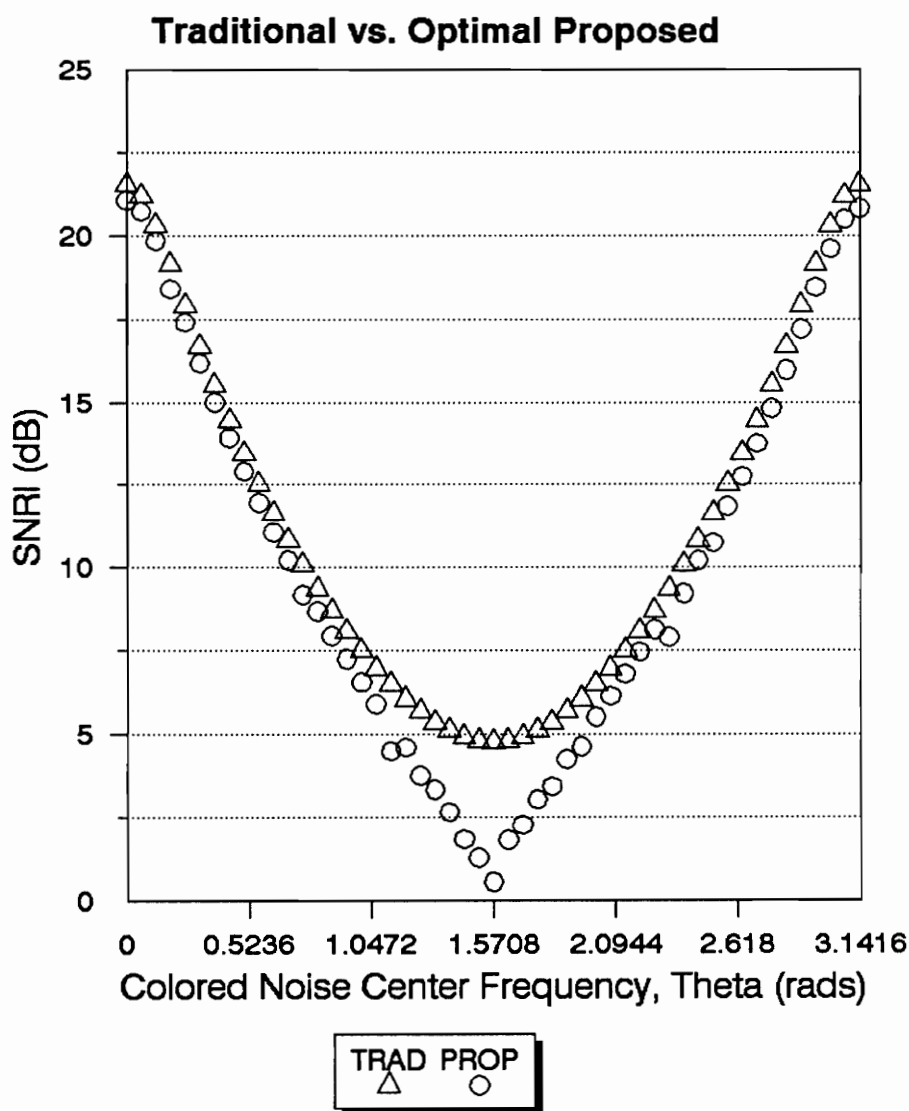


FIGURE 24. PLOT OF SNRI vs. CENTER FREQUENCY θ FOR $\rho = 0.8$
 TRAD. & PROP. SYSTEMS USE OPTIMAL PROPOSED VECTORS
 w/ ACTUAL AUTOCORRELATION SEQUENCE

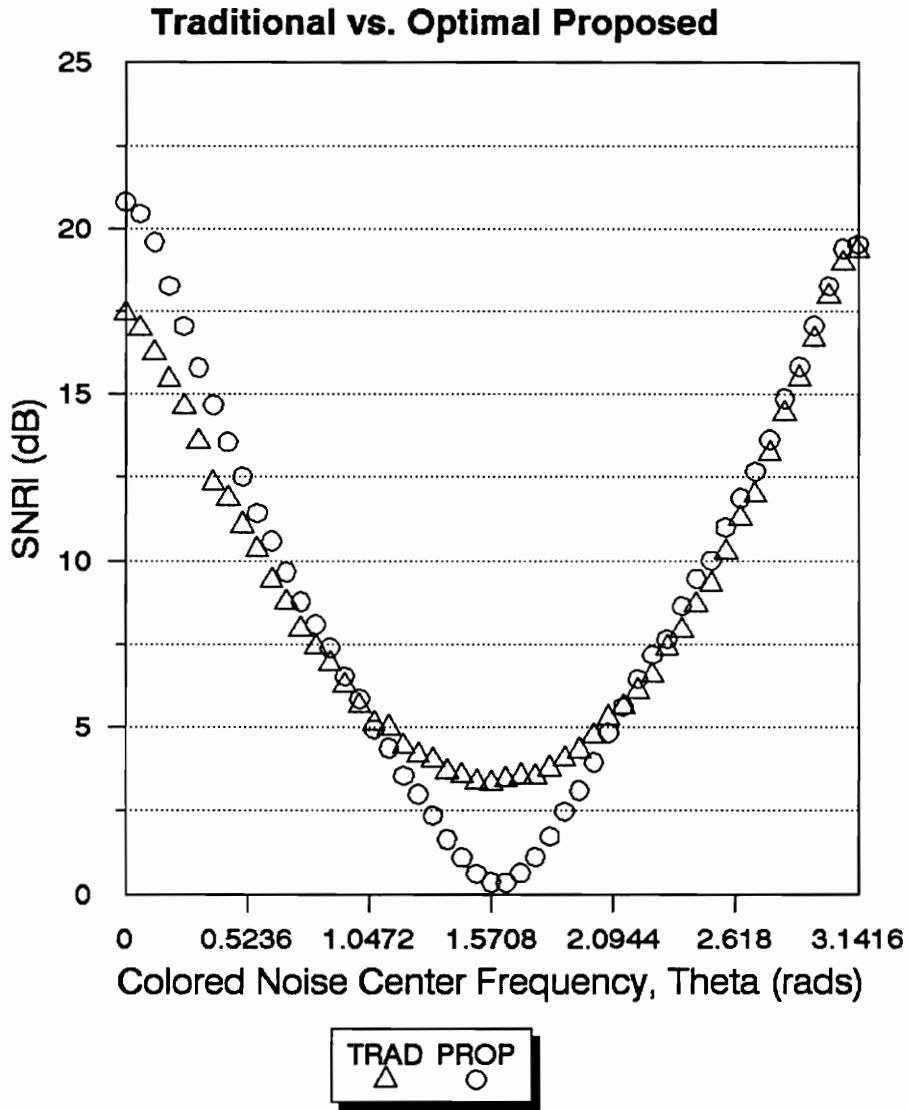


FIGURE 25. PLOT OF MEAN $\hat{\text{SNRI}}$ vs. CENTER FREQUENCY θ FOR $\rho = 0.8$
 TRAD. & PROP. SYSTEMS USE OPTIMAL PROPOSED VECTORS
 w/ ESTIMATED AUTOCORRELATION SEQUENCE

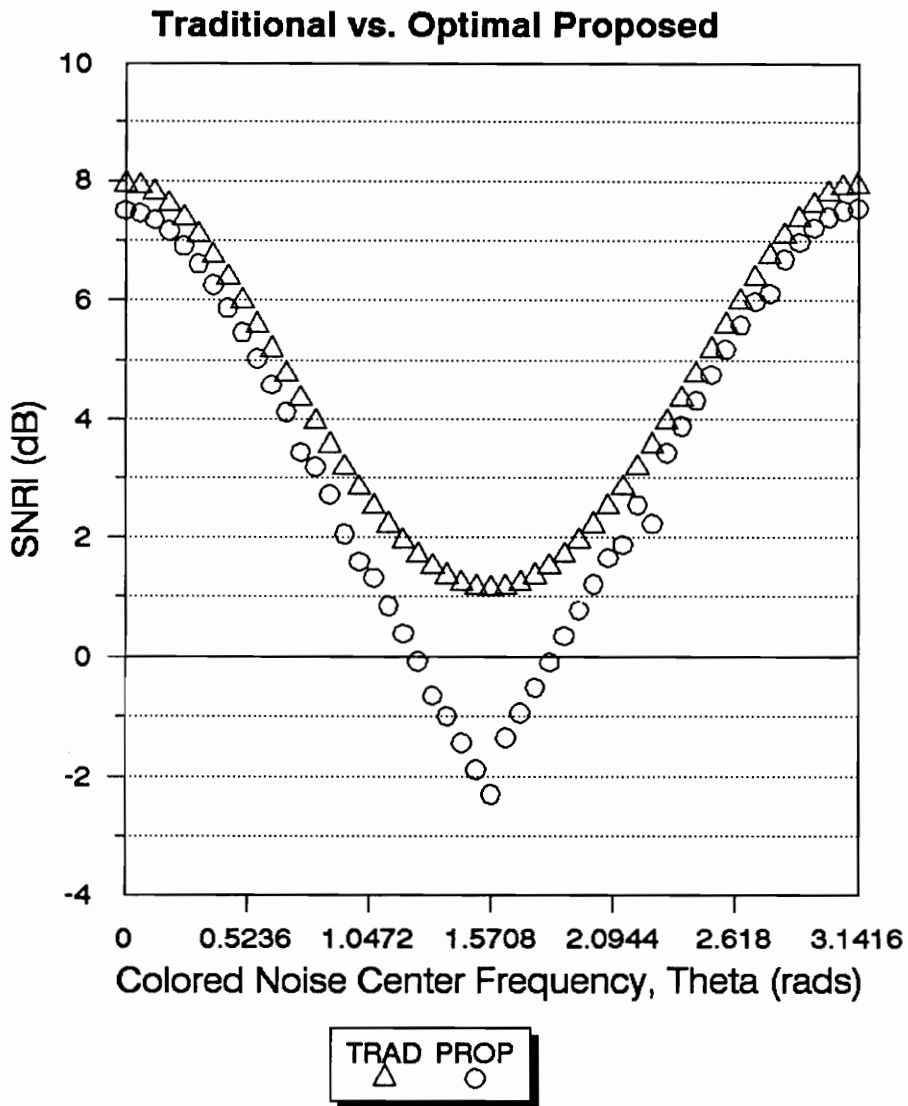


FIGURE 26. PLOT OF SNRI vs. CENTER FREQUENCY θ FOR $\rho = 0.5$
 TRAD. & PROP. SYSTEMS USE OPTIMAL PROPOSED VECTORS
 w/ ACTUAL AUTOCORRELATION SEQUENCE

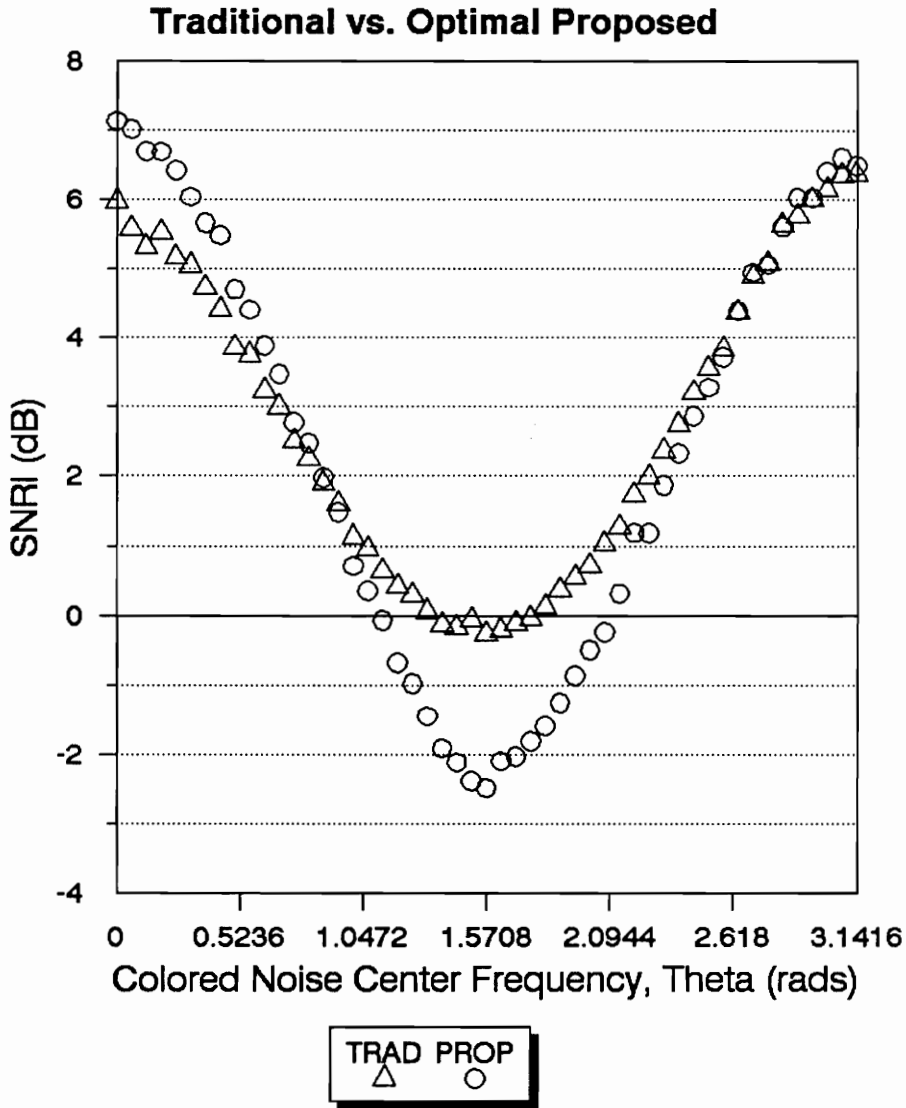


FIGURE 27. PLOT OF MEAN $\hat{\text{SNRI}}$ vs. CENTER FREQUENCY θ FOR $\rho = 0.5$
 TRAD. & PROP. SYSTEMS USE OPTIMAL PROPOSED VECTORS
 w/ ESTIMATED AUTOCORRELATION SEQUENCE

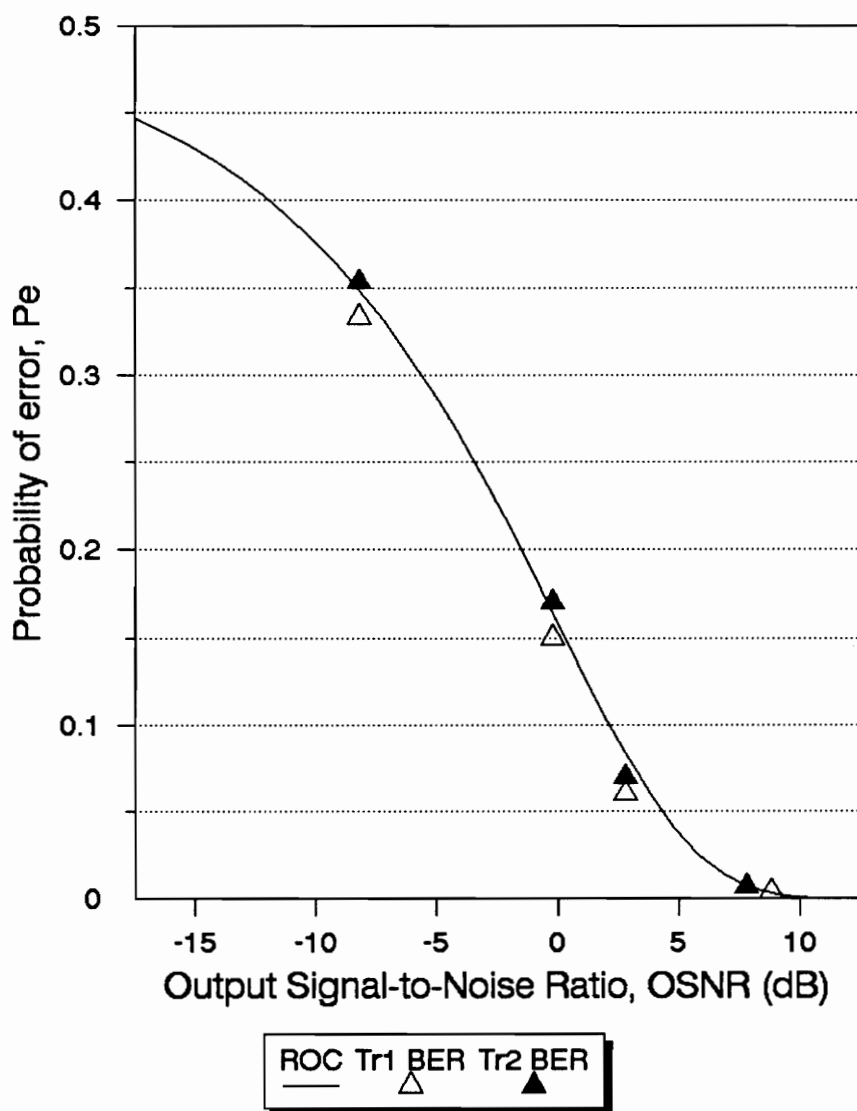
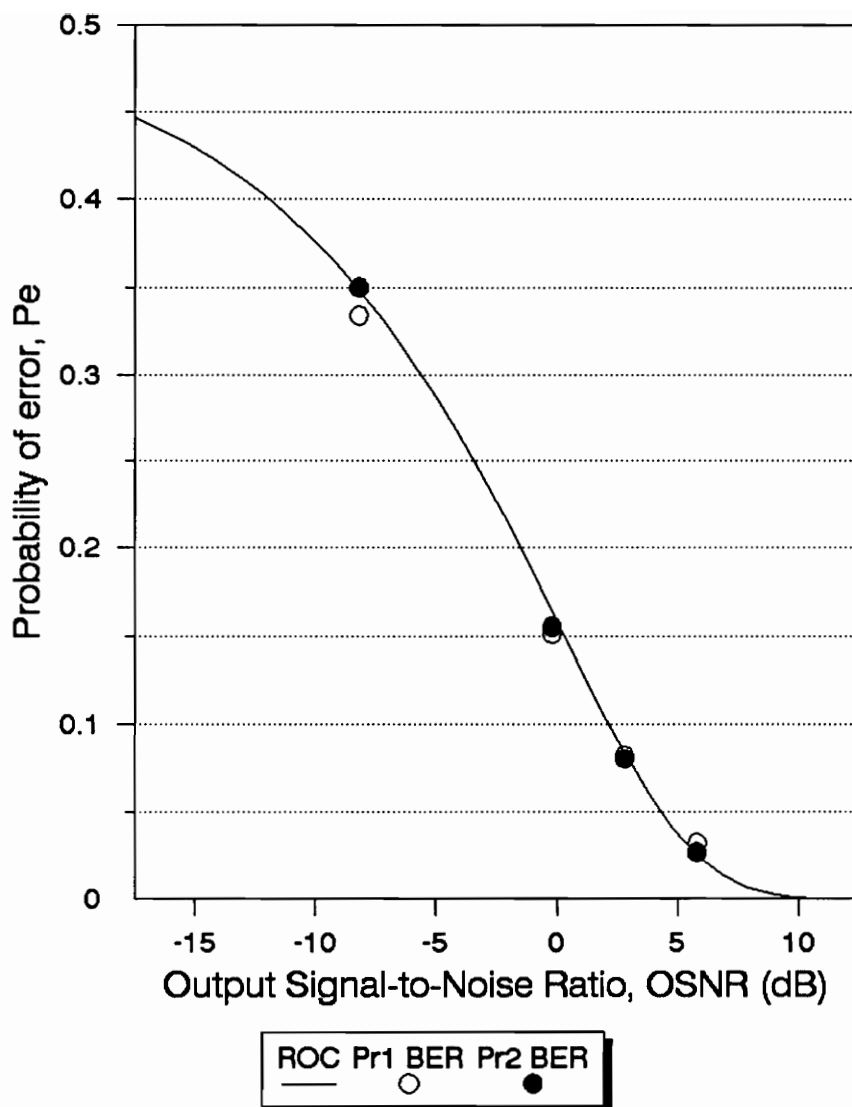


FIGURE 28. COMPARISON BETWEEN ROC + BER RESULTS
TRADITIONAL SYSTEM
ESTIMATED **AUTOCORRELATION SEQUENCE USED**



**FIGURE 29. COMPARISON BETWEEN ROC + BER RESULTS
PROPOSED SYSTEM
ESTIMATED AUTOCORRELATION SEQUENCE USED**

Table 4. Bit Errors / 1000 Bits vs. ISNR, Run @ $\theta = 0^\circ$, with $\rho = 0.95$.

Traditional system: Optimal proposed signal vectors

Proposed system: Optimal proposed signal vectors

System	Error Type	ISNR (dB)					
		0	-10	-20	-30	-40	-50
Trad.	1 0	0	0	0	0	73	187
	0 1	0	0	0	0	72	195
Prop.	1 0	0	0	0	1	76	189
	0 1	0	0	0	0	81	195
Trad.	1 0	0	1	27	160	221	241
	0 1	0	0	34	174	227	255
Prop.	1 0	0	0	0	2	79	195
	0 1	0	0	0	0	96	186

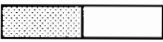
Actual AC values  Estimated AC values

Table 5. Bit Errors / 1000 Bits vs. ISNR, Run @ $\theta = 90^\circ$, with $\rho = 0.95$.

Traditional system: Optimal proposed signal vectors

Proposed system: Optimal proposed signal vectors

System	Error Type	ISNR (dB)					
		0	-10	-20	-30	-40	-50
Trad.	1 0	0	69	179	226	257	245
	0 1	0	65	184	223	246	251
Prop.	1 0	10	126	209	239	254	250
	0 1	8	128	211	237	247	246
Trad.	1 0	1	84	186	220	256	246
	0 1	1	81	198	234	255	248
Prop.	1 0	14	129	204	231	245	253
	0 1	11	137	212	239	257	241

Actual AC values  Estimated AC values

Table 6. Bit Errors / 1000 Bits vs. ISNR, Run @ $\theta = 180^\circ$, with $\rho = 0.95$.

Traditional system: Optimal proposed signal vectors

Proposed system: Optimal proposed signal vectors

System	Error Type	ISNR (dB)					
		0	-10	-20	-30	-40	-50
Trad.	1 0	0	0	0	0	73	182
	0 1	0	0	0	0	74	188
Prop.	1 0	0	0	0	1	83	188
	0 1	0	0	0	0	88	195
Trad.	1 0	0	0	0	21	133	197
	0 1	0	0	0	13	134	210
Prop.	1 0	0	0	0	24	131	207
	0 1	0	0	0	15	134	209


Actual AC values  Estimated AC values

Table 7. Bit Errors / 1000 Bits vs. ISNR, Run @ $\theta = 0^\circ$, with $\rho = 0.8$.

Traditional system: Optimal proposed signal vectors

Proposed system: Optimal proposed signal vectors

System	Error Type	ISNR (dB)					
		0	-10	-20	-30	-40	-50
Trad.	1 0	0	0	58	168	229	242
	0 1	0	0	61	187	222	233
Prop.	1 0	0	0	63	174	227	245
	0 1	0	0	70	195	223	236
Trad.	1 0	4	21	110	199	234	235
	0 1	2	23	119	202	233	233
Prop.	1 0	0	1	63	178	239	247
	0 1	0	0	69	183	228	235

Actual AC values

--	--

 Estimated AC values

Table 8. Bit Errors / 1000 Bits vs. ISNR, Run @ $\theta = 90^\circ$, with $\rho = 0.8$.

Traditional system: Optimal proposed signal vectors

Proposed system: Optimal proposed signal vectors

System	Error Type	ISNR (dB)					
		0	-10	-20	-30	-40	-50
Trad.	1 0	23	147	213	235	249	254
	0 1	20	145	217	239	255	253
Prop.	1 0	71	182	226	237	251	251
	0 1	67	183	232	245	240	260
Trad.	1 0	42	163	214	241	252	243
	0 1	33	159	213	228	249	255
Prop.	1 0	70	191	220	238	254	267
	0 1	74	183	221	235	249	259


Actual AC values  Estimated AC values

Table 9. Bit Errors / 1000 Bits vs. ISNR, Run @ $\theta = 180^\circ$, with $\rho = 0.8$.
Traditional system: Optimal proposed signal vectors
Proposed system: Optimal proposed signal vectors

System	Error Type	ISNR (dB)					
		0	-10	-20	-30	-40	-50
Trad.	1 0	0	0	61	177	229	252
	0 1	0	0	62	175	229	243
Prop.	1 0	0	0	71	181	231	257
	0 1	0	0	67	189	234	247
Trad.	1 0	0	2	90	187	238	239
	0 1	0	5	87	190	233	245
Prop.	1 0	0	0	80	186	240	240
	0 1	1	2	87	191	235	237


Actual AC values  Estimated AC values

Table 10. Bit Errors / 1000 Bits vs. ISNR, Run @ $\theta = 0^\circ$, with $\rho = 0.5$.
Traditional system: Optimal proposed signal vectors
Proposed system: Optimal proposed signal vectors

System	Error Type	ISNR (dB)					
		0	-10	-20	-30	-40	-50
Trad.	1 0	2	112	197	229	250	254
	0 1	4	103	196	234	237	245
Prop.	1 0	3	117	197	234	243	253
	0 1	5	111	201	236	240	247
Trad.	1 0	18	121	212	247	234	246
	0 1	24	129	215	238	239	259
Prop.	1 0	6	105	199	232	240	257
	0 1	7	127	201	239	253	258

Actual AC values Estimated AC values

Table 11. Bit Errors / 1000 Bits vs. ISNR, Run @ $\theta = 90^\circ$, with $\rho = 0.5$.

Traditional system: Optimal proposed signal vectors

Proposed system: Optimal proposed signal vectors

System	Error Type	ISNR (dB)					
		0	-10	-20	-30	-40	-50
Trad.	1 0	63	180	226	244	256	246
	0 1	66	175	222	238	245	252
Prop.	1 0	108	189	238	249	255	247
	0 1	114	209	228	239	242	245
Trad.	1 0	77	173	235	251	247	245
	0 1	86	187	234	247	249	263
Prop.	1 0	111	191	236	247	229	254
	0 1	111	207	233	253	253	258


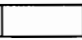
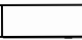
Actual AC values  Estimated AC values 

Table 12. Bit Errors / 1000 Bits vs. ISNR, Run @ $\theta = 180^\circ$, with $\rho = 0.5$.

Traditional system: Optimal proposed signal vectors

Proposed system: Optimal proposed signal vectors

System	Error Type	ISNR (dB)					
		0	-10	-20	-30	-40	-50
Trad.	1 0	2	111	195	229	238	252
	0 1	3	109	203	236	245	245
Prop.	1 0	4	115	202	225	239	250
	0 1	3	115	206	239	246	249
Trad.	1 0	12	134	205	236	248	255
	0 1	15	127	208	242	242	250
Prop.	1 0	11	128	200	232	251	255
	0 1	13	124	200	235	246	246

Actual AC values  Estimated AC values 

5.0 RECEIVER SELECTOR DESIGN

As seen from the SNRI curves and the BER results presented in the previous chapter, the proposed MAMF communication system deteriorates to a lesser degree, generally, than the traditional MAMF communication system under the use of estimated correlations. Hence, the proposed system appears to be more robust than the traditional system against changes in noise color. Nevertheless there are certain noise realizations θ , for instance when $75^\circ \leq \theta \leq 110^\circ$, for which the traditional system outperforms the proposed system.

Thus, in order to ensure the best possible probability of detection and discrimination of the transmitted bits, it is desirable as well as reasonable to design a selector whose responsibility would be to choose the MAMF receiver which performs better for an estimated noise realization $\hat{\theta}$ and $\hat{\rho}$. The vector entering the receiver is \mathbf{r}_a as seen from (2.19). The vector \mathbf{r}_a can be interpreted by the receiver as the traditional noise corrupted transmitted vector or the proposed noise corrupted transmitted vector depending on which is deemed most appropriate. Hence, this chapter first presents the estimation of the colored noise center frequency and bandwidth parameters, θ and ρ respectively. Next, based on the estimates $\hat{\theta}$ and $\hat{\rho}$, a decision can be made on which system performs better by utilizing the SNRI data that has been obtained already under the same autocorrelation estimator conditions (Figures 23, 25, 27). The theory behind the aforementioned procedure as well as its implementation are also contained in this chapter which concludes with BER results obtained in order to compare the traditional MAMF receiver, the proposed MAMF receiver and the [traditional/proposed] MAMF receiver in which the selector is incorporated.

5.1 NOISE CENTER FREQUENCY & BANDWIDTH ESTIMATOR

In a practical implementation, the only data available at the receiver is the 16-dimensional measurement vector \mathbf{r}_a as given in (2.19). The Toeplitz noise autocorrelation matrix \mathbf{R}_w is constructed from the noise vector \mathbf{w}_g , but no other information concerning the noise is available. In order to be able to make a decision on which communication system to pick for better detection, accurate estimates of the noise bandwidth and center frequency parameters must be obtained. This can be accomplished by the Burg method, an autoregressive (AR) spectral estimation method. This particular method is used because narrowband colored noise is well described by taking a Gaussian white noise process with $\sigma^2 = 1$ and coloring it with an autoregressive Infinite Impulse Response (IIR) digital filter as used and described in Section 3.1.

The Burg method uses the noise samples w_n to estimate the reflection coefficients $\{k_1, k_2, \dots, k_p\}$ and then uses the Levinson algorithm (Appendix B) to obtain the AR parameter estimates. The reflection coefficient estimates are calculated by minimizing estimates of the prediction error power for different order predictors in a recursive manner. Specifically, the Burg method for estimation of the AR parameters of an AR(p) filter is [6],

$$\hat{r}_w(0) = \frac{1}{N} \sum_{n=0}^{N-1} |w_n|^2 \quad (5.1)$$

with

$$\begin{aligned} \hat{\rho}_0 &= \hat{r}_w(0) \\ \hat{e}_{0,n}^f &= w_n \quad n = 1, 2, \dots, N-1 \\ \hat{e}_{0,n}^b &= w_n \quad n = 0, 1, \dots, N-2 \end{aligned}$$

where $N = 8$. Then,

$$\hat{k}_k = \frac{-2 \sum_{n=k}^{N-1} \hat{e}_{k-1,n}^f (\hat{e}_{k-1,n-1}^b)^*}{\sum_{n=k}^{N-1} (|\hat{e}_{k-1,n}^f|^2 + |\hat{e}_{k-1,n-1}^b|^2)} \quad k = 1, 2, \dots, p \quad (5.2)$$

$$\hat{\rho}_k = (1 - |\hat{k}_k|^2) \hat{\rho}_{k-1} \quad (5.3)$$

$$\hat{a}_{k,i} = \begin{cases} \hat{a}_{k-1,i} + \hat{k}_k \hat{a}_{k-1,k-i}^* & \text{for } i = 1, 2, \dots, k-1 \\ \hat{k}_k & \text{for } i = k \end{cases} \quad (5.4)$$

Notice that if $k = 1$, then $\hat{a}_{1,1} = \hat{k}_1$. Also,

$$\begin{aligned} \hat{e}_{k,n}^f &= \hat{e}_{k-1,n}^f + \hat{k}_k \hat{e}_{k-1,n-1}^b & n = k+1, k+2, \dots, N-1 \\ \hat{e}_{k,n}^b &= \hat{e}_{k-1,n-1}^b + \hat{k}_k^* \hat{e}_{k-1,n}^f & n = k, k+1, \dots, N-2 \end{aligned} \quad (5.5)$$

The Burg method yields estimated poles that are on or inside the unit circle due to the property $|\hat{k}_k| \leq 1$. Therefore a minimum-phase (stable) AR digital filter can be associated with this method. Since an AR(2) model is desirable, the filter has a transfer function described by,

$$\begin{aligned} H(z) &= \frac{b_0 z^2}{(z - \hat{z}_1)(z - \hat{z}_2)} \\ &= \frac{b_0 z^2}{z^2 - (\hat{z}_1 + \hat{z}_2)z + \hat{z}_1 \hat{z}_2} \\ &= \frac{b_0 z^2}{z^2 + \hat{a}_{2,1}z + \hat{a}_{2,2}} \end{aligned} \quad (5.6)$$

where $b_0 = (1 - \hat{\rho}) |e^{j\hat{\theta}} - \hat{\rho} e^{-j\hat{\theta}}|$ and is defined such that the peak magnitude response is normalized to unity. In addition, \hat{z}_1 and \hat{z}_2 are the estimated poles, and $\hat{a}_{2,1}$ and $\hat{a}_{2,2}$ are the estimated AR coefficients which are computed using the Burg algorithm. From this point the coefficients $\hat{a}_{2,1}$ and $\hat{a}_{2,2}$ will be referred to as \hat{a}_1 and \hat{a}_2 respectively for simplicity. Hence, in order to compute

the estimated poles the quadratic equation can be used on the denominator of (5.6). Therefore,

$$\hat{z}_{1,2} = \frac{-\hat{a}_1 \pm \sqrt{\hat{a}_1^2 - 4\hat{a}_2}}{2} \quad (5.7)$$

If

$$\Delta \triangleq \sqrt{\hat{a}_1^2 - 4\hat{a}_2} \geq 0 \quad (5.8)$$

then the poles are real and (5.7) is used for the pole calculation. Automatically,

$$\hat{\rho} = \max\{ |\hat{z}_1|, |\hat{z}_2| \} \quad (5.9.a)$$

If $|\hat{z}_1| > |\hat{z}_2|$, then,

$$\hat{\theta} = \begin{cases} 0 & \text{if } \hat{z}_1 > 0 \\ \pi & \text{if } \hat{z}_1 < 0 \end{cases} \quad (5.10.b)$$

If $|\hat{z}_2| > |\hat{z}_1|$, then,

$$\hat{\theta} = \begin{cases} 0 & \text{if } \hat{z}_2 > 0 \\ \pi & \text{if } \hat{z}_2 < 0 \end{cases} \quad (5.10.c)$$

If $\Delta < 0$, the poles are complex conjugates. Then, as in (3.1), (5.6) can be manipulated to yield,

$$\hat{\rho} = \sqrt{\hat{a}_2} \quad (5.10.a)$$

$$\hat{\theta} = \cos^{-1} \left[-\frac{\hat{a}_1}{2\hat{\rho}} \right] \quad (5.10.b)$$

The colored noise center frequency and bandwidth parameter estimates can thus be computed from the results of the Burg algorithm according to equations (5.10) or (5.9).

5.2 DECISION ON MAMF RECEIVER SYSTEM

Under the circumstances presented in the previous section and having available the data given in the mean SNRI curves (see Chapter 4) one can pinpoint, in the area of operation, which of the two systems performs better in a statistical sense.

By using Figures 23, 25, and 27 one can create a 3-D graph (x vs. y vs. z) θ vs. mean SNRI vs. ρ that will serve as the database for the simulation. Since these figures were produced when both systems used the optimal proposed signal vector it is required that the actual bit transmission take place under the same circumstances. Thus, for a $\hat{\theta}$, three SNRI values can be obtained by linear interpolation, each corresponding to a different ρ (: 0.5, 0.8, 0.95). By using polynomial interpolation, $\overline{\text{SNRI}}$, the mean SNRI value corresponding to both $\hat{\theta}$ and $\hat{\rho}$ for a particular communication system, can be determined. Specifically, the Lagrange form of polynomial interpolation is used due to its accuracy and simplicity as compared to similar methods.

5.2.1 Lagrange Interpolation of mean SNRI data

Let us assume that $f(\rho_j)$ is the mean SNRI value of ρ_j at a specific $\hat{\theta}$. Then there is a unique interpolating polynomial such that $p(\rho_j) = f(\rho_j)$ for $0 \leq j \leq n$. This is the interpolating polynomial of the Lagrange form and is defined by the following relations [11],

$$p(\hat{\rho}) = \sum_{j=0}^n f(\rho_j) \beta_j(\hat{\rho}) \quad (5.11)$$

where,

$$\beta_j(\hat{\rho}) = \prod_{i=0, i \neq j}^n \frac{(\hat{\rho} - \rho_i)}{(\rho_j - \rho_i)} \quad i \neq j \quad (5.12)$$

and $n = 2$, $\rho_0 = 0.95$, $\rho_1 = 0.8$, $\rho_2 = 0.5$.

The Lagrange form was checked for accuracy over various colored noise center frequencies (θ 's). Figures 30, 31, and 32 present the $\overline{\text{SNRI}}$ curves for both communication systems using the Lagrange form for every ρ , for θ 's of 0° , 90° , and 180° respectively. Note that when $\hat{\rho} = \rho_2 = 0.5$, $\hat{\rho} = \rho_1 = 0.8$, and $\hat{\rho} = \rho_0 = 0.95$, $p(\hat{\rho}) = f(\rho_j)$ for $j = 0, 1, 2$ as expected.

There are a few interesting cases that should be mentioned which are the result of the interpolation technique and the particular ρ -points used. In Figure 30, when $0.53 \leq \hat{\rho} \leq 0.73$, then $p_T(\hat{\rho}) > p_P(\hat{\rho})$. In other words, the interpolated curves suggest that for $\theta = 0^\circ$, and for that specific range of $\hat{\rho}$'s, the traditional system performs better than the proposed system. In addition, note that for the interpolatory curve produced for the proposed system, a minimum appears at $\hat{\rho} = 0.56$. This indicates that the $\overline{\text{SNRI}}$ at $\rho = 0.56$ is less than the $\overline{\text{SNRI}}$ at $\rho = 0.5$ at a $\theta = 0^\circ$. The same observation can be made for the interpolatory curves produced for both systems in Figure 31, when $\theta = 90^\circ$. For Figures 30 and 31,

$$f(\rho_2) - p(0.56) \approx 0.1 \text{ dB} \quad (5.13)$$

The aforementioned situations contradict the previous observation made in Section 4.2.2, that mean SNRI decreases with decreasing ρ and are, obviously, unacceptable. The reason for the behaviors of the interpolatory curves of Figures 30 and 31, is the interpolation itself. The interpolation was conducted from only three available data points, or $n = 2$. This, in addition with ρ_j not being equally spaced, resulted in the aforementioned situations. For $n > 2$, the interpolation would be more accurate due to the larger number of true data points. With ρ_j equally spaced any undesirable minima in the interpolatory curves would most likely be avoided. In order to have so many true data points, SNRI curves would have to be created for that many ρ 's.

For Figure 31, the $\overline{\text{SNRI}}$ minimum at $\hat{\rho} = 0.56$ is present for both communication systems. Since the purpose of the selector is to choose one of the two systems, this unique behavior does not produce any major influence on the

decision and subsequently on the output of the selector. This is not the case with Figure 30. At $\theta = 0^\circ$ whenever $0.53 \leq \hat{\rho} \leq 0.73$, the selector will choose the traditional system over the proposed system, resulting in an incorrect decision. Since the $\overline{\text{SNRI}}$ values computed from the interpolation are also affected, a restriction can be included to set the $\overline{\text{SNRI}}$ at the value attained at $\rho = 0.5$, whenever it falls below it. If (5.13) is true, the small error produced can be considered an approximation error.

Hence, using the Lagrange method, a $\overline{\text{SNRI}}$ value can be obtained for both communication systems. By picking the largest value of the two, one can choose a communication system based on the estimates $\hat{\theta}$ and $\hat{\rho}$ as well as the SNRI database, for that particular bit transmission.

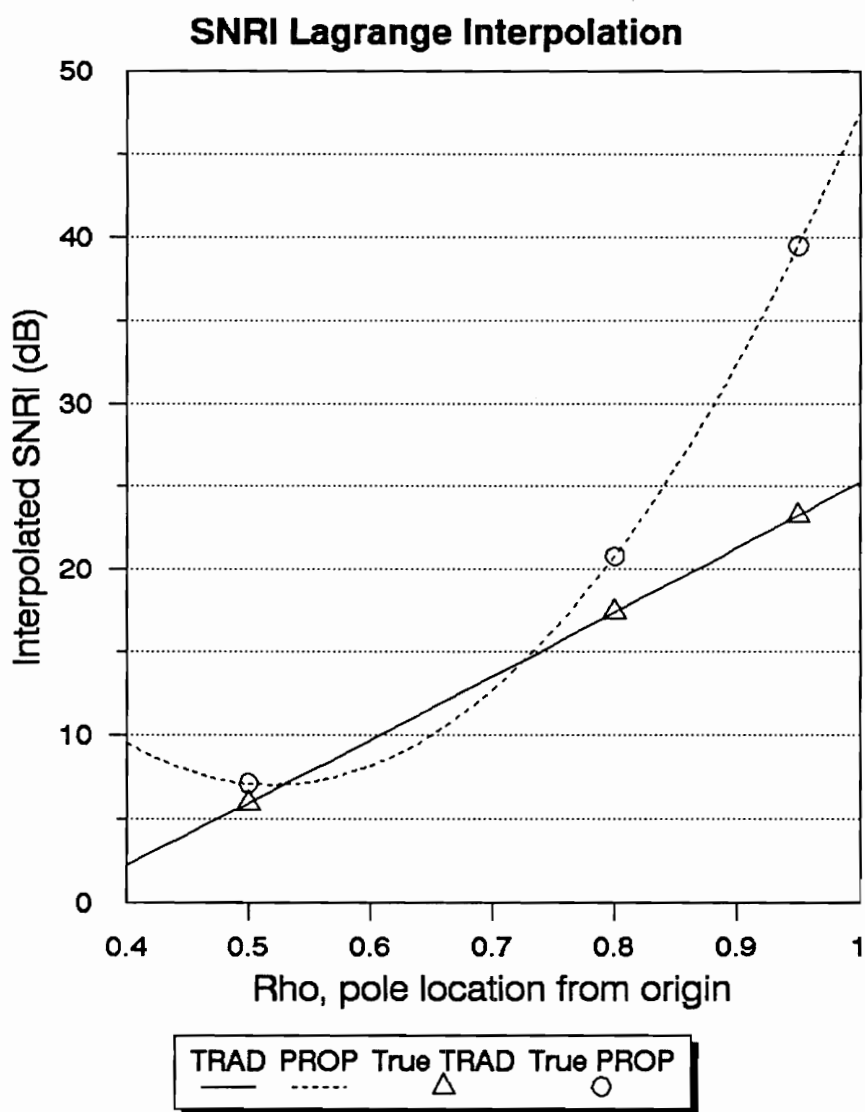


FIGURE 30. $\overline{\text{SNRI}}$ vs. NOISE BANDWIDTH PARAMETER $\hat{\rho}$
 INTERPOLATORY SNRI CURVE FOR $\theta = 0$
 TRADITIONAL & PROPOSED COMMUNICATION SYSTEMS

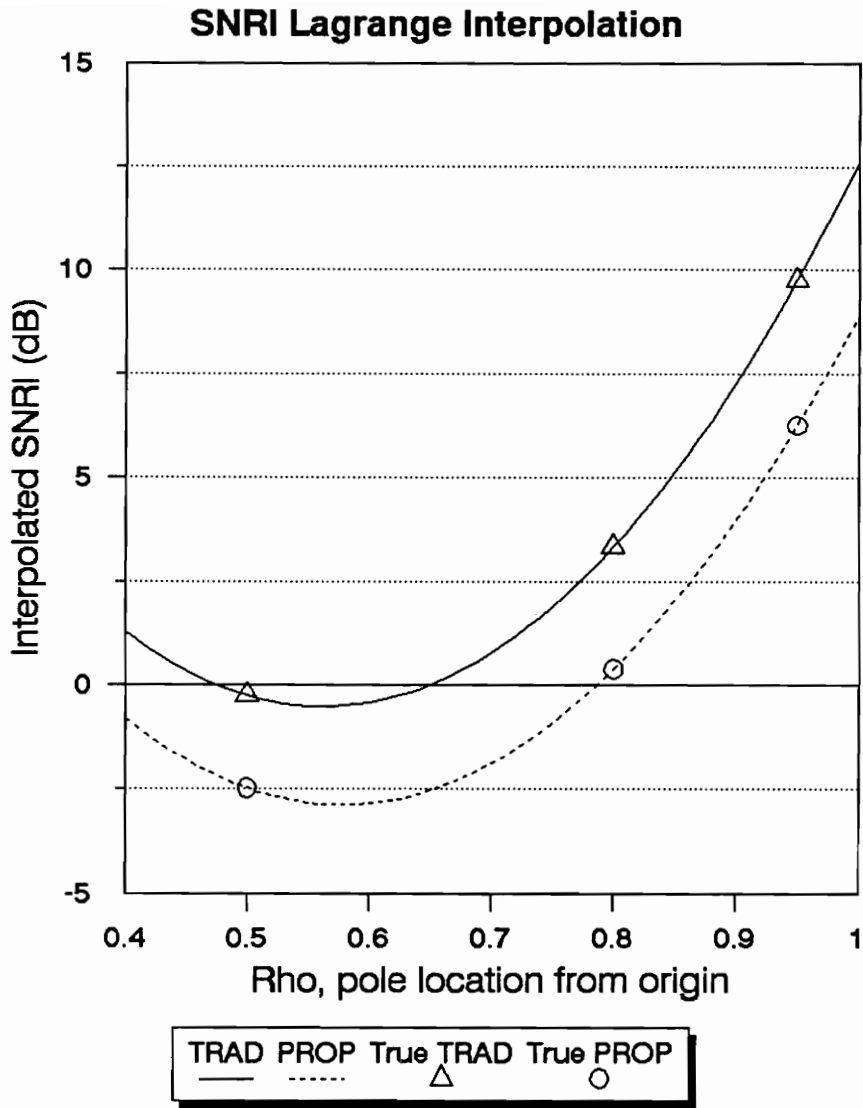


FIGURE 31. $\overline{\text{SNRI}}$ vs. NOISE BANDWIDTH PARAMETER $\hat{\rho}$
INTERPOLATORY SNRI CURVE FOR $\theta = \frac{\pi}{2}$
TRADITIONAL & PROPOSED COMMUNICATION SYSTEMS

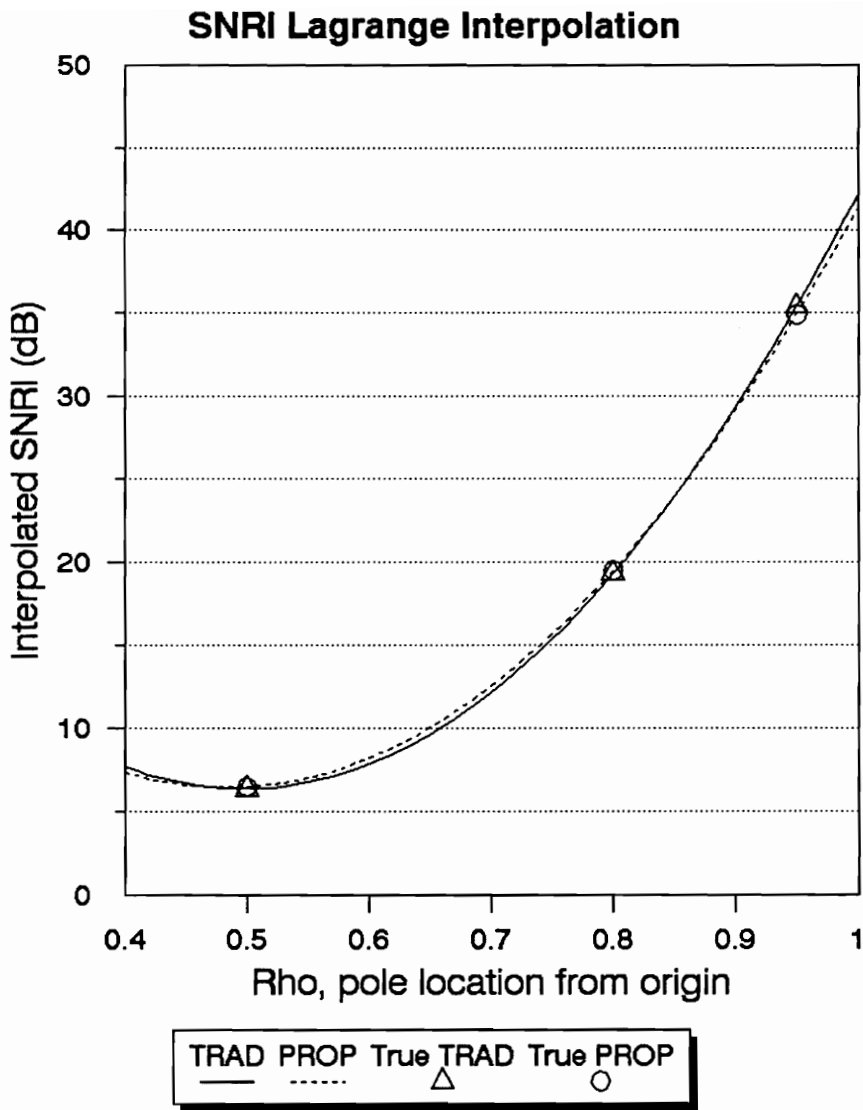


FIGURE 32. $\overline{\text{SNRI}}$ vs. NOISE BANDWIDTH PARAMETER $\hat{\rho}$
 INTERPOLATORY SNRI CURVE FOR $\theta = \pi$
 TRADITIONAL & PROPOSED COMMUNICATION SYSTEMS

5.2.2 Estimator / Selector Implementation

The estimator developed in Section 5.1 provides estimates of the bandwidth and frequency parameters of the colored noise. Based on these estimates as well as the mean SNRI curves (Figures 23, 25, and 27), a selector is designed which chooses a MAMF receiver system for the data processing. The selector compares the $\overline{\text{SNRI}}$ values for the proposed and the traditional systems at $\hat{\theta}$ and $\hat{\rho}$, and chooses the system with the highest value. In this way a minimum BER, on the average, can be assured for that particular bit transmission.

As a test, noise was generated with bandwidth parameter $\rho = 0.95$ and center frequency $\theta = 0^\circ$, $\theta = 90^\circ$, and $\theta = 126^\circ$, to create Tables 13, 14, and 15 respectively. For every bit transmitted the estimates $\hat{\theta}$ and $\hat{\rho}$ were computed using the estimator presented in Section 5.1. Based on these values the most appropriate communication system was picked and the BER were computed according to that communication system scheme as a function of ISNR. Every simulation consists of the transmission of 1000 bits, using estimated noise autocorrelation values in order to simulate as closely as possible a realistic situation. The BER presented in Tables 13B, 14B, and 15B are computed with both communication systems using the optimal proposed vectors and are the average of three simulations. Tables 13A, 14A, and 15A display the most vital statistics of these simulations as a function of ISNR.

Specifically, the maximum-likelihood estimates $\hat{\rho}$ and $\hat{\theta}$ and \hat{P}_e are presented. Let us assume that $\hat{\rho}_j$ and $\hat{\theta}_j$ are the colored noise bandwidth and center frequency parameter estimates, respectively, computed by the estimator for the j -th bit transmission. Then, $\hat{\rho}$ and $\hat{\theta}$ are computed in the following manner [10]:

$$\hat{\rho} = \frac{1}{B} \sum_{j=1}^B \hat{\rho}_j \quad (5.14.a)$$

$$\hat{\theta} = \frac{1}{B} \sum_{j=1}^B \hat{\theta}_j \quad (5.14.b)$$

where B is the number of bits transmitted (1000 in this case). Similarly, assume that $\hat{P}_{e,j}$ is the probability of error estimate calculated from the ROC curves in Figure 9 or 11, associated with the j -th bit, for either the traditional system or the proposed system. Then, \hat{P}_e is,

$$\hat{P}_e^{(P)} = \frac{1}{B} \sum_{j=1}^B \hat{P}_{e,j}^{(P)} \quad (\text{Proposed system}) \quad (5.14.c)$$

$$\hat{P}_e^{(T)} = \frac{1}{B} \sum_{j=1}^B \hat{P}_{e,j}^{(T)} \quad (\text{Traditional system}) \quad (5.14.d)$$

Equations (5.14.c) and (5.14.d), illustrate the computation method of \hat{P}_e for both the proposed system and the traditional system. Since for every bit transmission the selector chooses the best performing communication system in terms of SNRI based on $\hat{\theta}$ and $\hat{\rho}$, the \hat{P}_e for the selector system is computed in the following manner:

$$\hat{P}_e^{(S)} = \frac{1}{B} \sum_{j=1}^B \hat{P}_{e,j}^{(S)} \quad (5.14.e)$$

where

$$\hat{P}_{e,j}^{(S)} = \begin{cases} \hat{P}_{e,j}^{(P)} & \text{if the proposed system was picked for the } j\text{-th bit} \\ \hat{P}_{e,j}^{(T)} & \text{if the traditional system was picked for the } j\text{-th bit} \end{cases}$$

Furthermore, the number of times each communication system was picked for a specific number of bits transmitted is displayed in Tables 13A, 14A, and 15A as well as the average $\overline{\text{SNRI}}$ values for the traditional and proposed communication systems, as computed based on the estimated $\hat{\rho}$ and $\hat{\theta}$.

From Tables 13A, 14A, and 15A, one can observe the accuracy of the estimates. Let us consider the $\hat{\theta}$ in Table 13A. The estimate deviates from the true value about 4.3° whereas in Tables 14A and 15A, the estimate deviates only about 0.3° from the corresponding true value. Since the average $\hat{\theta}$ is computed according to (5.14.b), and θ is assumed throughout this work to be in the range

of $0 \leq \theta \leq \pi$, the average is shifted towards the positive side since there are no negative θ 's to compensate for. This accounts for the deviation of the $\hat{\theta}$ in Table 13A. Consider also the $\hat{\rho}$ in Table 13A. The $\hat{\rho}$ is very close to the true value of 0.95. However, in Tables 14A and 15A, the estimate deviates from the true value by about 0.07 units. The reason for this observation is that for $\theta = 0^\circ$ the poles of the colored noise AR(2) filter are real (Figure 6). Then, from Section 5.1, it is very likely that $\Delta \geq 0$ in (5.8) and thus (5.9) is used to obtain the estimated poles. As a consequence, the $\hat{\rho}$ is quite accurate. When $\theta = 90^\circ$ or $\theta = 126^\circ$ it is very unlikely that (5.9) will ever be used to provide the autoregressive parameter estimates. More likely, (5.10) is used, in an effort to fit a pair of complex conjugate poles to the noise data.

Table 13A. Statistics / 1000 Bits vs. ISNR, Estimated AC values.
True $\theta = 0^\circ$, True $\rho = 0.95$

ISNR (dB)	$\hat{\rho}$	$\hat{\theta}$ ($^\circ$)	T/P	T. $\overline{\text{SNRI}}$ (dB)	P. $\overline{\text{SNRI}}$ (dB)
-0	0.969	4.3	1/999	23.1752	38.9009
-10	0.970	4.5	1/999	23.1705	38.5903
-20	0.969	4.5	2/998	23.1439	38.6507
-30	0.970	4.5	1/999	23.1969	38.8273
-40	0.972	4.2	0/1000	23.2976	39.1324

Table 13B. Bit Errors / 1000 Bits vs. ISNR, Estimated AC values.
True $\theta = 0^\circ$, True $\rho = 0.95$

System	Error Type	ISNR (dB)				
		0	-10	-20	-30	-40
Proposed	0 1	0	0	0	1	73
	1 0	0	0	0	0	92
	$\hat{P}_e^{(P)}$	0.000	0.000	0.000	0.002	0.168
Traditional	0 1	0	1	30	157	225
	1 0	0	0	29	156	233
	$\hat{P}_e^{(T)}$	0.001	0.009	0.080	0.310	0.437
Selector	0 1	0	0	0	1	73
	1 0	0	0	0	1	92
	$\hat{P}_e^{(S)}$	0.000	0.000	0.001	0.002	0.168

Table 14A. Statistics / 1000 Bits vs. ISNR, Estimated AC values.
True $\theta = 90^\circ$, True $\rho = 0.95$

ISNR (dB)	$\hat{\rho}$	$\hat{\theta}$ ($^\circ$)	T/P	T. $\overline{\text{SNRI}}$ (dB)	P. $\overline{\text{SNRI}}$ (dB)
-0	0.890	90.7	992/8	9.2826	5.9476
-10	0.890	90.0	990/10	9.0455	5.7987
-20	0.890	90.4	993/7	9.7183	6.3421
-30	0.888	90.5	989/11	8.7189	5.4299
-40	0.892	89.9	995/5	8.9568	5.6398

Table 14B. Bit Errors / 1000 Bits vs. ISNR, Estimated AC values.
True $\theta = 90^\circ$, True $\rho = 0.95$

System	Error Type	ISNR (dB)				
		0	-10	-20	-30	-40
Proposed	0 1	16	139	208	262	248
	1 0	16	141	211	222	253
	$\hat{P}_e^{(P)}$	0.046	0.301	0.434	0.479	0.493
Traditional	0 1	3	84	198	243	233
	1 0	2	86	196	224	254
	$\hat{P}_e^{(T)}$	0.005	0.170	0.380	0.462	0.487
Selector	0 1	3	84	198	243	233
	1 0	2	86	196	223	254
	$\hat{P}_e^{(S)}$	0.005	0.171	0.380	0.462	0.487

Table 15A. Statistics / 1000 Bits vs. ISNR, Estimated AC values.
True $\theta = 126^\circ$, True $\rho = 0.95$

ISNR (dB)	$\hat{\rho}$	$\hat{\theta}$ ($^\circ$)	T/P	T. $\overline{\text{SNRI}}$ (dB)	P. $\overline{\text{SNRI}}$ (dB)
-0	0.888	125.9	547/453	12.4576	12.1196
-10	0.881	126.4	502/498	13.6442	13.2758
-20	0.878	126.3	511/489	12.6576	12.3205
-30	0.880	126.0	504/496	13.8262	13.3799
-40	0.881	126.6	480/520	13.1205	12.8133

Table 15B. Bit Errors / 1000 Bits vs. ISNR, Estimated AC values.
True $\theta = 126^\circ$, True $\rho = 0.95$

System	Error Type	ISNR (dB)				
		0	-10	-20	-30	-40
Proposed	0 1	0	49	173	217	232
	1 0	1	41	189	240	254
	$\hat{P}_e^{(P)}$	0.001	0.085	0.330	0.444	0.482
Traditional	0 1	2	48	181	211	242
	1 0	1	45	186	220	269
	$\hat{P}_e^{(T)}$	0.005	0.094	0.332	0.445	0.482
Selector	0 1	1	46	179	211	240
	1 0	0	42	180	227	268
	$\hat{P}_e^{(S)}$	0.004	0.086	0.332	0.444	0.482

The three θ 's picked for the above results were such so as to illustrate the three possible different cases in choosing a receiver system. The $\theta = 0^\circ$ case, presents the possibility of the proposed system outperforming the traditional system whereas the $\theta = 90^\circ$ case presents the opposite. Finally, the $\theta = 126^\circ$ case presents the possibility of the two systems being equivalent in terms of mean SNRI. Note that with an arbitrary noise color distribution one of the above three cases arises at any particular noise color. Also note, from Tables 13A, 14A, and 15A that the selector is clearly capable of distinguishing which system performs better since for the $\theta = 0^\circ$ case the proposed system was picked for the reception 999 times in 1000. Furthermore, in the $\theta = 90^\circ$ case the traditional system was picked for the reception approximately 992 times in 1000 and in the $\theta = 126^\circ$ case the choosing is approximately 500 in 1000.

In an attempt to illustrate the advantage of having a selector incorporated in the design, the average BER were computed for each system, for the three different colored noise center frequencies as a function of ISNR. Generally, if Θ is defined as the random variable such that,

$$\Theta(\theta) = \theta \quad \text{for } 0 \leq \theta \leq \pi$$

then the average of the function $\text{BER}(\Theta)$ for a specific ISNR is,

$$E\{\text{BER}(\Theta)\} = \int_{-\infty}^{\infty} \text{BER}(\theta) p(\theta) d\theta \quad (5.14)$$

where $p(\theta)$ is the probability density function of Θ . For the discrete case (5.14) becomes,

$$E\{\text{BER}(\Theta)\} = \sum_{j=1}^F \text{BER}(\theta_j) P(\theta_j) \quad (5.15)$$

where F is the number of colored noise center frequencies considered for the calculation of the average ($T = 3$ in this case), and $P(\theta_j)$ is the probability of the colored noise having a center frequency of θ_j . If $p(\theta)$ is a uniform probability density function, then a colored noise sequence has equal probability of

containing any center frequency. Hence,

$$p(\theta) = \frac{1}{F} \Rightarrow P(\theta_j) = \frac{1}{3} \quad j = 1, \dots, F$$

and (5.15) becomes,

$$\begin{aligned} E\{\text{BER}(\Theta)\} &= \frac{1}{F} \sum_{j=1}^F \text{BER}(\theta_j) \\ &= \frac{1}{3} \sum_{j=1}^3 \text{BER}(\theta_j) \end{aligned} \quad (5.16)$$

Specifically, the total BER were obtained for a particular ISNR and θ from Tables 13B, 14B, and 15B. Next, the average (over all three θ 's) BER was computed for each receiver system as well as the selector system according to (5.16). Table 16 presents these results. The most desirable system is the system with the smallest average BER and is displayed with a gray shading. Clearly, it is advantageous to incorporate the selector in the communication system since it provides the best averages for all ISNR's except -40 dB. The -40 dB case, though, is of little importance due to the large number of BER under any circumstances.

The BER averages presented in Table 16 can be confirmed by applying (5.16) to the estimated probability of error function $\hat{P}_e(\Theta)$ which is computed independently from the BER. Thus, (5.16) becomes,

$$E\{\hat{P}_e(\Theta)\} = \frac{1}{F} \sum_{j=1}^F \hat{P}_e(\theta_j) \quad (5.17)$$

where $\hat{P}_e(\theta_j)$ can be found in the Tables 13B, 14B, and 15B. The \hat{P}_e averages are presented in Table 17. As before, the most desirable system is the system with the smallest average \hat{P}_e and is displayed with gray shading. Again, the advantage a communication system has with the selector incorporated in the design, is evident. This is logical since the selector combines and utilizes either the proposed system or the traditional system only when they function at their

best.

From Tables 16 and 17 one can confirm the correlation of \hat{P}_e and BER. For instance, for an ISNR = -10 dB the average BER for the selector system is 86 bits out of 1000, whereas the average \hat{P}_e is 0.086 - an exact match. For an ISNR = -30 dB, the average BER for the traditional system, the proposed system and the selector system are 403.67/1000, 314/1000 and 302/1000 respectively. The average \hat{P}_e for these systems are 0.406, 0.308, and 0.303 respectively, resulting in a very close correlation with the aforementioned BER averages. Thus, it is possible to use the \hat{P}_e estimates to predict what would happen at ISNR of 10 dB or 20 dB, without computing the BER which is not only a costly, but a time-consuming procedure as well.

Table 18 is an extension of Table 17, in order to include the average \hat{P}_e values for ISNR of 10 dB and 20 dB. It should be mentioned that these cases represent typical communication system situations with BER on the order of $1/10^6$. Again the selector system is predicted to outperform both the traditional and the proposed system.

Table 16. Receiver System BER Averages for $\rho = 0.95$

ISNR = 0.0 dB	SYSTEM	Traditional	Proposed	Selector
	$\theta = 0^\circ$	0	0	0
	$\theta = 90^\circ$	5	32	5
	$\theta = 126^\circ$	3	1	1
	AVER	2.667	11.00	2.000
ISNR = -10.0 dB	SYSTEM	Traditional	Proposed	Selector
	$\theta = 0^\circ$	1	0	0
	$\theta = 90^\circ$	170	280	170
	$\theta = 126^\circ$	93	90	88
	AVER	88.000	123.33	86.00
ISNR = -20.0 dB	SYSTEM	Traditional	Proposed	Selector
	$\theta = 0^\circ$	59	0	0
	$\theta = 90^\circ$	394	419	394
	$\theta = 126^\circ$	367	362	359
	AVER	273.33	260.33	251.00
ISNR = -30.0 dB	SYSTEM	Traditional	Proposed	Selector
	$\theta = 0^\circ$	313	1	2
	$\theta = 90^\circ$	467	484	466
	$\theta = 126^\circ$	431	457	438
	AVER	403.67	314.00	302.00
ISNR = -40.0 dB	SYSTEM	Traditional	Proposed	Selector
	$\theta = 0^\circ$	458	165	165
	$\theta = 90^\circ$	487	501	487
	$\theta = 126^\circ$	511	486	508
	AVER	485.33	384.00	386.67

Table 17. Receiver System \hat{P}_e Averages for $\rho = 0.95$

ISNR = 0.0 dB	SYSTEM	Traditional	Proposed	Selector
	$\theta = 0^\circ$	0.001	0.000	0.000
	$\theta = 90^\circ$	0.005	0.046	0.005
	$\theta = 126^\circ$	0.005	0.001	0.004
	AVER	0.004	0.016	0.003
ISNR = -10.0 dB	SYSTEM	Traditional	Proposed	Selector
	$\theta = 0^\circ$	0.009	0.000	0.000
	$\theta = 90^\circ$	0.170	0.301	0.171
	$\theta = 126^\circ$	0.094	0.085	0.086
	AVER	0.091	0.129	0.086
ISNR = -20.0 dB	SYSTEM	Traditional	Proposed	Selector
	$\theta = 0^\circ$	0.080	0.000	0.001
	$\theta = 90^\circ$	0.380	0.434	0.380
	$\theta = 126^\circ$	0.332	0.330	0.332
	AVER	0.264	0.255	0.238
ISNR = -30.0 dB	SYSTEM	Traditional	Proposed	Selector
	$\theta = 0^\circ$	0.310	0.002	0.002
	$\theta = 90^\circ$	0.462	0.479	0.462
	$\theta = 126^\circ$	0.445	0.444	0.444
	AVER	0.406	0.308	0.303
ISNR = -40.0 dB	SYSTEM	Traditional	Proposed	Selector
	$\theta = 0^\circ$	0.437	0.168	0.168
	$\theta = 90^\circ$	0.487	0.493	0.487
	$\theta = 126^\circ$	0.482	0.482	0.482
	AVER	0.469	0.381	0.379

Table 18. Receiver System \hat{P}_e Averages $\times 10^{-6}$ for $\rho = 0.95$

ISNR = 10.0 dB	SYSTEM	Traditional	Proposed	Selector
	$\theta = 0^\circ$	0.762	0.000	0.000
	$\theta = 90^\circ$	101.1	244.2	137.0
	$\theta = 126^\circ$	105.1	4.448	56.34
	AVER	68.99	82.88	64.45

ISNR = 20.0 dB	SYSTEM	Traditional	Proposed	Selector
	$\theta = 0^\circ$	0.000	0.000	0.000
	$\theta = 90^\circ$	0.031	0.034	0.031
	$\theta = 126^\circ$	0.000	0.000	0.000
	AVER	0.010	0.011	0.010

6.0 SUMMARY AND CONCLUSIONS

The primary goal of this thesis was the design of an optimal detector for a MAMF communication system, capable of detecting and discriminating the transmitted signal vectors. The optimal detector utilizes the noise corrupted signal vector, the encoding signal vectors and the noise autocorrelation matrix in order to make a decision on which bit was most likely communicated. The detector is characterized by the Receiver Operating Characteristic (ROC). The ROC is illustrated by a plot of probability of error P_e vs. Output Signal-to-Noise Ratio (OSNR), and provides a theoretical standard for the performance of the detector. For optimal detector performance in binary communication, the signal vector encoding the "1" bit must be the negative of the signal vector encoding the "0" bit. In addition, the encoding signal vector must be the eigenvector associated with the minimum eigenvalue of the Toeplitz colored noise autocorrelation matrix, so that a minimum probability of error P_e , is ensured.

The traditional and the proposed MAMF communication systems were compared prior to the incorporation of their respective detectors in terms of Signal-to-Noise Ratio Improvement (SNRI), whereas Bit Error Rate (BER) comparison studies could be performed following the incorporation of the detector in each system. A close correlation was observed between the BER and the ROC for both the traditional and the proposed systems, for actual and estimated noise autocorrelation values. From the close correlation observed under any circumstances, one can predict the performance of the detector, in terms of probability of error, by using the ROC curve.

The absolute maximum attainable SNRI for the traditional and the

proposed systems was calculated over various colored noise center frequencies θ , in order to set an upper envelope of performance for narrowband noise. The SNRI absolute maxima that can be attained for less narrowband noise and broadband noise were also calculated. These results indicated that the traditional system was theoretically capable of outperforming the proposed system at every colored noise center frequency. In addition, as the noise became more broadband, the absolute maximum attainable SNRI decreased for every individual colored noise center frequency.

The two MAMF communication systems were compared when the traditional system was optimized for a specific θ_{opt} , thus using as its encoding signal vector the eigenvector associated with the smallest eigenvalue of the Toeplitz colored noise autocorrelation matrix generated at that θ_{opt} . The proposed system used randomly picked symmetric and skew-symmetric encoding signal basis vectors. When the colored noise center frequency was in the vicinity of θ_{opt} , the traditional system outperformed the proposed system, since the traditional system was optimized for that θ . However, once the colored noise center frequency deviated from the vicinity of θ_{opt} , the SNRI for the traditional system dropped and sometimes attained a negative decibel value which implied degradation, rather than improvement, as the performance of the receiver. The proposed system seemed to be more robust as its SNRI curve was more well-behaved.

The two MAMF communication systems were also compared when the traditional system was optimized for a θ_{opt} and the proposed system used as its encoding signal basis vectors the vectors that almost attain the theoretical SNRI maximum of the system. Hence both systems were considered to be optimized. When colored noise was generated for a specific θ , and the noise autocorrelation was estimated, the BER increased by 8% for the proposed system and 17% for the traditional system relative to the BER calculated with the actual noise autocorrelation values. Hence the proposed system deteriorated in a lesser degree than the traditional system, thereby indicating robustness. However, for another θ , the opposite occurred. From these results one can get an indication of the need for a selector which will be able to choose, based on colored noise

estimates for every bit transmission, the best performing receiver.

The behavior of both communication systems under a practical situation where both systems use the signal vectors for which the proposed system is optimal, was also investigated. As the colored noise became more broadband, the actual SNRI and mean SNRI values decreased. Since the magnitude response of the signal vector used was broadband, it is logical that narrowband noise was more distinctive than broadband noise, thus resulting in a high SNRI relative to the SNRI obtained when broadband noise was used. At different colored noise bandwidths, when actual noise autocorrelation values were used, the traditional communication system outperformed the proposed system. This is an important observation when taking into consideration that the optimal proposed signal vectors were used. When estimated autocorrelation values were used, the proposed communication system was more robust in the sense that it deteriorated to a lesser degree than the traditional system. Nevertheless, there were certain areas in the colored noise center frequency spectrum where the proposed system outperformed the traditional system and vice versa. For instance, the proposed system was clearly more desirable when θ was in the range of $0^\circ - 30^\circ$, while the traditional system performed better in the $75^\circ - 110^\circ$ range.

Therefore, in order to ensure the best possible probability of detection and discrimination of the transmitted bits, it was desirable as well as reasonable to design a selector whose responsibility would be to choose the MAMF receiver which performs better for an estimated noise realization $\hat{\theta}$ and $\hat{\rho}$. Based on the estimates $\hat{\theta}$ and $\hat{\rho}$, a decision could be made on which system performs better by utilizing the already existing SNRI data. The [traditional/proposed] MAMF communication system, which incorporates the selector, performed better, on the average, than either the traditional MAMF communication system or the proposed MAMF communication system alone. For instance, for an ISNR of -20 dB, the average BER for the [traditional/proposed] MAMF system was 251/1000 whereas the average BER for the proposed and traditional MAMF systems were 260/1000 and 273/1000 respectively.

APPENDIX

This chapter consists of two sections. The first section presents the Gram-Schmidt orthonormalization and the second section presents the Levinson algorithm. Although both procedures can be found in the literature ([9], and [6] respectively), they are included in this chapter for fast reference due to their importance.

Appendix A. (Gram-Schmidt Orthonormalization Process)

Let us assume that $\mathbf{f}_1, \mathbf{f}_2, \dots, \mathbf{f}_n$ are any n basis vectors. Then one can always construct orthonormal basis vectors $\mathbf{g}_1, \mathbf{g}_2, \dots, \mathbf{g}_n$ by using the Gram-Schmidt orthonormalization recursive scheme which is given by the following equations:

$$\begin{aligned}\mathbf{h}_1 &= \mathbf{f}_1 \\ \mathbf{h}_2 &= \mathbf{f}_2 - a_{21}\mathbf{f}_1 \\ &\vdots \\ \mathbf{h}_n &= \mathbf{f}_n - a_{n,n-1}\mathbf{f}_{n-1} - \dots - a_{n1}\mathbf{f}_1\end{aligned}$$

where

$$\begin{aligned}a_{n1} &= \frac{\langle \mathbf{f}_n, \mathbf{h}_1 \rangle}{\langle \mathbf{h}_1, \mathbf{h}_1 \rangle} \\ &\vdots \\ a_{n,n-1} &= \frac{\langle \mathbf{f}_n, \mathbf{h}_{n-1} \rangle}{\langle \mathbf{h}_{n-1}, \mathbf{h}_{n-1} \rangle} \quad n \geq 2\end{aligned}$$

where $\langle \mathbf{x}, \mathbf{y} \rangle$ denotes the inner product of the vectors \mathbf{x} and \mathbf{y} . Hence, the normal basis is obtained by normalizing the \mathbf{h}_n vectors as follows,

$$\mathbf{g}_n = \frac{\mathbf{h}_n}{\|\mathbf{h}_n\|} \quad \forall n \quad (\text{A.1})$$

where $\|\mathbf{x}\|$ denotes the norm of the K -dimensional vector \mathbf{x} in the following manner:

$$\|\mathbf{x}\|^2 = \langle \mathbf{x}, \mathbf{x} \rangle$$

The vectors $\mathbf{g}_1, \mathbf{g}_2, \dots, \mathbf{g}_n$ form an orthonormal basis of the linear space spanned by the basis vectors $\mathbf{f}_1, \mathbf{f}_2, \dots, \mathbf{f}_n$.

Appendix B. (Levinson Algorithm)

The Levinson algorithm was originally designed to solve the Yule-Walker equations or,

$$\Phi \mathbf{a} = \mathbf{b} \quad (\text{B.1})$$

where Φ is an $N \times N$ Hermitian matrix of the following structure:

$$\Phi = \begin{bmatrix} \varphi(0) & \varphi(-1) & \dots & \varphi(-N+1) \\ \varphi(1) & \ddots & & \vdots \\ \vdots & & \ddots & \vdots \\ \varphi(N-1) & \dots & \dots & \varphi(0) \end{bmatrix}$$

In addition the vectors \mathbf{a} and \mathbf{b} are of the following structures:

$$\mathbf{a} = [\mathbf{a}(1) \ \mathbf{a}(2) \ \dots \ \mathbf{a}(N)]^T$$

$$\mathbf{b} = -[\varphi(1) \ \varphi(2) \ \dots \ \varphi(N)]^T$$

If Φ denotes the autocorrelation matrix, then one may determine the AR parameters by solving the set of linear equations of (B.1). Gaussian elimination could be used but would require N^3 operations. Due to the special structure of the Φ matrix, though, the Levinson algorithm requires N^2 operations. The algorithm recursively computes the parameter sets $\{a_1(1), \rho_1\}$, $\{a_2(1), a_2(2), \rho_2\}$, ..., $\{a_N(1), \dots, a_N(N), \rho_N\}$ where ρ_j is the prediction error power at order j . The final set at order N is the desired solution of (B.1). The recursive algorithm is initialized by,

$$a_1(1) = -\frac{\varphi(1)}{\varphi(0)}$$

$$\rho_1 = (1 - |a_1(1)|^2)\varphi(0)$$

with the recursion for $k = 2, 3, \dots, N$ given by

$$a_k(k) = - \frac{\varphi(k) + \sum_{l=1}^{k-1} a_{k-1}(l)\varphi(k-l)}{\rho_{k-1}} \quad (\text{B.2.a})$$

$$a_k(i) = a_{k-1}(i) + a_k(k) a_{k-1}^*(k-i) \quad i = 1, 2, \dots, k-1 \quad (\text{B.2.b})$$

$$\rho_k = (1 - |a_k(k)|^2)\rho_{k-1} \quad (\text{B.2.c})$$

The reflection coefficients are given by,

$$k_k = a_k(k)$$

The Levinson algorithm can also be used to solve any set of linear equations of the form,

$$\Phi \mathbf{c} = \mathbf{d} \quad (\text{B.3})$$

where the vectors \mathbf{c} and \mathbf{d} are of the following formats:

$$\mathbf{c} = [c(1) \ c(2) \ \dots \ c(N)]^T$$

$$\mathbf{d} = [d(1) \ d(2) \ \dots \ d(N)]^T$$

Then the recursive algorithm is initialized by

$$c_1(1) = - \frac{\varphi(1)}{\varphi(0)}$$

$$\rho_1 = (1 - |c_1(1)|^2)\varphi(0)$$

and equations (B.2) become for $k = 2, 3, \dots, N$,

$$c_k(k) = - \frac{d(k) + \sum_{l=1}^{k-1} c_{k-1}(l)\varphi(k-l)}{\rho_{k-1}} \quad (\text{B.4.a})$$

$$c_k(i) = c_{k-1}(i) + c_k(k) c_{k-1}^*(k-i) \quad i = 1, 2, \dots, k-1 \quad (\text{B.4.b})$$

$$\rho_k = (1 - |c_k(k)|^2)\rho_{k-1} \quad (\text{B.4.c})$$

BIBLIOGRAPHY

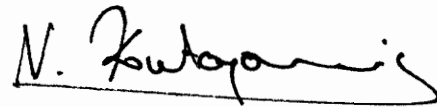
- [1] C. T. Chen, *Linear System Theory and Design*. Holt, Rinehart and Winston, New York, 1984.
- [2] R. Deutsch, *Estimation Theory*. Prentice-Hall Inc., New Jersey, 1965.
- [3] K. A. Becker, *Effects of Spectral Estimation on Matched Filter Design*. M.S. Thesis, Virginia Polytechnic Institute & State University, May 1985.
- [4] A. A. (Louis) Beex, and J. M. Wilson, "Robust Communication in a Time-Varying Noisy Environment," International Conference on Acoustics, Speech, and Signal Processing, (ICASSP '88), April 11-14, New York, NY, pp. 1546-1549.
- [5] A. D. Whalen, *Detection of Signals in Noise*. Academic Press Inc., California, 1971.
- [6] S. M. Kay, *Modern Spectral Estimation - Theory & Application*. Prentice-Hall Inc., New Jersey, 1988.
- [7] A. Papoulis, *Probability, Random Variables, and Stochastic Processes*. McGraw-Hill, New York, 1965.
- [8] H. Stark, *Probability, Random Processes, and Estimation Theory for Engineers*. Prentice-Hall Inc., New Jersey, 1986.

- [9] N. Mohanty, *Random Signals, Estimation, and Identification - Analysis and Applications*. Van Nostrand Reinhold Company Inc., New York, 1986.
- [10] D. Kazakos, *Detection and Estimation*. Computer Science Press, New York, 1990.
- [11] L. W. Johnson, *Numerical Analysis*. Addison-Wesley Publishing Company, Massachusetts, 1982.
- [12] J.P. Dugre, A.A. Beex, and L.L. Scharf, "Generating Covariance Sequences and the Calculation of Quantization and Rounding Error Variances in Digital Filters," *IEEE Transactions on Acoustics, Speech, and Signal Processing*, vol. ASSP-28, pp. 102-104, February 1980.
- [13] E. Arthurs and H. Dym, "On the optimum detection of digital signals in the presence of white gaussian noise," *IRE Trans. Commum. Syst.* CS-10, No. 4, pp. 336-372, December 1962.
- [14] B. M. Oliver, "Thermal and quantum noise," *IRE Proc.*, May 1965.
- [15] J. R. Pierce, "Physical sources of noise," *IRE Proc.*, May 1956.
- [16] J. H. Miller and J. B. Thomas, "Detectors for discrete-time signal in non-gaussian noise," *IEEE Trans. Inform. Theory* IT-18, pp. 241-250.
- [17] M. Schwartz, "Effects of signal fluctuation on the detection of pulse signals in noise," *IRE Trans. Inform. Theory* IT-2, No. 2, pp. 66-71, 1956.
- [18] M. Schwartz, "On the detection of known binary signals in gaussian noise of exponential covariance," *IEEE Trans. Inform. Theory*, IT-11, No. 3, pp. 330-335, 1965.

- [19] B. O. Steensen and N. C. Stirling, "The amplitude distribution and false-alarm rate of filtered noise," *IEEE Proc.*, January 1965.
- [20] T. Kailath, "A general likelihood-ratio formula for random signals in gaussian noise," *IEEE Trans. Inform. Theory*, IT-15, No. 1, pp. 350-361, 1969.
- [21] T. Kailath, "The innovations approach to detection and estimation theory," *IEEE Proc.*, Vol. 58, No. 5, pp. 680-695, 1970.
- [22] T. Kailath, "A projection method for signal detection in colored gaussian noise," *IEEE Trans. Inform. Theory*, IT-13, No. 3, pp. 441-447, July 1967.
- [23] C. W. Helstrom, "Solution of the detection integral equation for stationary filtered white noise," *IEEE Trans. Inform. Theory*, IT-11, No. 3, pp. 335-339, 1965.
- [24] J. Makhoul, "On the eigenvectors of symmetric Toeplitz matrices," *IEEE Trans. on Acoustics, Speech, and Signal Processing*, Vol. ASSP-29, No. 4, pp. 868-872, August 1981.
- [25] J. M. Wilson, *Robust Communication in a Time-Varying Noisy Environment*. M.S. Thesis, Virginia Polytechnic Institute & State University, November 1987.

VITA

Nickos Sotirios Kontoyannis was born on January 28th, 1968 in Enid, Oklahoma USA. He graduated from the "Helliniki Paedia" High School in 1985 in Athens, Greece. He attended the Stevens Institute of Technology in Hoboken, NJ and received his Bachelor's of Engineering degree with High Honor with Thesis in Electrical Engineering with a Humanities minor in May 1989. In September of the same year he came to VPI & SU to complete a Master's of Science degree in Electrical Engineering. He is the recipient of the 1989 Sheehan Biomedical Research Award and a member of Tau Beta Pi and IEEE.

A handwritten signature in black ink, reading "N. Kontoyannis". The signature is written in a cursive style with a horizontal line underneath the name.